From Bottom Water to Mode Water: A Compendium of Water Masses

Y. Plancherel[a]

[a]*Department of Earth Sciences, University of Oxford, Oxford, OX1 3AN, UK*

Abstract

While global coupled climate models do, for the most part, resolve the main structure of the ocean, that is, models possess bottom waters, deep waters, intermediate waters and central waters, the ability of global climate models varies greatly in their ability to resolve the water masses regionally. The temperature and salinity distribution simulated by models also show significant biases. Water masses, although difficult to define quantitatively, can provide a useful framework to evaluate and discuss model simulations and biases. The literature on water mass properties is spread widely in the literature, however, making it hard to evaluate what the salient features of each water mass are.

A review of the world's most prominent bottom waters, deep waters, intermediate waters and central waters is presented here, including a discussion of formation mechanisms, thermohaline and biogeochemical properties, variability and formation rates. Water masses originating at high polar latitudes are discussed first, with a comparative description of the freshwater and sea ice conditions in the Arctic and Antarctic regions. Low salinity intermediate waters are described next, followed by high salinity intermediate waters that originate from evaporation basins. The central waters that ventilate the thermocline are discussed last, including a presentation of the five types of mode waters.

One recurrent theme of the synthesis presented here is that overflows, entrainment at the overflows, water mass formation and export is often impacted by small bathymetric features, such as the Maud Rise in the Weddell Sea, the Orphan Knoll in the Labrador Sea, the depth and width of continental shelves or the presence of canyons cutting through the shelf break. Mode and intermediate water formation are critically dependent on the winds and on the cycling of the mixed layer. Some water masses, such as ESTMW in the North Pacific, can also depend critically on peculiarities of the seasonal cycle of the buoyancy flux. As water mass formation often requires cold winter air bursts, small zonal or meridional shifts in the winds can have a dramatic impact on the formation characteristics of water masses.

Keywords: Water mass, Bottom Water, Deep Water, Intermediate Water, Mode Water, Hydrography

Contents

1. Introduction

In spite of its limitations and the fact that it is over a century old, the concept of water masses in oceanography, defined here in analogy to "air masses" as finite bodies of water having common origin and histories, remains a useful practical construct to summarize modern and paleo-data, interpret model results and compare models with data. Judging from its prevalence in the oceanographic literature, there is clearly value and interest in better understanding the concept of water mass. Porting this concept to a consistent and rigorous quantitative analysis is a difficult task but use of the concept has proven useful in a multitude of studies. Because the concept of a water mass is perceived as semi-quantitative at best, water mass names tend to be assigned loosely. Names are often adapted based on the particular purpose of a study. As such, it can be difficult to find a consensus in the published nomenclature of water masses and their properties. Names can be assigned to water masses based on their geographical location (i.e. North Atlantic Central Water), their origin (i.e. Mediterranean Sea Overflow), to explain differences in tracer properties (i.e. Classical and Upper Labrador Sea Water) or their role in maintaining the vertical stratification (i.e. Intermediate or Deep Waters). These loose definitions can make the task of comparing and appreciating results pertaining to these water masses challenging. One is often faced with the case where similar names are used that define water masses differently or different names are used that describe a similar body of water.

While there exist many articles discussing particular water masses, only few provide a synthesis summarizing this information. One of the earliest global summaries of the world's water masses was provided by Sverdrup et al. (1942) in *Chapter XV: The Water Masses and Currents of the Ocean*. Sverdrup et al. (1942) provide schematic generalized whole water column θ/S diagrams organized by basins (Atlantic, Indian, South Pacific and North Pacific), reproduced here in Figure 1, and a map containing the approximate boundaries of the distribution of Mode Waters (they refer to them as central water masses or upper water masses) with estimates of their formation areas (their Figures 209A and 209B). This summary does not include the high-latitudes.

These characteristic θ/S diagrams and approximate distribution maps have been updated and modified by Mamayev (1975) and Emery & Meincke (1986) (Figure 2). These authors have also contributed maps of the approximate distribution of intermediate (550-1500 m), deep and bottom waters (>1500m) as well as summary tables of thermohaline θ/S indices (Mamayev (1975), his Table XV, Ch. 8), also known as water types. In contrast, Emery & Meincke (1986) provides water mass θ/S ranges. Unlike Sverdrup et al. (1942), however, Mamayev's perspective was on the understanding of water mass mixing as evaluated from vertical profiles. Consequently, his θ/S diagrams (his Figures 97 to 101) were developed to highlight mixing pathways and thermohaline indices (water types), rather than for regional categorization. The θ/S diagrams of Emery & Meincke (1986) incorporate some update in term of water mass nomenclature relative to Mamayev (1975), although they still do not provide a synthesis of the water masses at high-latitudes.

Some of the most complete collections of information on the distribution and formation characteristics of the ocean water masses can be found in Tomczak & Godfrey (1994), and more recently Talley et al. (2011). Both textbooks introduce the field of oceanography through a global presentation of the hydrography of all major ocean basins, with schematic maps of the dominant circulation patterns, cross sections and θ/S diagrams.

The goal of this study is to review the water mass literature, to describe the climatological water mass structure of the ocean interior, and to discuss the general properties of water mass. Since variability increases in amplitude and frequency near the surface, the concept of water mass loses some of its meaning in the mixed layer. For this reason, regional waters masses from the top few tens of meters located and those located equatorward of the subpolar regions are not discussed here, even if these have been mentioned in the literature. The water masses discussed below provide a detailed picture of the world's hydrographic structure with a focuse on some important formation processes at a scale that should provide useful as a basis against which global circulation model results can be compared. The $1^o \times 1^o$ gridded World Ocean Atlas 2005 climatology (WOA05, Locarini et al. (2006)) is used throughout this review for illustrative purposes and this is conceptually representative of the targetted saptial and temporal scales relevant for this review.

An overview of the global observed volumetric θ/S distribution of the ocean is presented first. Volumetric θ/S distributions have the advantage of being able to give a good representation of the full scatter of the ocean properties, while also providing a sense of importance (volume). Water masses are then discussed in sequence, starting with waters that form in polar regions and proceeding towards the tropics. Deep and bottom waters originate in cold polar regions, where the haline component of density dominates the thermal component in setting the overall stratification (Carmack, 2007). Water mass formation in these regions is dominated by the process of convection and by the interactions between ice and seawater. The subpolar regions, origin of the intermediate waters, are essentially transition regions that can be extremely susceptible to climate perturbations and are convergence regions for fresh cold polar waters and warm and salty subtropical waters. Their location is associated with the storm tracks. Water mass formation mechanisms in these regions are affected by both thermohaline processes and winds. The tropics are characterized by high evaporation rates and steady trade winds. These regions are home to the subtropical gyres and the associated swift western boundary currents (WBC). These are the physical settings that largely control the formation of mode waters.

2. General overview

Annotated global and regional volumetric θ/S distributions, $(\theta/\mathrm{S})_{vol}$, computed from the annual WOA05 climatology with bin intervals δS=0.01 psu and $\delta\theta$=0.05 ^{o}C, are shown in Figure 3. The water mass nomenclature attempts to use commonly used denomitations (Table 2). A list of general acronyms is also given in Table 1. The volumetric distributions are presented

with two different color schemes. In Figure 3a, the discrete color palette corresponds to the relative cumulative volume distribution calculated after sorting the $(\theta/S)_{vol,i}$ pairs in decreasing order from the θ/S pair accounting for the largest volumes to the pairs accounting for the smallest volumes. Color breaks are shown where the cumulative volume, divided by the total ocean volume, reaches subjectively selected fractions (e.g. 50, 70, 90%, etc, as indicated). Fractions were chosen to highlight certain features, such as the mode water volumetric ridges. Panels b-i (Figure 3) use a base-10 logarithmic scale to increase contrast. Black contours, the volumetric skeleton, reproduced in all panels, mark the locations of the color-breaks from the global $(\theta/S)_{vol}$ distribution from Figure 3a. A selection of σ_θ isopycnals are also shown for reference.

Figure 3a shows the typical ζ-shape characteristic of θ/S curves, with the following main features:

- a warm and fresh equatorial region whose salinity is low due to the high precipitation associated with the Inter-Tropical Convergence Zone (ITCZ)
- a subtropical salinity maximum produced by the high evaporation at these latitudes dominated by the trade-winds
- a subpolar salinity minimum that forms from both equatorward transport of fresher waters from higher latitudes and high precipitation under the storm tracks
- a relatively higher salinity maximum characteristic of the deep water formation regions and processes, representing the combination of surface cooling and mixing between relatively fresh subpolar and polar waters and poleward moving saltier waters from the subtropics, and, in the Southern Ocean mostly, the concentration of salt by the process of brine rejection
- a very cold polar region with salinities that vary owing to freshwater fluxes from precipitation and rivers (Arctic, i.e. presence of large drainage basins), calving and melting ice-shelves, and melting and brine rejection from the seasonal sea-ice cycle.

Because of the localized and seasonal nature of bottom water formation at polar latitudes, the presence of residual low-salinity water in the upper layer of the ocean, particularly in the Southern Ocean, reflects the seasonal cycle of the buoyancy fluxes and the rate at which this cold fresh layer is exported equatorward by Ekman transport. As such, the presence or absence and hydrographic properties of waters such as the WW and AASW (see Figure 3d and e) carry interesting implications for the diagnosis of circulation models. These water masses are not only reflecting the boundary fluxes and the mixed layer dynamics, but are themselves precursors of other water masses in the overall water mass system, such as AABW and AAIW. These water masses are part of a characteristic "box-shaped" complex of water masses located at low-temperatures in the $(\theta/S)_{vol}$ diagrams (-2.2 to 3^oC, dash pink line, Figure 3d) that appears to be unique to the Southern Ocean regions. There, the θ/S structure forms a "box" that is closed on the warmer/saltier side by the mixed region between AAIW, CDW, and the AABW components, and on the colder/fresher side by the nearly isothermal WW and the nearly isohaline AASW (with a broad volumetric mode centered around 34 psu, Figure 3a, d, e).

The $(\theta/S)_{vol}$ of individual basins, all having the typical ζ-shape, are shown in panels 3d, f, g, i. Aside from this main structure, which is explained mostly by the latitudinal variation of the large-scale surface heat and freshwater fluxes, 3a shows clearly the separation between the central waters of the Southern Hemisphere, the North Atlantic and the North Pacific. The Pacific is about 2 salinity units fresher than the Atlantic between 15 to 20^oC. While the exact controls on inter-basin salinity offsets are not totally understood, the typical explanation invovles a combination between the excess precipitation in the Pacific of water that has originally evaporated in the Atlantic and oceanic circulation-induced freshwater transport (Broecker, 1997). The global circulation and the inter-basin salinity contrast are closely linked, however (Seidov & Haupt, 2002). In order for a model to achieve the correct salinity contrast between the North Atlantic and the North Pacific, it is necessary for that model to simulate the correct balance between both oceanic and atmospheric freshwater transport. This is a challenging task, which makes the Pacific to Atlantic salinity contrast a simple but interesting and stringent model diagnostic.

While the volumetric ridges characteristic of the central waters in each basin are fairly linear, they tend to be slightly concave upwards, particularly towards the colder side of the tropical salinity maxima (Figure 3d, f, g, i). This slight curvature is in fact the signature of cabbelling (Mamayev, 1975; Carmack, 2007), a nonlinear mixing process that increases density of a mixture. Cabbelling occurs when warm salty waters lay over colder fresher waters: the typical situation that separates Subtropical waters from Intermediate Waters. This layering pattern exists in all basins. It is reflective of the latitudinal heat and moisture fluxes in each basin and each hemisphere, and of the source water characteristics that ventilate the thermocline. Where density gradients are mostly controlled by temperature, in the subtropical regions, these regions are coined "alpha-oceans", whereas regions where density stratification is mostly driven by salinity differences are called "beta-oceans" (Carmack, 2007). "Alpha" regions tend to be regions of Ekman convergence, favorable for subduction. "Beta" regions tend to be characterized by cyclonic (counter-clockwise in the Northern Hemisphere) circulations and are regions of Ekman divergence, or upwelling. The competition between Ekman upwelling and downwelling, and surface stratification affects the ability of these regions to maintain deep mixed layers and ventilate the interior. Since upwelling brings isopycnals upwards, closer to the surface, this is a particularly important process that affects the formation mechanisms of Mode Waters in different hydrographic basins. For example the difference between the strength of the salinity stratification explains the difference between the volumetric importance of North Atlantic and North Pacific subpolar mode and intermediate waters. Upwelling, cy-

clonic conditions which bring isopycnals to the surface, are also critical for the preconditioning of convective regions, such as in the Greenland gyre (arguably a part of the North Atlantic subpolar cyclonic circulation system).

Aside from these main structures, each basin also possesses a suite of $(\theta/S)_{vol}$ signatures , which may not be very important volumetrically, but that can readily be identified and that reflect regional climate processes or important oceanographic features. Ocean basins tend to have fresher subtropical regions on the East than on the western side of the basin, with characteristic water mass signatures, owing to the atmospheric circulation and associated precipitations patterns. Surface waters are fresher in the East because of increased precipitation west of the Andes, Rocky Mountains and Continental Europe. These waters are the ESTMWs and are found in all basins, although to varying degrees. They are less pronounced in the Atlantic because of the Agulhas leakage (Beal et al., 2011) and the eastward extending North Atlantic Current, which both inject salty waters to the eastern side of the basin. Extreme cases exist in the Pacific, with the formation of South Pacific Eastern Subtropical Mode Water (SPESTMW), which combines the eastern precipitation excess with the equatorward propagating leftover waters that do not contribute to the formation of AAIW in the Southeastern Pacific (Wong & Johnson, 2003). These also have a North Pacific equivalent (North Pacific Eastern Shallow Salinity Minimum Water, NPESSMW), which constitute part of the California Current and are the subtropical consequences of the cold and fresh subpolar North Pacific Subarctic Surface Water (NPSASW) from the Western Subarctic and Alaska gyres in the North Pacific. The upper layers of the Indian Ocean hold a complex set of water masses (Stott et al., 2009). The Indonesian Throughflow injects waters from the Pacific (Indonesian Through-flow Water, ITW), the Arabian Sea receives extremely salty inputs from the Persian Gulf and the Red Sea evaporation basins, contributing to the formation of Persian Gulf Water (PGW), Red Sea Water (RSW), Arabian Sea Surface Water (ArSSW), Western Indian Surface Water (WISW) and influencing the deep water characteristic (Indian Deep Water, IDW) through the process of salt fingering (You, 2000, 2002a). The Bay of Bengal (between India and Thailand) accumulates large amounts of freshwater from both direct precipitation and because it is the end-point of the drainage basin that collects the inland precipitation of the Asian Monsoon (Kang et al., 2002) (Bay of Bengal Water, BBW).

3. Water masses of the high-latitudes

As first posited by Benjamin Thompson (Count Rumford) based on the observation that deep waters at mid-latitude are colder than surface waters at these locations and the knowledge that waters at high latitudes are cooler than those at low latitude, cold waters filling the deep ocean originate from the polar regions and drive a kind of planetary heat engine (Thompson, 1800). The basic idea still stands: heat is transported from the low latitude and is released at the poles where waters sink owing to the gain in density. The role of salt stratification, winds, atmospheric buoyancy fluxes and turbulence greatly complicate the discussion, however, such that one now prefers to talk of a "Meridional Overturning Circulation (MOC)" rather than a "Thermohaline Circulation (THC)" (Kuhlbrodt et al., 2007).

The study of the polar seas has always been data limited, however. Much of what is known, or has been inferred, about polar hydrography and biogeochemistry stems from few samples. More often than not, experiments have not been repeated and variability near the sampling sites has not been properly assessed. Deep waters originate poleward of 50° where the effects of seasonality are particularly important (Hoppema et al., 1995; Gibson & Trull, 1999; Jennings et al., 1984; Nilsen & Falck, 2006; Bruhwiler et al., 2011). The few samples available at these latitudes suggest that interannual to decadal-scale variability is important at high latitudes (Orsi et al., 2001; Fahrbach et al., 2004) and that important aspects of polar ventilation are missing owing to the biases in the available database (Whitworth, 2002). However, some confidence can be gained as some distinctive features are found repeatedly at different sites and ventilation processes are suggested from specific tracers, for example the V-shaped front located at the Antarctic shelf break in association with the Antarctic Coastal Current or the presence of CFCs in the deep Greenland Basin. Other features, however, such as Gordon (1978)'s Weddell chimney, which has been interpreted as a convective chimney in the Weddell Sea, indicative of open ocean convection, remains unreplicated.

The race to the poles has long been finished, however. Today, interest in the polar oceans and deep water formation is no longer a matter of national prestige but is mostly focused around theories of global climate change (Hay, 1993). It is known that perturbation of the polar regions can affect climate on different space and time scales. For instance, salinity perturbations originating from the Arctic or the Labrador Sea/Baffin Bay may greatly affect the convective activity in the North Atlantic on the interannual time-scale (Dickson et al., 1988; Belkin et al., 1998; Proshutinsky et al., 2002). Similar but longer perturbations are believed to be responsible for the shutdown of the Atlantic MOC during Heinrich events (McManus et al., 2004), what circulation model experiments seem to suggest also (Manabe & Stouffer, 1995). While it is generally sufficient to reduce the discussion to summary water masses, such as NADW and AABW, in the climate discussion, a more detailed understanding of the mechanisms leading to the production of these deep and bottom waters, that integrate the net effects of different ventilation processes and requires the interactions of many lesser known water masses locally, can be helpful to further understand variability on time scales shorter than the ocean overturning time scale and to better characterize the sensitivity of ocean ventilation in the polar regions, particularly in the context of anthropogenic climate change.

The water masses that ventilate the global deep ocean are of considerable importance for climate (Hay, 1993) as they influence heat (Stouffer et al., 2006b; Boé et al., 2009b) and carbon (Sarmiento & Toggweiler, 1984; Siegenthaler & Wenk, 1984; Knox & McElroy, 1984; Toggweiler et al., 2003a,b) uptake in the long-term. The hydrographic conditions characteristic of the North Atlantic and Southern Ocean Deep Water systems are shown in panels 3b and e, respectively. The discussion

of deep waters starts with a presentation of the Arctic region (Figure 3h). Given the importance of the end-products NADW and AABW in the oceanographic literature, the following discussion is organized in a way to contrast the formation mechanisms of these two water masses originating at high-latitudes. A detailed description and characterization of the water masses found in both polar regions is provided. The physical settings of the oceanic Arctic and Antarctic regions are briefly described. This is followed by a comparison of the freshwater budget in the polar regions, highlighting the relevance of key fluxes for the hydrographic situation that characterizes each location, focusing on rivers, ice shelves and sea-ice dynamics.

3.1. The water mass system of the North Atlantic and the Arctic

3.1.1. The Arctic and Greenland-Iceland-Norwegian Seas

Geographical setting. The hydrographic properties of the Mediterranean Arctic and the Greenland, Iceland, Norwegian (GIN) Seas are very different from the other basins and these regions are easily identifiable on the $(\theta/\mathrm{S})_{vol}$ space (Figures 4 and 3h). The strongly salinity stratified Arctic Mediterranean Sea (Figure 4) is made up of four large basins north of the Fram Strait (the Nansen, Amundsen, Makarov and Canadian Basins) and of the Nordic Seas (Greenland, Norwegian and Iceland Seas - note the Iceland Sea is located north of Iceland, whereas the Iceland Basin is located south of Iceland). The Nordic Seas are themselves separated from the North Atlantic Ocean by the Greenland-Scotland Ridge (Meincke et al., 1997). The Nansen and Amundsen Basins, as they are only separated by the small and deep Gakkel Ridge, are often considered together and called the Eurasian Basin. Similarly, the Makarov Basin is often folded into the Canadian Basin. The Lomonosov Ridge, with a depth between 850 m and 1600 m (Tomczak & Godfrey, 1994), separates the Eurasian and the Canadian Basins. The Arctic Ocean communicates with the Atlantic and the Pacific through only four passages: 1) through the Fram Strait, located west of Spitsbergen, 2) through the Barents Sea, east of Spitsbergen, 3) through the Canadian Archipelago into Baffin Bay and 4) through the Bering Strait (45 m deep, 85 km wide). Of these passages, only the 450 km wide Fram Strait, with depths between 2500-3000 m, permits exchange of deep water between the Eurasian basin and the Greenland Basin. The Greenland-Scotland Ridge, however, limits that connection with the subpolar North Atlantic to the 600 m deep Denmark Strait and the Iceland-Scotland channel. This channel is 400 m deep between Iceland and the Faroe Island and reaches 800 m in the Faroe Bank Channel, between the Faroe Islands and the Faroe Bank just south of the Faroe Islands (Tomczak & Godfrey, 1994). The 600 m deep Wyville-Thomson Ridge passage separates the Faroe Bank from Scotland (Saunders, 2001). The Arctic Sea is surrounded by land or shallow marginal seas: Barents Sea (100-350 m), Kara Sea (100 m), Laptev Sea (10-40 m), East Siberian Sea and Chukchi Sea (20-60 m). These marginal seas typically sit on broad continental shelves (up to 600-800 km wide).

Water mass overview. A good understanding of the hydrography in the Arctic is warranted as this basin closes the thermohaline loop (Mauritzen & et al., 2011). The ocean and the atmosphere over the Arctic also respond quickly and with large amplitude to increasing atmospheric greenhouse gases concentrations (Serreze & Francis, 2006; Peterson et al., 2006; Chapman & Walsh, 2007; Bates & Mathis, 2009).

The water mass structure of the Arctic, including the GIN Seas and the Bering Sea (BS) is shown in Figure 3h. The σ_θ contours provide an impression of the overall vertical structure of the Arctic region, that is mostly governed by salinity variations between source waters and by the freeze-melt process. The surface layers are very fresh and very cold (Arctic Shelves Water, ASW), owing to a combination of sea-ice melt and river discharge, mostly on the Siberian shelf (Dai et al., 2009). Because of the dominantly cyclonic circulation in the Arctic, the freshwater layer is thickest in the convergent Canadian Basin (Gow & Tucker, 1990; Proshutinsky et al., 2002; McPhee et al., 2009) where local brine production is not able to erode the halocline directly in the center of the basin. The growing ice-edge is located towards the continental shelves (Belchansky et al., 2008), mostly off the Siberian coasts and the Barents and Kara Seas, where summer ice-free conditions are favored by river runoff and by the cyclonic circulation of warmer waters of Atlantic origin. This is also where seasonal brine rejection is concentrated in winter. Sinking of brine-enriched water (High Salinity Arctic Shelf Water, HSASW) on the shallow shelves and subsequent lateral mixing at the shelf break (suggested by magenta arrows on figure 3h) is thought to contribute to the the formation of the halocline (Upper/Lower Halocline Water, U/LHW) and to the slow ventilation of the deep basins (Aagaard et al., 1985; Carmack, 1990; Rudels & Quadfasel, 1991; Rutgers Van Der Loeff et al., 1995; Carmack et al., 2008).

Mixing with waters intruding from the Atlantic, which is typically warmer and saltier (Atlantic Water, AW), occurs at a variety of specific locations depending on the entry route of the AW in the Nordic Seas and around Spitsbergen or over the Barents Sea. Mixing with AW contributes to the formation of various levels of Arctic Intermediate Waters whose exact properties depend on location and on the mixing and cooling associated with each route (Polar Intermediate Water - PIW, Upper/Lower Arctic Intermediate Water - U/LAIW) (Swift & Aagaard, 1981; Rudels et al., 1991, 1994). Heat subducted and transported into the Arctic by AW is not lost to the atmosphere in the Arctic as this layer is protected by the strong halocline above it. AW perturbations are able to recirculate into the Arctic with a time scale of 10-20 years and later influence the intermediate layer properties in the Nordic Seas upon exiting the Arctic through the Fram Strait, indirectly modifying slightly intermediate waters in the GIN seas. Since modified AW is a precursor of NADW (Strass et al., 1993; Rudels et al., 1994; Mauritzen, 1996; Karcher et al., 2008; Tanhua et al., 2008; Messias et al., 2008), perturbations of the northward heat and salt transport into the Arctic may induce a mode of variability of the North Atlantic overturning. An Arctic-Atlantic connection between interior temperature and salinity properties of the Arctic and multi-decadal variability (>40 years) of the overturning was in fact recently found in a model study (Frankcombe & Dijkstra, 2011).

The deep waters of the Arctic and GIN Seas evolve from

densest (cold and fresh Greenland Sea Deep Water (GSDW) and Norwegian Sea Deep Water (NSDW)) to lightest (warm and salty Eurasian Basin Deep Water (EBDW) and Canadian Basin Deep Water (CBDW)) along the circulation path characteristic of these water masses starting from GSDW, NSDW, through the Fram strait into EBDW and CBDW (Aagaard et al., 1985). Heat and salt accumulate into CBDW because of its relative isolation from the other basins. Its long residence time and mixing with both the AW and occasional brine-enriched plumes sinking off the Siberian shelves (HSASW) slowly enrich its salinity and explain the warmth of CBDW relative to the other waters in the region. Because of open-ocean convection occurring in the Greenland Sea, GSDW and NSDW are better ventilated and richer in oxygen and other anthropogenic tracers (Anderson & Jones, 1991; Bonisch & Schlosser, 1995; Dickson et al., 1996; Tanhua et al., 2009). Convection depth mostly affects the intermediate layer but tracer concentrations indicate that this process is occasionally able to ventilate the whole water column (Aagaard & Carmack, 1989; Chen et al., 1990; Schlosser et al., 1991; Boenisch et al., 1997; Marshall & Schott, 1999).

Ventilation of the deep Arctic. The deep Arctic Basin is less well ventilated than the deep waters surrounding the Southern Ocean. The Canadian Basin, especially, is isolated from the other basins by the Lomonosov Ridge and is capped off by a freshwater lid. MacDonald & Carmack (1993) estimated ^{14}C ages of 500 years for the deep Canadian Basin. More recently, Tanhua et al. (2009), used measurements of CFCs and SF_6 made in the Arctic and applied the theory of transit time distributions (TTD) to estimate the ventilation rate and the anthropogenic carbon burden of the different Arctic basins. They obtained similar age estimates as MacDonald & Carmack (1993) in the Canadian Basin and confirmed that the Eurasian Basin (200-300 years) is better ventilated, suggesting that the Lomonosov Ridge is an efficient barrier between the main deep basins of the Arctic. The mean age patterns obtained by Tanhua et al. (2009) are also consistent with the cyclonic dominance of the large scale Arctic circulation, showing younger waters richer in both CFC and anthropogenic carbon along the Siberian shelves than along the Canadian coast.

The deep and intermediate results of Tanhua et al. (2009) do show some patchiness in estimates for mean age, however, with isolated locations showing much lower ventilation ages than others. Such patterns are consistent with episodic and localized convective events. In support of this interpretation, Aagaard & Carmack (1994) noted that the temperature field is also particularly inhomogenous in the Canada Basin. These authors also establish, based on time-series measurements that the production of Arctic Bottom Waters on the shelves is very sporadic. Aagaard & Carmack (1994) also find ages of order 500 years. Their ultimate interpretation is quite a bit more dramatic, however, as they suggest that ventilation of the Canadian Basin stopped 500 years ago, which appears to be a time when sea ice cover became more important and the time when the whale hunting Thule culture of the region went extinct.

The geological sedimentary neodymium record at the North Pole, recovered on the Atlantic side of the Lomonosov Ridge at about 1250 m, indicates the the relative influence of AW and brine-enriched shelf waters on the intermediate waters of the Arctic have varied substantially over the past 15 million years (Haley et al., 2008). While the modern hydrographic situation relies heavily on the penetration of AW, the neodymium isotopic data suggest that the influence of the North Atlantic on the Arctic was reduced prior to 2 Myr. The production of brine-enriched shelf waters played a dominant role for the ventilation of AIW during that time. Oscillations of similar magnitude exist between the glacial and inter-glacial periods of the Quaternary, indicating increased brine production on the Siberian shelves and a reduced inflow of AW during glacial periods.

Aagaard et al. (1985) inferred the broad-scale patterns of ventilation in the Arctic Ocean by analyzing the evolution of temperature and salinity of the deep waters. They show that the deep waters of the Greenland Sea are the coldest (T<-1^{o}C) and freshest (S<34.90 psu) of all Arctic basins and that the temperatures and salinities of the deep Arctic Basins increase in the following order: GSDW, NSDW, EBDW, CBDW. Aagaard et al. (1985) conclude that shelf waters formed by brine rejection, formed at a relatively low rate, are the only source of new water to the bottom Canadian Basin. They further note that the bottom waters of the Canadian Basin have anomalously high salinities. While this could be a relict feature of an older time, as suggested by Aagaard & Carmack (1994), an alternative and probably more valid explanation is that the shelf waters mix intensely with Arctic Intermediate Waters as they sink to the deep Canadian Basin. This entrainment of warm and salty intermediate waters would explain the higher temperatures and salinities found below the sill depth of the Lomonosov Ridge. In the Eurasian Basin, on the other hand, the shelf water ventilation process is complemented by lateral exchange across the Fram Strait between the Greenland Sea and the Eurasian Basin. This inflow of fresh and cold Greenland Sea Deep Water explains the lower temperature and lower salinity of the Eurasian Basin relative to the Canadian Basin.

Aagaard & Carmack (1989) make the interesting observation that deep penetrative convection is only possible when the overlying surface water is fresher than the underlying water mass acting as a barrier between the surface and the deep when temperature is the dominant cause of densification (i.e. excluding the case of brine rejection and cabelling instability). This is a consequence of the non-linearity of the equation of state of seawater. If we assume that convective overturn is possible when the density of the surface water mass (1) is equal to that of the underlying water mass (2): $\sigma_\theta(1) = \sigma_\theta(2)$. Because the slope of deep isopycnals in the θ/S space is shallower than the slope of shallower isopycnals, when $\sigma_\theta(1) = \sigma_\theta(2)$ one also has the non-intuitive condition $\sigma_z(1) > \sigma_z(2)$, thus the surface water may penetrate through the underlying barrier without further cooling (Figure 6a). If the salinity of the overlying surface water is higher than the underlying water mass acting as a barrier, at the time when overturning is possible ($\sigma_\theta(1) = \sigma_\theta(2)$), the densities at depth prevent further sinking of the surface water mass without further buoyancy forcing: $\sigma_z(1) < \sigma_z(2)$ (Figure 6b). Since atmospheric cooling stops when the water par-

cel leaves the surface, further cooling is only possible to the depth of the mixed layer. The hydrographic situation in the polar Arctic and Antarctic regions is such that case I (fresher surface, saltier subsurface) prevails. In such situation, ventilation tends to be an "all or nothing" process owing to the thermobaric instability (Killworth, 1983; Marshall & Schott, 1999). Case II (saltier surface, fresher subsurface) corresponds to the situation encountered typically in the subtropical and perhaps subpolar regions, where the ventilation process is better described by "Stommel's demon" captured in the theory of "subduction" (Stommel, 1979; Luyten et al., 1983). The subduction process is described in more detail in the Mode Water section below.

Since the water exchanges in the Denmark Strait (leading to production of Denmark Strait Overflow Water, DSOW) and the Iceland-Scotland overflows are believed to be largely controlled hydraulically by the pressure difference across the sills (400-800 m depth) between the Irminger-Iceland Basins and the Greenland-Norwegian Basins (Whitehead, 1998; Kosters, 2004), and because the overflow and associated entrainment processes exert a strong control on the final properties and formation rates of the deep waters in the North Atlantic (Winton et al., 1998; Smethie & Fine, 2001; Yashayaev & Clarke, 2008; Haine et al., 2008), an accurate depiction of Arctic and GIN hydrography depends on and will generate better global simulations of the deep waters and of the overall water mass stack in the Atlantic (Fogelqvist et al., 2003; Born et al., 2009; Mahlstein & Knutti, 2011).

Given the resolution of global climate models and the hydrographic complexity of the Arctic, an accurate model depiction of the Arctic is a challenging target for coupled global circulation models. The hydrography of the Arctic depends on a plethora of peculiar oceanic features such as the inflow of warm and salty water from the North Atlantic Drift, Norwegian and Spitsbergen Currents, water mass transformation in the Barents Sea, Bering Strait freshwater inflow, sea-ice dynamics and sea-ice export into the North Atlantic, and on continental shelf processes (sinking of brine enriched waters, runoff). It is not surprising that existing evaluations of the CMIP3 model suite in the Arctic (Holland et al., 2007; Boé et al., 2009a; Holland et al., 2010; Mahlstein & Knutti, 2011) show dramatic differences amongst the models and with the observations with regards to mean surface ocean salinity distribution, sea-ice dynamics, precipitations patterns, radiative feedback and freshwater transport in and out of the basin.

3.1.2. The situation in the North Atlantic

Water mass overview. A schematic of the dominant circulation of the North Atlantic in shown in Figure 5 for reference. The North Atlantic water mass system (Smethie et al., 2000), including the GIN Seas (south of Fram Strait and excluding the Barents Sea) and the subpolar North Atlantic to 50°N, is shown in Figure 3b, where the overflow process from the GIN seas is shown by the magenta arrow connecting the GIN Seas with the warmer volumetric mode between 2-4°C. The East Greenland Current (EGC) and West Greenland Current (WGC) branches are also indicated by magenta lines in this figure. While the waters in the Denmark Strait Overflow are measurably fresher and colder than those in the Iceland-Scotland Overflow, which are slightly warmer and saltier owing to larger influence of waters from the Atlantic in the Norwegian Sea (Fogelqvist et al., 2003; Lherminier et al., 2007), this difference in the overflow characteristic is not easily recognizable in Figure 3b.

Waters spilling over the Denmark Strait Overflow (about 2 Sv, Ivanov et al. (2004)) gain volume through entrainment and feed much of the Deep Western Boundary Current (DWBC, 2-9 Sv, Bacon (1998)). Some water is able to sink to the bottom and maintain a relatively cold and fresh signature relative to the layer overlying it, which is characterized by a relative salinity maximum and is often called North East Atlantic Deep Water (NEADW, Yashayaev & Clarke (2008)). NEADW contains a mixture of warmer and saltier Iceland-Scotland Overflow Water (ISOW, also about 2 Sv), which has entrained a water mixture of North Atlantic origin composed of Subpolar Mode Water (SPMW) (McCartney & Talley, 1982; Brambilla & Talley, 2008; Brambilla et al., 2008), recirculating Labrador Sea Water (LSW) and perhaps some fraction of waters of subtropical origin, over the Iceland-Scotland overflow along its spreading path in the Iceland Basin. The modified ISOW meanders southward to cross the Reykjanes Ridge through the Charlie-Gibbs Fracture zone (Saunders, 1994, 2001; Whitehead, 1998) and propagates around the Irminger basin, mostly as a topographically constrained boundary flow, where it interacts with DSOW. This evolving mixture further circulates into the Labrador Basin where it is further modified by LSW, before being exported out of the subpolar region in the form of a southward DWBC flowing along the American coast (Pickart & Smethie, 1993; Yashayaev & Clarke, 2008). The intermediate/deep stratification in the North Atlantic is thus, from the bottom upwards, characterized by a cold layer of intermediate salinity, a slightly warmer salinity maximum layer, and a thick layer that constitutes varieties of LSW characterized by a salinity minimum in the subpolar region (Figure 3b). The formation characteristics and export of LSW varieties has been discussed extensively, see for instance Lazier (1973), Talley & McCartney (1982), Clarke & Gascard (1983), Gascard & Clarke (1983), Clarke & Coote (1988), Pickart (1992), Smethie et al. (2000), Smethie & Fine (2001), Pickart et al. (2002), Pickart et al. (2003b), Yashayaev et al. (2007) and Yashayaev (2007). LSW is a thick, relatively cold and fresh water mass, which, in essence, serves as the North Atlantic counterpart to AAIW in the Southern Ocean (Figure 3b,d) and constitutes the intermediate water of the North Atlantic. This water mass will be discussed in more detailed in a following section on low salinity intermediate waters.

Influence of the overflows. Because the overflows between the GIN Seas and the North Atlantic are mostly governed by the horizontal pressure gradients at the sill depth, overflow transports do not tend to experience large high-frequency seasonal or interannual variability (Dickson et al., 1990; Saunders, 1990; Mauritzen, 1996; Riemenschneider & Legg, 2007), even if the ventilation processes in the GIN Seas are highly seasonal or episodic and vary substantially from year to year (Dickson et al., 1996). This is partly a consequence of the relative unifor-

mity of the deep water column in the GIN Seas (Aagaard et al., 1985). This uniformity is due to both effective mixing when convective events occur, and residence times of order 20 years typical of the GIN Seas (Fogelqvist et al., 2003), a timescale which is consistent with the decadal variability that seems to typify the overflows (Bacon, 1998). Recent results from an SF_6 dye injection at intermediate depth in the central Greenland gyre also suggests that the transit time from this site, where deep convection occurs, to the overflows is about 2.5 years, at which time dilution of the initial patch is important and die concentrations at the overflow are small (Olsson et al., 2005; Messias et al., 2008).

On the other hand, chlorofluorocarbon (CFC) results of Smethie & Fine (2001) and Fogelqvist et al. (2003) show that waters located south of the Denmark Strait, near the sill depth, are younger than waters at equivalent depth north of the sill (i.e. mainly varieties of AIW). Note that AIW is not the densest waters in the GIN Seas. AIW is believed to contain a substantial amount of recirculating AW (Mauritzen, 1996). The particular composition and origin of the waters feeding the overflows from the GIN seas is not clear, with shallow convection north of Iceland being possibly important (Swift & Aagaard, 1980, 1981; Killworth, 1983; Swift, 1984; Fogelqvist et al., 2003; Karstensen et al., 2005; Messias et al., 2008; Kasajima & Johannessen, 2009). Nevertheless, this across sill contrast in CFC-derived apparent age suggests that variability of the pressure gradient across the overflow may in fact be influenced, aside from perturbations in the GIN Seas, by changes in the ventilation processes that modify hydrographic properties of the subpolar North Atlantic (LSW, SPMW), and allows for possible resonance effects between different modes of variability specific to the GIN seas and to the subtropical and subpolar North Atlantic. These water masses, especially LSW, experience substantial interannual variability (Yashayaev et al., 2007; Yashayaev, 2007; Yashayaev & Clarke, 2008; Haine et al., 2008) and appear to be vulnerable to a suite of episodic (Dickson et al., 1988; Belkin et al., 1998) and climatic perturbations (Dickson et al., 1996).

Theoretical considerations suggest that entrainment is inversely proportional to the density contrast between the sinking plume and the surrounding waters. Consequently, a denser LSW (i.e. colder or saltier) should result in a decreased density contrast with AIW, what would increase entrainment and the DWBC flux. Bacon (1998) briefly discusses the possible link between entrainment strength at the overflow and its downstream influence on the volume flux of the deep western boundary current (DWBC), and the density contrast between LSW and the average AIW properties flowing across the sill (Turner, 1986; Legg et al., 2006). The analysis of Bacon (1998) of 22 historical sections in the Irminger Sea does not seem to support the hypothesis presented at the beginning of this paragraph, however. Bacon (1998) attributes the main source of overflow variability to temperature perturbations in the GIN seas rather than to variations in LSW density. On the other hand, the results of Bacon (1998) also reveal that DWBC fluxes from years 1966 and 1967 do not follow the linear trend between GIN air temperature and DBWC volume flux, which is the core of the argument that is used to argue that conditions in the GIN seas to govern overflow variability. Overflow entrainment during these years appear to be controlled by different processes, possibly due to the extreme sea-ice conditions in the GIN seas at that time (Mysak et al., 1990; Bacon, 1998), suggesting perhaps a saturation of the air-sea flux control at this time on the GIN ventilation region and an increased influence of the subpolar North Atlantic LSW on the overflow process. This period also seems to coincide with anomalous heat trapping in the AW of the Arctic (Swift et al., 2005).

Ventilation of the North Atlantic. At the Grand Banks, NADW is estimated to be composed of 37% ISOW, itself composed of 15% entrained SPMW and 22% eastern overflow, 32% LSW and 31% DSOW (western overflow) (Swift, 1984). These estimates, however, do not take into account the AABW component highlighted by McCartney (1992), such that they are all upper limit estimates (Haine et al., 2008). Estimates of the volume flux at the sills for both the DSOW and ISOW are about 3 Sv and 2-2.7 Sv, respectively (Haine et al., 2008). These fluxes double subsequent to entrainment in the overflows, with the majority of the additional volume coming from the SPMW. Formation rates of LSW appear much more variable, however (Haine et al., 2008), ranging from 2 to 8.6 Sv. Recent estimates seem to suggest average values between 3-5 Sv after 1990. LSW formation is prone to large interannual variations (by almost one order of magnitude), as suggested from the different data-based estimates and GCM-based estimates. Data and model estimates of LSW formation do not converge, except in projecting an impression of low formation in the 1980s and higher formation in the 1990s (Haine et al., 2008). LSW is viewed as one of the most variable components of NADW and is sensitive to climate change (Stouffer & et al., 2006; Stouffer et al., 2006a). Although the high CFC plume associated with LSW can be traced to the equator and shows the importance of the DWBC for the export of this water mass (Weiss et al., 1985; Smethie et al., 2000), it is unclear how LSW formation variability influences the overturning circulation (Marotzke & Scott, 1999; Spall & Pickart, 2001) as much of LSW recirculates in the North Atlantic (Smethie et al., 2000). Analysis of historical data and modeling experiments show, however, that buoyancy loss in the Labrador Sea and the properties of the DWBC influences the path of the Gulf Stream, which in turn may affect climate over the North Atlantic (Dickson et al., 1996; Yeager & Jochum, 2009).

Processes affecting ventilation in the GIN Seas and in the North Atlantic are not purely local, however. Dickson et al. (1996) speaks of coordinated convective activity between the GIN Seas, STMW formation regions off North America, and LSW formation centers. These large-scale correlations are the consequence of one dominant mode of climate variability in the region known as the North Atlantic Oscillation (NAO). Analysis of historical data shows that storm activity in the GIN Seas and cold air bursts off the Atlantic North American coasts appear to be correlated, resulting in deep ventilation in the GIN Seas and increased production of STMW in the North Atlantic subtropical gyre. This situation also seems to be asso-

ciated with increased freshwater delivery to the Labrador Sea, which increases stratification and limits the convection depth in that basin, resulting in shallower LSW ventilation. Associated changes in the wind patterns may also result in less upwelling in the Labrador Sea subpolar gyre, limiting the density of newly formed LSW. The NAO index was high in the 1920s and in the 1990s, corresponding to increased weather intensity in the GIN Seas and a southwestward migration of the storm track over America and the Western North Atlantic. These periods are characterized by maximal convection in the Labrador Sea. On the other hand, the NAO index was particularly low in the 1880s and in the 1960s, when Labrador Sea convection appears to have been shallow. Downstream changes in LSW properties in agreement with NAO dominated variability in the Labrador Sea region have been detected downstream near Bermuda (Curry et al., 1998).

Connectivity between the ventilation processes in the GIN seas, the overflow characteristics and the subtropical and subpolar gyre was also suggested in Orvik & Niiler (2002), Hakkinen & Rhines (2004), Hatun et al. (2005), Hansen et al. (2004) and Hansen et al. (2008), among others, although from the alternative perspective of the warm/salty water northward flowing branch. The focus in these studies is on the return flow of AW into the GIN seas, investigating both the North Atlantic processes influencing the pathway and characteristics of the North Atlantic Drift at key passages and the evolution of the Norwegian Atlantic Current (NwAC). The dynamics of the subpolar gyre, particularly the shape of the subpolar gyre (see Figure 5), can impede the northward flow of subtropical waters in the GIN regions, and thereby influences the fractions of SPMW and STMW that develops into AW (Hakkinen & Rhines, 2009). Gyre dynamics in the North Atlantic seems to be strongly associated with the NAO, such that the return flow of AW is one component of the interconnected processes proposed by Dickson et al. (1996). The relative importance of the processes governing the variability of the overflow on different time scales and the dynamics of inter-gyre water mass exchange is not yet well understood with regards to their effects on the overturning circulation. Nonetheless, the hydrographic contrast between subpolar water masses, particularly LSW, and the hydrography of the GIN seas, particularly AIW, surely can be exploited into a potential diagnostic for model evaluation.

Synthesis. In summary, the water masses of the North Atlantic and the Arctic are quite well characterized in their mean state, but variability is large and poorly constrained. These regions are prone to large interannual variations, which can mask the signal expected from greenhouse-induced climate change. The North Atlantic is the best sampled ocean, but data in the Arctic are sparse. Much remains to be learned about the processes ventilating the deep Arctic, particularly the importance of episodic plumes sinking off the Siberian shelves and their interactions with the warm and salty intermediate layer of Atlantic origin. The current generation of global climate models is, to a large degree, incapable of simulating the hydrography in the Arctic. It is not clear if better simulations of the Arctic will result in substantially better representations of NADW characteristics, however, as global constraints exert also a strong influence on the heat and salt balance of the North Atlantic (Bryan, 1986; Saenko et al., 2004). It is clear, however, that better NADW simulations will benefit from more correct representations of the overflow densities and the entrainment process.

3.2. The water mass system of the Southern Ocean

3.2.1. Geographical setting

In contrast to the Northern Atlantic and the Arctic, whose exchange with the rest of the world is influenced or limited by overflows, the polar Southern Ocean (Figure 7) is not bounded by shallow sills on the equatorward side and communicates with all ocean basins through multiple deep passages (Whitehead, 1998). There is a dynamical barrier to ocean exchange, however: the Antarctic Circumpolar Current (ACC) system. Antarctica is bordered by four large basins separated by broad and relatively deep ridges and plateaus: the Weddell-Enderby, South Indian, Southwest Pacific and Southeast Pacific Basins. Continental shelves around Antarctica are typically narrow, except the Weddell and Ross Sea continental shelves, which reach 400 km in width and 400 m in depth.

3.2.2. Characterization of Antarctic Bottom Water

The consolidated product of the densest Southern Ocean water masses is often referred to as AABW (highlighted with grey ellipse on Figure 3e). AABW is recognizable as a temperature and salinity minimum layer near the bottom, with relatively high oxygen and other gas concentrations in the Southern Ocean (Foldvik & Gammelsrod, 1988). At lower latitudes, AABW distinguishes itself from NADW by being fresher and colder, but other nutrient-based (Broecker, 1974; Broecker et al., 1985b, 1998) and isotopic (Broecker et al., 1985a) tracers also show readily identifiable differences between the Northern and Southern source waters. Definitions of AABW vary extensively (see Table 3, Naveira-Garabato et al. (2002)) depending on the extent of the region considered. Frequently proposed operational AABW definitions in the Southern Ocean are waters colder than 0°C (Hellmer & Bersch, 1985; Whitworth & Orsi, 2006) or water denser than the lightest water not found in the Drake Passage ($\gamma_n > 28.27$ kg/m^3 Orsi et al. (1999, 2002); Orsi & Wiederwohl (2009)). The exact partitioning of the total production into particular source regions remains poorly constrained as overflows can be episodic, have been under-sampled (Jacobs, 2004; Gordon et al., 2009) and new sources of waters (most ventilate only to intermediate or deep depth, not to the bottom) are discovered over time as increasing fractions of the Antarctic coast are explored (Jacobs, 2004; Williams et al., 2010).

Total AABW production estimates suffer from the lack of coherence amongst AABW definitions, but holistic independent assessments of the total AABW production appear to asymptote nonetheless towards values of 15-20 Sv (Stommel & Arons, 1960b; Gill, 1973; Broecker et al., 1998; Orsi et al., 2002), roughly similar to estimates of NADW production and estimates of overturning in the North Atlantic (Broecker et al., 1985a; Smethie & Fine, 2001; Talley et al., 2003; Lumpkin &

Speer, 2007). As discussed by the CFC-based assessment of Orsi et al. (2002), the range (15 to 20 Sv) appears to depend on the treatment of entrainment of LCDW in the ACC (Orsi et al., 1999).

AABW, like NADW, is a mixture of water masses and not a true water mass in the sense that its source is not well-defined at the surface but depends on a variety of regional sources and ventilation processes. NADW and AABW are practical constructs that integrate complex mixing histories (Gebbie & Huybers, 2011) and ventilation processes. The average composition of these broadly and loosely defined summary water masses, however, form a useful framework that can be used to discuss global scale climate shifts over long periods because NADW and AABW properties integrate the general surface boundary conditions and internal dynamical ocean processes of the high latitudes. Particular components of AABW or NADW, however, may be more or less vulnerable to climate or regional perturbations and each component may respond with different magnitudes and different time scales, what may alter the overall AABW composition (Foldvik & Gammelsrod, 1988; Adkins et al., 2002). With regards to AABW and NADW representation in models, the average model biases in AABW or NADW cannot easily be linked to particular ventilation processes (Matsumoto et al., 2004). In this case, more detailed and regional analyses are often useful (Santoso & England, 2008; Kerr et al., 2009). The following paragraphs provide an overview of the water masses of the Southern Ocean relevant to the formation and export of AABW.

Overall, AABW consists of a mixture of LCDW (which is characteristically warm and salty in the Southern Ocean as it contains a large fraction of waters originating in the North Atlantic), varieties of near-freezing water masses of variable salinities found on the continental shelves around Antarctica and a permanent cold and fresh subsurface layer (Winter Water, WW; Carmack & Foster (1975); Gordon et al. (1984)) formed as a by-product of the mixed-layer and buoyancy seasonal cycles (Foster & Carmack, 1976; Hellmer & Bersch, 1985; Orsi et al., 2002; Jacobs, 2004). Since the properties of CDW are quite uniform relative to the other constituents, peculiarities in types of bottom waters mostly vary owing to the amounts and types of shelf waters injected in the different regions around the Antarctic continent. Spatial variability is affected mostly by local geographical features, such as the size and shape of the ice-shelf cavities (Foldvik & Gammelsrod, 1988; Grosfeld et al., 1997; Losch, 2008), topographic constraints (i.e. Berkner Island, Maud Rise, etc.; Bagriantsev et al. (1989); Gordon & Huber (1995); de Steur et al. (2007)), the width of the continental shelf and the depth of the shelf break, which limits or dictates the influence and properties of WDW that penetrates over the continental shelves (Orsi et al., 1993; Chavanne et al., 2010), and the presence or absence of icebergs at key locations. Climatic variability also plays a role on various time-scales (Foldvik et al., 1985; Comiso & Gordon, 1996; Robertson et al., 2002; Fahrbach et al., 2004; Gordon et al., 2007; Meredith et al., 2008; Gordon et al., 2010; Meredith et al., 2011), although natural variability along the Antarctic coast and its effect on ventilation processes remains poorly constrained by data.

3.2.3. Processes affecting the formation of AABW

The mixing processes and the properties of precursor water masses that form AABW (Orsi et al., 1999) are discussed, amongst others, in Gill (1973), Foster & Carmack (1976), Weiss et al. (1979), Jacobs et al. (1985), Foster et al. (1987), Foldvik & Gammelsrod (1988), Weepernig et al. (1996) and Jacobs (2004). Different formation mechanisms co-exist, more or less prominently, around Antarctica. Carmack & Killworth (1978) suggest that circum-Antarctic sinking of waters off the shelf break is likely, in agreement with a more recent study investigating the role of tidal mixing (Whitworth & Orsi, 2006) on the Ross Sea shelf as a driver of dense water formation, but that it is rare that sinking plumes reach the bottom. Sources of variable characteristics and magnitudes, dominated by different formation processes, that ventilate the deep and bottom layers have been reported at various locations around Antarctica. Gordon & Tchernia (1972), Rintoul (1998), Whitworth (2002) and Williams et al. (2010) report on the formation of species of Adélie Land Bottom Water (ALBW) at various locations off the Adélie Land associated with the Adélie and Mertz Depressions. Gordon (1974), Jacobs & Georgi (1977), Nunez Vaz & Lennon (1996), Wong et al. (1998a) and Yabuki et al. (2006) show evidence for bottom water formation from Prydz Bay (Prydz Bay Bottom Water, PBBW), located off the Amery Ice Shelf. Carmack & Killworth (1978) show interleaving signatures of freshly ventilated waters at mid-depths off Wilkes Land, and Carmack (1977) finds evidence of formation in the Davis Sea, just east of Prydz Bay.

As discussed in the following, owing to the various mixing mechanisms, particularly the tidal mixing (which is not affected by climate perturbations), and the role of Ice Shelf Waters (ISWs), perennial formation of forms of bottom or deep water is observed in the Southern Ocean (Gill, 1973; Gordon et al., 2009). The types of ventilation processes or mixing interactions, which are not mutually exclusive, are essentially mixing on the continental shelf between upwelled deep water and near-freezing ice-shelf products, mixing at the shelf break in association with the Antarctic Slope Front (ASF, Gill (1973); Jacobs (1991); Heywood et al. (2004); Ou (2007); Baines (2009); Chavanne et al. (2010)), and direct deep convection in association with polynyas on the shelves or in the open ocean.

Complex mixing patterns on continental shelves with ISW contributions describe the situation of the major bottom water production areas: the Weddell Sea, Prydz Bay, Adélie Land and the Ross Sea. Particular relationships between water masses indicative of the formation process of AABW are illustrated by black and dashed magenta (for shelf waters) line segments on Figure 3e. The deep water varieties characteristic of the Ross or Weddell Sea gyres (Ward Deep Water, WDW, (Gill, 1973)), where most of the bottom water production takes place, are slightly cooler and fresher version of LCDW owing to modification over time by shelf water plumes aided by its substantial recirculation and residence time in the Weddell and Ross gyres (Foldvik et al., 1985; Orsi et al., 1993; Gordon et al., 19934, 2004). WDW is injected onto the continental shelves (≈500 m

deep) bordering Antarctica (Foster et al., 1987), where this water interacts with WW at the ASF and cold and low salinity waters on the shelves (Low Salinity Shelf Water, LSSW), resulting in Modified Warm Deep Water (MWDW), a freshened and colder version of WDW. Injection of WDW onto the shelf and mixing at the shelf break has been shown to be strongly modulated by tides (Foster et al., 1987; Whitworth & Orsi, 2006), which translates into the overflow (mixing product) variability exhibiting a strong tidal signature (Whitworth & Orsi, 2006; Gordon et al., 2009). In fact, numerical modeling experiments suggest that tides of the right amplitude (not necessarily the strongest) and phase may enhance bottom water production by up to 70% (Wang et al., 2010).

Sea-ice production near the edge of ice-shelves and around polynyas enrich near-freezing surface waters with brine, resulting in the densest waters of the Southern Ocean (High Salinity Shelf Water, HSSW, Gill (1973)). HSSWs, owing to their densities either overflow off the shelf break (Gordon et al., 2009) or sit on the continental shelves and enter ice-shelf cavities, where their residence times is of order ≈5 years (Jacobs et al., 1985; Trumbore et al., 1991). The fate of these waters depends greatly on the local topography. Upon interaction at depth with the ice underneath the ice-shelf cavity, where pressure decreases the freezing point of seawater (Lewis & Perkin, 1986; Jacobs et al., 1979b; Foldvik et al., 2004; MacAyeal, 1984; Price et al., 2008), HSSW melts ice underneath the shelf cavity. This decreases its salinity and its temperature to temperatures that are below the freezing point at surface pressure. This supercooled water mass is known as ISW (Jacobs et al., 1979b). If of sufficient density (Fahrbach et al., 1994), ISW is then exported off the shelves via topographic channels, troughs and depressions to variable depths (Foldvik et al., 1985; Price et al., 2008; Gordon et al., 2009). Isotopic analyses (Weepernig et al., 1996) in the Weddell Sea reveal that a significant fraction of the WSDW (20%) is ventilated by ISW and HSSW, while the isotopic composition of WSBW suggests a relative dominance of HSSW. Complex plume dynamics, thermobaricity, the possibility of hydraulic jumps, the effect of rotation on the overflows, the tidal phase and the relative position of the ASF all influence the final resting depth of particular overflows (Killworth, 1977; Condie, 1995; Gordon et al., 2004; Foldvik et al., 2004). By similar ice-water interactions underneath the ice-shelves, MWDW that enters the ice-shelf cavity forms LSSW upon exiting.

There exists a spectrum of shelf waters, however, and the particular properties of HSSW, LSSW and ISW vary substantially between locations. HSSW and LSSW are, for historical reasons, named differently in the Weddell Sea near the Filchner ice shelf: WSW and ESW, respectively. However, due to the strong influence of regional topography on the shelves, the separation into East and West is relative and I do not recommend this nomenclature. These waters, as indicated by their isotopic signatures, appear to form in a similar fashion in the Ross and Weddell Sea and seem to have similar roles at both locations (Jacobs et al., 1985). While the importance of LSSW is not clear (it seems to contribute mostly to AASW, (Jacobs et al., 1979a) and to the transformation of WDW into MWDW), HSSW, as a precursor of ISW and as a direct bottom water contributor, appears to be a fundamental component for the ventilation of the Southern Ocean (Gordon et al., 2009). While HSSW and brine-enriched shelf waters in general contribute to the ventilation of the bottom waters, their net effects on the average salinity of the bottom waters is not large as the bulk of the salinity signature of the bottom water arises from the mixing between CDW and fresher near surface waters (WW, LSSW, AASW) (Toggweiler & Samuels, 1995).

The ASF is a dynamical barrier that separates the dense waters on the shelves from the waters of the open ocean (Chavanne et al., 2010). It is often described as a V-shaped feature on latitude-depth sections crossing the shelf break. The presence of that front is identifiable in most hydrographic properties located at the shelf break and it represents a quasi-circumpolar westward flowing current that reaches depths in excess of 1000 m (Jacobs et al., 1985). It is a region of lower sea ice cover in winter and a major route of iceberg transport (Jacobs et al., 1979a; Jacobs, 1991). Its width at the surface is of order half a degree or less (Jacobs et al., 1985), but its surface signature is weak and it mostly exists below 200 m (Baines, 2009). The V-shape indicates that isopycnals from both sides slope downward, which is atypical as most fronts only have one branch of the V (Baines, 2009). Its dynamics are not well understood (Ou, 2007; Baines, 2009). While the offshore branch of the V appears to be associated with a typical along-shore current, possibly generated by katabatic winds and Ekman flux (Baines, 2009) or the wind-induced ice motion that separates brine release regions (on shelves) from melt regions (offshore) (Ou, 2007), the onshore branch of the V is mostly likely due to the sinking of dense shelf water plumes. In fact, the V-shape is indicative of different dynamical regimes that interact at that location (Baines, 2009). Evidence that the two branches of the V are not necessarily linked is that the onshore branch is not visible everywhere the offshore branch exist (Baines, 2009). As such, the presence of the V-shape structure at the shelf break appears to necessitate denser overflows from shelves.

Models suggest that the front is an important component limiting the properties of AABW as it is a location where strong entrainment of WDW and, especially, surface WW and AASW occurs (Ou, 2007; Baines, 2009). It is also a region where warm/salty waters mix with fresh/cold waters, which is a necessary condition for cabbelling, a process believed to be important at the front (Jacobs, 2004). The overall entrainment of fresh and near-freezing waters from the surface, most likely in the form of WW (in the center of the V) is a critical control on the ultimate salinity of AABW.

The last process that is believed to ventilate the deep Southern Ocean is convection (Gordon, 1978). While not directly observed, convection has been inferred from tracers (Gordon, 1978; Foldvik et al., 1985). The process is associated with polynyas, in that upwelling of deep waters, which are warmer, supply heat to maintain sea-ice free condition above the convective region. Freezing at the surface cools the water and rejects brine, increasing the salinity of the surface water, which is fresher than WDW, to densities sufficient for overturning to occur (Martinson et al., 1981; Martinson, 1990). Upwelling of deep waters is also the main reason for the sharp and rapid de-

cline of the Antarctic sea-ice cover in spring (Gordon, 1981). In contrast, the halocline in the Arctic limits heat exchange from the warm/salty AW, allowing for sea-ice to persist longer in the year. Budget calculations show that only about 50% of the heat necessary to account for spring heating of the mixed layer is supplied from air-sea fluxes (Gordon, 1981), the rest must come from below.

One region with a quasi-permanent polynya is located in the Weddell gyre, West of Maud Rise. Cells of WDW, which appear to originate through interaction of the wind-driven gyre with the local topography, have been observed to propagate into the Weddell gyre (Gordon & Huber, 1984; Bagriantsev et al., 1989; Gordon & Huber, 1995; Holland, 2001; de Steur et al., 2007). These eddies inject heat and salt and contribute to the maintenance of a polynya in the region. These eddies also bend isopycnals upwards, closer to the surface mixed layer. Gordon & Huber (1984) suggests that the frequency with which such WDW cells may be injected can destabilize the pycnocline in the region and increase the frequency of convective events. The process also appears to be modulated by the wind regime in the Weddell gyre and is influenced by larger scale synoptic climate patterns, such as the Southern Annular Mode (Gordon et al., 2007).

Polynyas have been detected at multiple locations around Antarctica (Gordon & Comiso, 1988; Comiso & Gordon, 1996; Tamura et al., 2008; Comiso, 2010), but their overall contribution for the ventilation of the deep Southern Ocean is not yet clear. Jacobs (2004) estimates the contribution of the Weddell Polynya to be of order 1.6 to 3.2 Sv. The importance of convection in the Southern Ocean appears to be small (Jacobs, 2004) relative to its role in the GIN Seas, where it is the dominant ventilation process (Carsey & Roach, 1994). With the continental shelves covered with grounded ice-sheets during the Last Glacial maximum (Mackintosh & et al., 2011), it is likely that polynyas may have been the dominant ventilation pathway of the Southern Ocean Deep Waters at that time (Smith et al., 2010).

One interesting point with regards to the convective process is that a mixture of WDW and WW forms MWDW (Figure 3e) and not bottom waters. Clearly, brine rejection is necessary for the density of the mixture to be sufficiently high. Early theories of Southern Ocean ventilation proposed the concept of critical salinity (S_{crit}) (Mosby, 1934; Kelley, 1994); that is the salinity necessary for near surface waters close to the freezing point (WW) to exceed the density of the waters below them (WDW). Based on the Southern Ocean conditions, a value of S_{crit}=34.6 was suggested (Mosby, 1934), obtained by projecting the WDW-WSBW mixing line to the freezing point (indicated by an annotated magenta segment on Figure 3e). This value of S_{crit} apparently separates LSSW and HSSW, suggesting that shelf waters saltier than S_{crit} sink, while waters fresher than S_{crit} are too light and contribute to LSSW and eventually AASW. Using conditions of the Weddell Polynya, Martinson et al. (1981) proposed a convective model for polynyas, incorporating the time remaining in the cooling season, or the time available for brine production, setting a limit on how much salt can be released. This implies a low-salinity limit, beyond which the water is too fresh to ever become dense enough before sea-ice melts resets the stratification. These waters will invariably escape the Southern Ocean as AASW and their probable next chance for subduction will be associated with the formation of AAIW (Figure 3d). The salinity limits suggested by Martinson et al. (1981) range between about 34.52 and 34.36. These values are shown on Figure 3e and seem to bracket the interaction region between WW and MWDW rather well.

3.2.4. Export of AABW

Equatorward export out of the Southern Ocean is affected by the presence of a circumpolar topographic barrier and the presence of a dynamical barrier (the Antarctic Circumpolar Current). Export of bottom water out of the Southern Ocean occurs via deep western boundary currents along ridges (Stommel & Arons, 1960a). Eight deep passages (deeper than 3500m) located between 50° and 60°S account for most of the export (Orsi, 2010). Most of the equatorward export is in the form of Antarctic Circumpolar current bottom water (ACCbw) (Orsi, 2010), a relatively warmer and saltier mixture than primary AABW beyond the ACC. The transport accounted for by each passage out of the Southern Ocean does not necessarily appear to be a function of the distance from the formation site or formation rate at the closest site. The purity of the AABW exported is a function of the mixing imposed on this water mass as it crosses the ACC, however. For instance, Whitworth et al. (1991) measured a net export out of the Weddell Sea into the Argentine Basin along the eastern flank of the Ewing Bank, west of the Georgia Bank, of about 1.9 Sv (waters colder than 0.2°C, 8.2 Sv northwestward minus 6.3 Sv of southeastward recriculation). Fukamachi et al. (2010), on the other hand, report on a strong net (8 Sv) northwestward transport of AABW (waters colder than 0°C, 16.4 Sv northwestward minus 8.4 Sv of southeastward recriculation) in a narrow boundary current on the eastern flank of Kerguelen Plateau. The Weddell Sea is believed to account for about 60% of the total 8.1 Sv of AABW formed in the Southern Ocean (Orsi et al., 1999). The topographic and dynamical barriers, mixing and water mass transformation in the Southern Ocean acts as a major control on the properties of AABW that is exported.

Little is known about the variability of the deep western boundary currents in the Southern Ocean. Fukamachi et al. (2010) report a standard deviation for their Kerguelen measurements of 5.6 Sv with a mean cross-array transport of 12.3 Sv based on two years of mooring data. Whitworth et al. (1991) find that, for the deep western boundary current only, the transport has a mean of 2.5 Sv and a standard deviation of 2.2 Sv. Whitworth et al. (1991) argue that most of the observed transport variability off Ewing Bank may not be due so much to the variability of the AABW component flowing north but to the meandering of the ACC (time-scale of 2-3 months), which is responsible for most of the recirculation, and the presence of eddies (1-2 weeks). Given the geographical and dynamical setting at the Kerguelen site and the dominance of the 3 months and the 2 weeks time-scales visible in the record, one would be tempted to conclude that ACC meandering and eddies also

dominates the variability at Kerguelen.

3.2.5. Variability

The relationship between the dominant climate modes of the Southern Ocean, and the formation process of AABW and its components are also not well characterized. Notable climate modes that have been shown to influence conditions, particularly sea ice, sea-surface temperature and pCO_2, in the Southern Ocean include El-Niño Southern Oscillation (ENSO), the Antarctic Dipole (AD) and the Southern Annular Mode (SAM). Studies on the effects of dominant climate modes on the property of the ocean interior is critically impaired by a lack of data in the Southern Ocean and have relied mostly on reanalysis products, models or limited temperature time-series measurements from few moorings (Yuan & Martinson, 2000, 2001; Lovenduski & Gruber, 2005; Lovenduski et al., 2007; Stammerjohn et al., 2008; Screen et al., 2010; McKee et al., 2011). The analysis of the vulnerability to climate variability of the different water masses and of the bottom water end-product in the Southern Ocean seems to be a topic of great interest for the coming years. Existing studies converge towards a prominent role of the winds, which affect the area covered by sea ice, sea ice export, as well as the strength and shape of the Weddell and Ross gyres, whose broad eastern return flows supply heat and salt to the polar coasts (Assmann & Timmermann, 2005).

3.2.6. Synthesis

The properties of the main water masses and the general stratification are well known in the Southern Ocean. Contrary to the situation in the Northern Atlantic, the Southern Ocean water masses tend to be very homogenous. The influence of CDW in the bottom water formation process makes the Southern Ocean rather insensitive to regional perturbations. This homogeneity, or lack of contrast between water masses, makes it difficult to identify patterns of variability on short temporal or spatial scales. The homogenous nature is due to strong mixing. While this makes monitoring the mean conditions of the Southern Ocean easy, this also strongly dilutes most signals or perturbations associated with the precursors of AABW, making it difficult to characterize variability in the region. Analysis of specific tracers and radiogenic isotopic fingerprinting methods, however, provide additional constraints that can be used to differentiate deep and bottom waters of similar temperatures and salinities but formed in different sectors around Antarctica and provide additional benchmarks against which to test models (Shodlock et al., 2001; van de Flierdt et al., 2004, 2006; Rodehacke et al., 2007b,a).

The volume of the Southern Ocean and the ocean volume that is ventilated from the Southern Ocean are large relative to the global ocean volume. For this reason, small biases or property anomalies in the Southern Ocean, even if barely detectable because of their lack of contrast with respect to the background conditions, translate usually into large biases or signals with regards to integrated quantities. One example is given by the measured changes in freshwater and heat storage (Helm et al., 2010). These and similar signals are locally small but have a major impact on global climate and on global nutrient budgets. Simulation of the hydrography of the Southern Ocean water masses by global coupled models appear reasonable with respect to the main water mass structure shown on the global volumetric θ/S diagram. At least, the agreement is better in the Southern Hemisphere than in the Northern Atlantic. This is not to say, however, that models resolve the water mass formation processes accurately in the South.

Less scatter exists between the models' representation of the thermohaline conditions in the South because bottom water is mostly a mixture of NADW with a fresher and colder end-member. As long as a model has both of these elements, for any reason, a model can produce bottom water of reasonably good temperature and salinity values. The volumetric θ/S distribution shows, however, that differences exist between the influence of NADW south of 30°S. When calculated only for the southernmost latitudes, the volumetric θ/S distribution of the models indicate substantial discrepancies with observations. These model biases suggest errors in the models' water mass formation processes of the precursor water masses constituting the colder and fresher end-member necessary to form bottom water.

3.3. The contrasting roles of Arctic rivers, Antarctic ice shelves and sea-ice dynamics

The mechanisms supplying freshwater to the polar Southern Ocean are quite different than those supplying freshwater to the Arctic. There are no large rivers in Antarctica and 45% of the Antarctic coast is bordered by vertical ice walls (200-300 m tall) reflecting the edges of ice-shelves. The largest ice shelves are the Filchner-Ronne ice-shelf in the Weddell Sea, the Ross ice-shelf in the Ross Sea and the Amery ice shelf in Prydz Bay (Figure 7). Smaller ice shelves include the Larsen C, east of the Antarctic Peninsula, the Riiser-Larsen and the Fimbul ice shelves along the Enderby coast in the eastern Weddell Sea, the West and the Shakelton ice shelves east of Prydz Bay along the Adelie Land, and the George VI and the Wilkins ice shelves bordering the Belinghausen sea, west of the Antarctic Peninsula. It is estimated that glacial meltwater contributes 0.06-0.07 Sv to the non-atmospheric freshwater input to the polar Southern Ocean (Carmack, 1990). In contrast, there are few ice-shelves (near the Ellesmere Islands, Northern Canada) in the Arctic owing to the lack of large glaciers there (Figure 4). Ice shelves exist around Greenland, however, shedding icebergs into the East Greenland Current and into the Labrador Sea. These icebergs tend to travel southward and their influence on the Arctic Sea is that they are exporters of freshwater and not a freshwater source. Their decay, nonetheless, has some impact on the salinity of the East Greenland Current and influences convection in the Labrador Sea downstream.

3.3.1. The role of rivers

Major rivers enter the Arctic Sea. Most of these rivers are located along the Siberian coast. The largest Arctic rivers are the Yenisei (0.019 Sv), the Ob (0.017 Sv), the Lena (0.016 Sv), the Mackenzie (0.011 Sv), the Pechora (0.004 Sv), the Severnay Dvina (0.0035 Sv), the Kotuy (0.0033 Sv), the

Kolyma (0.0032 Sv), the Pyasina (0.0027 Sv) and the Indigirka (0.0018 Sv). These rivers transport an estimated 0.105 Sv of freshwater from the continents (Carmack et al., 2008). This is an estimated 8.9% of the world's river runoff, 60% of the long-term average discharge of the Amazon (Dai et al., 2009) but only 0.67% of global atmospheric precipitations (Dai & Trenberth, 2002). The peak discharge for Arctic rivers occurs in June and results from spring snowmelt. Integrated precipitation in the Arctic drainage peaks in July (Dai & Trenberth, 2002). Interannual variability in Arctic river discharge is estimated to be about 5-20% of the mean annual flow, but seasonal variability can be up to 40-fold for the Yenisei and the Lena river. This is smaller, about 5-fold, for the Mackenzie (Carmack, 1990). Bryzgalo & Ivanov (2000) estimate that up to 90% of the total annual runoff occurs between June and September. Additional freshwater input arises from the seasonal sea ice meltwater, 0.079 Sv of freshwater entering from the Bering Strait and 0.067 Sv of net oceanic precipitation (Serreze et al., 2006). These numbers are calculated relative to a reference Arctic salinity of 34.8. The actual mass flux through the Bering strait is an order of magnitude larger 0.8±0.2 Sv (Melling et al., 2008), but the salinity difference between inflowing Pacific water and mean Arctic water is relatively small. The largest fraction of the freshwater is stored in the Beaufort gyre in the Canadian Basin (Melling et al., 2008; Peterson et al., 2006; McPhee et al., 2009).

The Arctic, through its role as a gatekeeper for freshwater, can alter the meridional overturning circulation by shutting off deep water production sites in the Northern Hemisphere. There is in fact as much freshwater stored in the Arctic as there is in all the lakes and rivers worldwide (assuming a reference salinity of 34.8 psu). The reservoir is about 10-15 times greater than the annual freshwater flux out of the Arctic (Carmack et al., 2008). The bulk of this storage is concentrated in the Canadian Basin and is the consequence of the Ekman-convergent anticyclonic Beaufort gyre, the only anticyclonic gyre of the Arctic Mediterranean Seas. The Beaufort gyre is also where sea ice is thickest (Belchansky et al., 2008). The Transpolar Drift (TSD) is a baroclinic front which separates the fresh polar waters in the Canadian Basin from the more saline surface water of the Eurasian Basin. Variability in the wind patterns, the buoyancy forcing, river runoffs or the Pacific-Atlantic trans-Arctic flow, which is believed to be driven by the higher sea level of the Pacific, itself the steric consequence of the relative freshness of the North Pacific compared to the North Atlantic (Melling et al., 2008), may influence the degree of leakage through this fragile front. Carmack et al. (2008) estimates that a leakage of 5% of the freshwater contained in the Canadian Basin is equivalent to one Great Salinity Anomaly (Dickson et al., 1988). This is sufficient to drastically decrease the convective activity in the Labrador and Greenland Sea.

Yamamoto-Kawai et al. (2009) recently reported on a surface freshening trend in the Arctic. Such a freshening trend would be expected given a strengthening of the global hydrological cycle, as implied by global warming (Holland et al., 2007). Using a combination of tracers, δ^{18}O and alkalinity, they were able to separate the sea-ice meltwater from the runoff component. They conclude that while sea-ice meltwater is the dominant component, runoff can account for about 30-50% of the trend in certain locations. Furthermore, they point out that there exists a link between river runoff and sea-ice melt. Since river runoff is warmer than the ocean, river runoff melts sea ice, further reducing surface salinity. The presence of rivers over the Siberian shelves explains partly why these shelves are able to remain free of sea-ice in summer (Figure 8). Incidentally, this is also where sea-ice growth is fastest in winter, such that cold brine-enriched surface polar water is able to form there and accumulate on the continental shelves. These brine-enriched waters are then able to ventilate the upper halocline, and perhaps the bottom occasionally, of the Arctic Mediterranean Seas (Carmack, 1990).

Another important role for Arctic rivers is that they contribute large nutrient fluxes, which tend to be rich in nitrate relative to phosphate. Most Arctic shelves are net weakly denitrifying systems (Nitishinsky et al., 2007). The riverine nutrient flux, together with the role of rivers in maintaining ice-free ocean regions also act to concentrate the primary production of the Arctic on the continental shelves (Anderson & Jones, 1991). Together with the limiting role of sea ice in air-sea gas exchange and other controls such as the wind forcing, river runoff ultimately impacts the metabolic state of the Arctic ecosystem with regards to carbon. While some Russian Seas are net autotrophic (i.e. Laptev Sea), others seem to be weakly net heterotrophic (East-Siberian Sea) (Nitishinsky et al., 2007). Overall, however, the Arctic is a net sink of carbon dioxide taking up an estimated 0.066-0.199 PgC/yr (Bates & Mathis, 2009). Based on expected responses of the Arctic to global warming, Bates & Mathis (2009) suggest that increased sea ice melt and river runoff will contribute a decrease in the saturation state of calcium carbonate. This effect may be partially mitigated by an expected increased primary production at the surface but remineralization at depth is expected to further decrease the saturation state in the subsurface, resulting in a total water column acidification.

3.3.2. Sea ice and ice shelves

While one of the main defining features of the Arctic is its riverine flux, the corresponding unique feature of the Antarctic region may be the presence of ice shelves and the role of these ice shelves in modifying seawater properties and its density. Since river discharge of freshwater is small in the polar Southern Ocean, the inherent seasonal variability of the freshwater flux is much less there. Seasonal variability in the Southern Ocean is dominated by sea-ice dynamics. Secondly, to maintain a steady state, the ice accumulation occurring on the Antarctic continent has to ultimately be evacuated to the ocean. Jacobs et al. (1979a) estimate an annual ice accumulation rate of 0.15 m/yr over an area of $14{\cdot}10^6$ km^2, corresponding to a equivalent freshwater flux of 0.067 Sv. This is roughly two thirds of the river flux entering the Arctic. The importance of the ice-melt in the Southern Ocean is then not so much in its mass, but rather in the mechanisms through which it is delivered. Jacobs et al. (1979a) argues that about 25% of that mass is evacuated in the form of basal melting under ice shelves and 75% as other processes, mostly icebergs calving and subsequent offshore melt-

ing.

Both the Arctic and the Southern Ocean are β-oceans (Carmack, 2007), stratified by a halocline. Yet, the mechanism by which freshwater is injected into each ocean and the contrasting magnitude of these fluxes suggests that the role and importance of the freshwater cap for limiting basin ventilation and the processes maintaining the halocline are different in each ocean. Unlike river runoff, which is constrained to the surface, the ice-water transformation involves not only a phase transition but melting can and does happen at depth underneath floating ice shelves tens to hundreds of meters deep. The thermodynamics of the former implies that this phase transition not only freshens the water but also cools it. In concert with the latter, which is important given that the freezing point of seawater (T_f) is depressed by pressure ($\frac{\partial T_f}{\partial p} \approx 0.00753°C/bar$), these two features are able to fuel the self-starting ice pump described by Lewis & Perkin (1986). These relatively fresher and colder seawater streams have noticeable signatures on hydrographic sections and contribute to the particular δ^{18}O isotopic signature of Antarctic Bottom Waters (Weiss et al., 1979; Jacobs et al., 1985; Toggweiler & Samuels, 1995; Price et al., 2008).

To put the buoyancy forcing of sea-ice formation into perspective, Aagaard & Carmack (1989) calculated that the distillation effect due to sea-ice formation is equivalent to that experienced by highly evaporative basins such as the Red Sea (2 m/yr). In the Arctic, the quasi-complete winter sea-ice cover insulates this salty lens from atmospheric cooling. In the Arctic, sea-ice tends to grow outward from the ice-edge such that the necessary conditions of brine rejection and atmospheric cooling are almost exclusively met over the deep ocean at the ice edge as the sea-ice expands. In contrast, sea-ice tends to form near the Antarctic coast and then be exported outwards, such that the equatorward ice-edge in the Southern Ocean does not necessarily represent the location of sea-ice formation and brine rejection and does not play a direct role in the ventilation process of the deep Southern Ocean. Moreover, mixing will dilute the brine layer equatorward there.

The different behavior of sea ice in the two polar oceans (Gow & Tucker, 1990) influences bottom water ventilation in the two regions. In the Arctic (Figure 8), the average sea-ice thickness is about 3 meters and represents a stable equilibrium of the seasonal melt/freeze cycle (Belchansky et al., 2008). In the Southern Ocean, sea-ice is thinner (0.5-2 meters). It is thinner in the Southern Ocean because it is mostly first-year ice everywhere. The thick Arctic sea ice is possible because it is largely an enclosed basin and because it is strongly salinity stratified, a necessary condition for sea-ice formation in the deep ocean (Aagaard & Carmack, 1989). This stratification limits the influence of vertical heat exchange on sea-ice melting.

Owing to strong katabatic winds and the fact that the Southern Ocean is not constrained by land equatorward, the melt and freeze cycle is spatially largely decoupled in the South, resulting in a distillation effect similar to the decoupling between regions of net evaporation and net precipitation. While sea-ice formation rates are strong near the Antarctic coast along leads and polynyas, melting tends to occur in the open ocean near the equatorward ice-edge (Figure 8). Sea-ice is exported offshore and does not tend to build up from year to year. The wind, current and wave shear at the ice edge as well as upwelling of heat, the thinness of the ice pack and the dominant frazil ice composition of the Antarctic sea-ice sheet further results in a higher likelihood of it breaking up (Gow & Tucker, 1990). This results in a large numbers of gaps or other openings all the way to the coastal sea-ice regions around Antarctica (Carmack, 1990).

The fresh surface layer of both polar oceans is characteristic for these regions and limits ventilation. The characteristics of the haloclines in the models differ widely, which affects the models' ability to produce deep and bottom waters. While poor halocline representations by models in the Arctic mostly affect the hydrography of that basin, the bottom waters formed in the Southern Ocean directly ventilate the world's ocean. As such, errors in the Southern Ocean representations of the halocline in the models is potentially more hurtful to climate simulations. The Arctic halocline is a large freshwater reservoir, however, and even if it may not be critical for models to capture Arctic hydrography very accurately, freshwater export out of the Arctic exerts an important control on North Atlantic convection.

4. Intermediate waters

Intermediate waters are typically found between 500 and 1500 m. They separate deep waters from the saltier and warmer central waters associated with the wind driven gyre circulation. There exist two types of intermediate waters: low salinity waters, such as Antarctic Intermediate Water (AAIW), Labrador Sea Water (LSW), North Pacific Intermediate Water (NPIW), and high salinity waters, such as Mediterranean Sea Overflow Water (MSOW), Red Sea Overflow Water (RSOW), Persian Gulf Overflow Water (PGOW), which tend to settle on density levels competing with the low salinity type. Low salinity intermediate waters form at subpolar latitudes, under the storm tracks in all basins, and transport freshwater equatorward. This freshwater comes from both excess precipitation over evaporation, and also from the flux of low salinity waters, driven by Ekman transport, as is the case for Antarctic Surface Water (AASW) in the Southern Hemisphere, or by other currents, such as the East Greenland and Baffin Island Currents out of the Arctic in the North Atlantic. High salinity waters, on the other hand, form from the outflows from evaporation basins characterized by estuarine circulations at low latitudes.

4.1. Low salinity intermediate waters

4.1.1. North Pacific

Overview. The North Pacific is the freshest of all basins (Figure 3), and North Pacific Intermediate Water is the freshest of all intermediate waters. The characteristic feature of NPIW is the salinity minimum of the subtropical North Pacific, which is closely associated with a density between 26.7-26.9 σ_θ (300-700 m) (Sverdrup et al., 1942; Talley, 1993). While the salinity of the subpolar North Pacific is also low, no salinity minimum exist in the subpolar North Pacific to the extent that it exists in

the subtropics. Salinity is low in the subpolar region, but it increases monotonically with depth in the subpolar North Pacific. The salinity minimum of the NPIW does not form a pycnostad, unlike LSW, arguing against convective mechanisms or subduction for its formation (Talley, 1993).

The challenge with NPIW is in explaining its main ventilation pathway. Climatologies show that isopycnals denser than σ_θ=26.8, characteristic of the subtropical salinity minimum in the subtropics, do not outcrop in the open North Pacific (Reid, 1965, 1969). Direct ventilation of the salinity minimum isopycnals from the surface is consequently not possible and other mechanisms maintain the salinity minimum. It is best to think of NPIW as a water mass system, of which the salinity minimum is only one component, composed of multiple layers that can be differentiated based on their dominant ventilation mechanisms (Talley & Yun, 2001; Shcherbina et al., 2003).

Isoneutral distribution of tracer properties. Global maps of various hydrographic properties are shown on Figure 9. Isoneutral γ_n = 26.8 is characteristic of the subtropical salinity minimum in the North Pacific. The isoneutral maps were calculated from the annual mean WOA05 climatology and the gridded GLODAP data product (Key et al., 2004). Properties shown are include physical tracers (the depth of the isoneutral, S, θ), biogeochemical tracers (O_2, NO_3, PO_4, Si), the anthropogenic tracer pCFC-11 (the partial pressure of CFC-11) and other quasi-conservative preformed nutrient tracers indicative of water mass origins (NO, Broecker (1974)), biogeochemical processes ($Si^\star$, Sarmiento et al. (2004a); $N*$, Gruber & Sarmiento (1997)) and a tracer indicative of the natural carbon disequilibrium (ΔC_{gasex}, Gruber & Sarmiento (2002)).

The topographic gradient of the γ_n = 26.8 surface shows clearly the location of the boundary between the subpolar and the subtropical region in the North Pacific (Figure 9a). The subpolar-subtropical boundary marks the location of the North Pacific Current, which includes the Kuroshio Extension in the West.

It is clear from panel 9d that the minimum salinity on this isoneutral is found in the Northeast, in the Oyashio region. Also, the salinity gradient between the subpolar and the subarctic region is not as clear as that suggested by panel 9a. The distribution of salinity on γ_n = 26.8 provides an impression of the main circulation of the NPIW salinity minimum layer underneath the subtropical gyre and particularly emphasizes the cross-gyre exchange on the eastern side of the North Pacific, south of the Alaskan gyre (You et al., 2003; Masujima & Yasuda, 2009). Other tracers, however, particularly O_2, $pCFC11$, NO, and $N^\star$ (Figure 9b, c, f), show local extrema in the North Pacific that are visibly associated with the Okhostk Sea (Yoshikawa et al., 2006) and the convergence region between the Kuroshio and the Oyashio (i.e. the Mixed Water Region (MWR) a hydrographically complex region at the confluence of the Oyashio and the Kuroshio and bounded to the East by the Tsungaru Current outflowing from the Sea of Japan). Figure 9j and k show the importance of the North Pacific for silicate cycling and for the low latitude export of this nutrient.

Figure 9l maps ΔC_{gasex}, a quantity that corresponds to the salinity normalized dissolved inorganic concentration, corrected for the effect of biological remineralization, calcium carbonate dissolution and the intrusion of anthropogenic carbon (Mikaloff-Fletcher et al., 2007). ΔC_{gasex} is a quasi-conservative tracer that captures the effect of air-sea fluxes across the surface on the natural carbon distribution and is a coarse measure of disequilibrium of the water with respect to pCO_2 at the time of water mass formation. Since the definition involves an arbitrary constants (here Alk_{ref}=2320 μmol/kg, DIC_{ref}=1986 μmol/kg, $PO_{4,ref}$=0.4 μmol/kg are used), only gradients in ΔC_{gasex} are meaningful. Where ΔC_{gasex} gradients go from low values to high values along a streamline in the mixed layer, this means that there is potential for the water to take up carbon by air-sea exchange. Generally, more positive ΔC_{gasex} values indicate waters closer to air-sea pre-industrial equilibrium, while smaller or more negative values indicate a greater degree of disequilibrium.

While ΔC_{gasex} is prone to many uncertainties (Mikaloff-Fletcher et al., 2007), it is interesting to note the differences between the distribution of oxygen (panel 9b) and ΔC_{gasex} (panel 9l), particularly in the Nortwestern subpolar Pacific, where a region with high oxygen is associated with a region of low ΔC_{gasex}. Better agreement between the two tracers exists southward of the Okhostk Sea outflow, however. This is likely a consequence of the fact that equilibration time-scales are shorter for oxygen than for carbon. This feature highlights the important role of the Okhostk Sea as a region of carbon uptake and export to the subsurface North Pacific.

Formation and ventilation. The upper-most layer (26.6≤ σ_θ ≤26.8) of the intermediate waters in the North Pacific can be ventilated directly from the surface in winter. Outcrops with densities approaching, but less than, 26.8 are found in the Gulf of Alaska (Van Scoy et al., 1991; Ueno & Yasuda, 2000; You et al., 2000, 2003), the Oyashio (Talley et al., 1995; Qiu, 1995) and the Southern Okhostk Sea (Talley, 1991; Yasuda, 1997). Ventilation in the Gulf of Alaska to these high densities is relatively rare, however, and is associated with episodic storm activity in the region (Van Scoy et al., 1991). The tritium budget for these isopycnals (Van Scoy et al., 1991) provides additional evidence in favor of this ventilation mechanism. The distribution of salinity on these lighter isopycnals also shows that a ventilation pathway to the interior of the gyre exists on the eastern side of the basin, from the Gulf of Alaska (You et al., 2003).

The bulk of ventilation is thought to occur in the Northwestern Pacific. Outcrop densities in the Oyashio, however, tend to be limited to the 26.6-26.7 isopycnals (Talley et al., 1995). This means that direct surface ventilation in the Western North Pacific is incapable, by itself, of accounting for the salinity minimum on a density of 26.8. Cabbelling along the Kuroshio Extension Front subsequent to mixing with northward Kuroshio water in the MWR has been invoked to explain the remaining density increase necessary to match the density of the salinity minimum (Talley & Yun, 2001; Yun & Talley, 2003). Yun & Talley (2003) estimate the cabbeling flux may be up to 2.3 Sv. This is a substantial fraction of the 3 Sv estimated to represent the net subpolar to the subtropical transport of new NPIW (Tal-

ley et al., 1995; Talley, 1997).

Cabbeling may not fully explain the low potential vorticity, high oxygen and high anthropogenic carbon content of NPIW, however (Talley, 1991; Ono et al., 2007). Denser waters (Okhostk Dense Shelf Waters, ODSW) are formed by brine rejection around the Sea of Okhostk, although mostly in the northern polynya (Gladyshev et al., 2003; Shcherbina et al., 2004a,b). These dense waters contribute to the formation of Okhostk Sea Mode Water (OSMW), which occupies the intermediate layers of the Okhostk Sea. OSMW outflows into the Oyashio, contributing to a fresh, cold, oxygen-rich, low potential vorticity subsurface layer (Yasuda, 1997; Wong et al., 1998b; Yasuda et al., 2002) to the Oyashio. This water is then exported southward along the western boundary, where it is further transformed in the MWR. The densest layers of NPIW (to σ_θ=27.6) are mostly formed by tidal mixing of OSMW, DSW and Pacific Deep Water along the straits linking the Okhostk Sea and the North Pacific. The deepest and largest of these Strait is the Bussol' Strait (2200 m sill depth) (Katsumata et al., 2004; Ono et al., 2007; Ohshima et al., 2010).

The role of NPIW in climate is not clear and is difficult to evaluate as models do not, in general, capture NPIW formation and export processes very well. NPIW has mostly three roles. First, as is suggested from Figure 9l, it captures a small fraction of the global uptake of anthropogenic carbon. Ono et al. (2003) estimate that new NPIW formed in the MWR captures about 35% (0.045 PgC/yr) of the anthropogenic carbon of the temperate North Pacific. Yasuda et al. (2002) estimate the the Okhostk Sea water component alone takes up 0.025 PgC/yr. Second, NPIW participates in the return of freshwater from the Pacific to the Indian through the Indonesian Throughflow via the Mindanao Current and the Makassar Strait (Gordon & Fine, 1996; Vranes et al., 2002; You et al., 2005; Talley & Sprintall, 2005). The silicate distribution on Figure 9j illustrates the connection between the North Pacific and the Indian. Finally, NPIW contributes to the export of silicic acid and nutrients from the subarctic North Pacific to low latitudes (Figure 9j, k), and thus contributes to fueling low-latitude primary productivity (Sarmiento et al., 2004a; Yoshikawa et al., 2006). Its high gas content (Figure 9b) also re-oxygenates the North Pacific thermocline (Yasuda et al., 2002).

Variability. Little is known about the variability of NPIW. One can hypothesize that the isopycnals of the MWR, the Oyashio and the Gulf of Alaska that are directly ventilated by winter surface processes are influenced by large-scale climate patterns, such as ENSO and PDO, as both affect the storm tracks. Large changes were observed by Joyce & Dunworth-Baker (2003) in the MWR that are correlated with the PDO. How this variability translates into production rate and properties of the salinity minimum in the subtropics is unclear, although Auad et al (2003), using a coarse model, investigated the effect of the 1976-1977 climate regime shift of the North Pacific on NPIW and found that NPIW perturbations influenced the properties of the California Current. These changes may help interpret variability observed on sediment cores recovered at intermediate depth from Santa Barabara Basin (Hendy & Kennett, 2003). Seasonality has also been shown to influence the formation of OSMW and the fluxes in and out of the Okhostsk Sea (Gladyshev et al., 2003; Ohshima et al., 2010). Finally, as mixing at the Kuril straits is mostly driven by tides, one would expect a tidal modulation of the mixing process there on a variety of timescales, including millennial, and so a downstream effect on the properties of NPIW. Much remains to be done with regards to modeling and understanding the variability of NPIW.

4.1.2. North Atlantic

Overview. The low salinity intermediate water of the North Atlantic is LSW (Figure 3b). Similarly to NPIW, it is also formed in the northwestern corner of the basin. LSW is the saltiest of all low-salinity intermediate waters. It is broadly characterized by a local mid-depth salinity minimum in the subpolar region, but it is best defined as a stratification (potential vorticity, PV) minimum (Talley & McCartney, 1982). Typical salinities of the vorticity minimum are 34.83-34.86 psu and typical potential temperatures are 2.8-3.2°C. Neutral densities of order 27.90-28.0 bracket the vorticity minimum (Faure & Speer, 2005). The salinity and temperature of LSW vary substantially in time such that the LSW nomenclature has evolved to include the year of production, the vintage (see for example Yashayaev (2007) and Yashayaev & Loder (2009)). When cast in the broader context of subpolar water masses and circulation, LSW can be thought of as the final product of a chain of transformation processes that occur around the subpolar gyre and collectively contribute to the formation of SPMW (McCartney & Talley, 1982; Brambilla & Talley, 2008). Below LSW in the Labrador Sea are NEADW and DSOW. The presence of the relatively warm and salty NEADW acts like a barrier that limits deep convection to depths of about 2500 m.

Isoneutral distribution of tracer properties. Global maps showing the distribution of various properties and tracers on the 27.95 isoneutral are shown in Figure 11. The depth of the 27.95 isoneutral in the North Atlantic shows the shallowest depth of this density layer to be in the Southern Labrador Sea and in the Irminger Sea (Figure 11a). The 27.95 isoneutral reaches a depth of around 2000 m in the subpolar region, but south of the Gulf Stream, the 27.95 level stabilizes around 1700 m in the Atlantic. The 27.95 isoneutral is deeper (2300 m) in the other basins, except the Southern Ocean. A map of the thickness of the water column contained between the 27.9 and 28 isoneutral surfaces highlights the presence of LSW, its extent and its southward export along the DWBC (Figure 13n). The thickness for the shallower layer (Figure 13m, 27.8$\leq \gamma_n \leq$27.9) also shows the thick layer in the Labrador Sea and the subpolar North Atlantic, but does not show the DWBC tongue south of the Gulf Stream separation.

Contrary to other intermediate waters (NPIW, AAIW), whose salinity minimum can be used to trace these waters far from their sources, the salinity minimum of LSW is typically only visible in the subpolar region of the North Atlantic (Talley & McCartney, 1982). Further south, mixing with salty Mediterranean water erodes the salinity minimum. Vertical profiles there show that salinity decreases monotonically from

the high surface salinities characteristic of the North Atlantic to the salinity typical of NADW or show a salinity maximum at intermediate depth (Figure 11d). Isopycnal mixing of LSW and MSOW contributes to the formation of UNADW (Talley & McCartney, 1982), which stands out by its high salinity in the Southern Ocean. Since MSOW is warm and salty, the distribution of temperature (Figure 11g) on γ_n=27.95 mimics mostly the distribution of salinity on this surface. While MSOW is clearly visible in salinity or temperature, the influence of MSOW cannot be easily detected using nutrient characteristics as these are similar to the background Atlantic conditions (Figure 11b, e, h, j, k; also see Kawase & Sarmiento (1985), Kawase & Sarmiento (1986) and Clarke & Coote (1988)).

Unlike NPIW, however (Figure 9), LSW has low nutrient concentrations. The characteristically low nutrient content of LSW is evident in panels 11e and h. The North Atlantic has the lowest silicate concentrations and lowest $Si^\star$ values (Figure 11j). The Atlantic has a characteristically higher $N^\star$ signature (on all density levels) than the Pacific. This is a reflection that nitrogen fixation exceeds nitrogen loss in the Atlantic, while the reverse is true in the Pacific (Gruber & Sarmiento, 1997). Nitrogen fixation having a large demand for iron, this interpretation is also consistent with the fact that atmospheric iron depositions are higher in the Atlantic (Karl et al., 2002). The importance of atmospheric iron to fuel primary production is being reassessed, however. Latest model results and measurement campaigns suggest that subsurface fluxes may be dominant (Tagliabue & Arrigo, 2006; Tagliabue et al., 2010). NO is low in the Atlantic (Figure 11f), with a minimum associated with MSOW. This MSOW NO minimum can be observed between $27.3 \leq \gamma_n \leq 28.1$. A weak maximum in $N^\star$ can be seen in the subtropical North Atlantic on γ_n=27.95, but this signal is likely to be the result of upper ocean circulation features (NAC, Azores Front, see Figure 5).

LSW contains large amounts of atmospheric gases, such as oxygen, tritium, CFC and anthropogenic carbon (Clarke & Coote, 1988; Rhein et al., 2002; Steinfeldt et al., 2009). These gases have been used to trace the spreading of LSW. Figure 11b, c and l show the expected maxima in the Labrador Sea for oxygen, pCFC-11 and ΔC_{gasex}. Note that oxygen and ΔC_{gasex} maxima need not be collocated: ΔC_{gasex} is corrected for remineralization and calcium carbonate dissolution, not oxygen. In the North Pacific for instance, ΔC_{gasex} is high in spite of oxygen being a minimum. In that case, the high ΔC_{gasex} values are evidence of the deep reaching influence of NPIW in the North Pacific. Since the distribution of chlorofluorocarbons is not affected by biology, CFCs have been used extensively to trace the fate of LSW in the North Atlantic, and particularly the export pathways of the freshly ventilated waters to the interior of the basin and to the Southern Hemisphere (Weiss et al., 1985; Smethie, 1993; Smethie et al., 2000; Smethie & Fine, 2001; Rhein et al., 2002; Kieke et al., 2006). The spreading of LSW is described in more details below.

The different types of Labrador Sea Water. Two types of LSW have been identified in the Northwestern Atlantic, ULSW and CLSW. The potential density intervals $27.68 \leq \sigma_\theta \leq 27.74$ and $27.74 \leq \sigma_\theta \leq 27.8$ have been used to define these two classes. Analyzing the temporal variation of the thickness of these intervals, Kieke et al. (2006) and Rhein et al. (2011) observed a strong anti-correlation between the thicknesses of these two types of intermediate waters. Yashayaev (2007) pointed out, however, that regional and temporal variability in the intensity of formation and characteristics of these water masses, in addition to the presence of other water masses such as Irminger Sea Water (IrSW) in the Labrador Sea, make these hard definitions rather imprecise in the Labrador Sea. Yashayaev (2007) warn that these fixed density definitions may be too broad such that the combined LSW product (CLSW+LSW), as defined by Kieke et al. (2006), does not reflect the known LSW variability described by volumetric surveys in the θ/S space.

CFC and oxygen concentrations are higher in DSOW and ULSW than in CLSW (Pickart, 1992; Smethie et al., 2000). During convection, CLSW mixes extensively with waters (NEADW, IrSW) that recirculate at mid-depth in the North Atlantic, which are older and lower in oxygen. High oxygen and CFC content in the DSOW of the Irminger Sea and the DWBC are consistent with source waters of the overflow that are well ventilated, indicative of shallow convection north of Iceland. The motivation to treat ULSW as a separate entity from CLSW is based on CFC and tritium measurements south of the Grand Banks (Clarke & Coote, 1988; Pickart, 1992; Pickart et al., 1996). South of the Grand Banks, ULSW is well represented by a CFC and a tritium maximum, indicating that this layer is better equilibrated with the atmosphere than CLSW, arguing for a separate formation mechanism for ULSW.

The nature of ULSW is unclear and debate exist with regards to the role of the Irminger Sea as a source of freshly ventilated intermediate water and whether or not it constitutes one component of ULSW that can be exported in the DWBC (Stramma et al., 2004). Part of the formation of ULSW is associated with eddies in the southern sector of the Labrador Sea (Pickart et al., 1996). Interaction of the cold/fresh Labrador Current with warmer/saltier water stemming from the North Atlantic Current results in mixtures that are lighter and better equilibrated than CLSW, being formed in part from a well-equilibrated subtropical component from the NAC. The influence and mixing of varieties of LSW with SPMW is highlighted with magenta arrows on Figure 3b, were small volumetric ridges are seen to connect SPMW with LSW.

A second component of ULSW may form in the Irminger Sea. On one hand, models show that deep mixed layers likely form in the Irminger Sea, a consequence of a low-level atmospheric jet that forms seasonally in the lee of Cape Farewell at the southern tip of Greenland (Doyle & Shapiro, 1999; Pickart et al., 2003b,a; Spall & Pickart, 2003; Moore & Renfrew, 2005). The Greenland tip jet induces a localized seasonal recirculation cell east of the tip of Greenland, in the Irminger Sea, which can be observed. This recirculation, as well as other recirculation cells in the northwestern Labrador Sea and in the southern Labrador Sea region (Lavender et al., 2000), represented in cartoon form on Figure 5a as dashed magenta circular arrows in the Northwestern Atlantic, prolong the residence time of the water in these cells and provides a means for the water

to experience the necessary heat loss for convective mixing to occur. Model simulations show this phenomenon can generate mixed layers as deep as 1600-1700 m in the Irminger Sea (Pickart et al., 2003a; Vage et al., 2008a), sufficiently deep to explain the low potential vorticity patch that can be observed between 600 and 1000 m in the region (Vage et al., 2008a).

This mechanism of ULSW formation is not unanimously accepted, however. In his original study on the characteristics and origin of ULSW in the DWBC, Pickart (1992) argued against the Irminger Sea as the source of ULSW. Pickart (1992) argued that for convectively formed intermediate water from the Irminger Sea to reach the DWBC, this water mass would have to be unmodified by deep convection in the Labrador Sea. Furthermore, for waters formed in the Irminger Sea to be the source of the CFC/tritium maximum defining ULSW in the DWBC, this water would have had to be in contact with the atmosphere more recently than ULSW formed in the southern Labrador Sea (i.e. be younger) and remain isolated from waters with lower CFC concentrations along its export pathway. Pickart (1992) judged both conditions improbable.

A second argument that minimizes the role of the Irminger USLW source revolves around transit times between the Labrador Sea and the Irminger Sea. Sy et al. (1997) obtained surprisingly fast connection times (of order half a year) between the Labrador Sea and the Irminger Sea. This stimulated Pickart et al. (2003b) to conjecture a local source in the Irminger Sea to explain the presence of an interior low vorticity patch that can be observed in the Irminger Sea. These fast transit times imply the presence of unrealistically swift currents between the two seas. Yashayaev et al. (2007) analyzed the propagation of LSW vintages throughout the subpolar region and found Labrador to Irminger Seas transit times of order 1-4 years for the shallower layers and 2-5 years for the deeper layers, longer than the ones proposed by Sy et al. (1997). Based on these slower transit times, Yashayaev & Loder (2009) questioned the necessity of a local origin for the Irminger subsurface low vorticity layer, pointing out that in the case of slower transports, the low vorticity in the interior of the Irminger Sea is not inconsistent with an advected signal from the Labrador Sea. While this is also consistent with the results of Vage et al. (2008a), who only observed mixed layer depths to 300-400 m in the Irminger Sea between 2003-2004, an earlier analysis by Centurioni & Gould (2004), using data from autonomous profiling floats collected between 1994 and 2003, revealed that deep mixed layers exceeding 800 dbar occasionally occur in the Irminger Sea.

Stramma et al. (2004) and Vage et al. (2011) proposed that the location of ULSW formation and the dominant ULSW formation process is likely to change in time, including both an Irminger Sea component and a southwestern component. At times when deep convection exists in the Labrador Sea (CLSW formation), the Irminger source is largely erased in the Labrador Sea and the dominant source is likely in the southern Labrador Sea, as originally proposed by Pickart (1992) and Pickart et al. (1996). When CLSW formation is weak, seasonally formed ULSW from the Irminger Sea is able to travel through the Labrador Sea and contribute to ULSW beyond the Labrador Sea.

Weakly convective periods also tend to show sharper horizontal density gradients between the rim currents of the Labrador Sea (West Greenland Current, Labrador Current, see Figure 5) and the interior of the Labrador Sea. Stramma et al. (2004) propose that these stronger density gradients act as a barrier to mixing, contributing to the conservation of the Irminger Sea component. Since baroclinic eddies form as part of the convection process (Gascard & Clarke, 1983; Lilly et al., 2003) and have been shown to be important for the formation of southern-type ULSW (Pickart et al., 1996; Stramma et al., 2004; Cuny et al., 2005b), quiescent conditions in the Labrador Sea imply weaker formation of southwestern-type ULSW and a dominance of the Irminger type.

Formation of Classical Labrador Sea Water. Production of CLSW in the interior Labrador Sea is episodic (Lazier, 1973; Lazier et al., 2002; Yashayaev, 2007; Yashayaev et al., 2008). Convective activity translates into variable temperature and salinity characteristics of the CLSW vintages. Intense convection results in fresh and cold CLSW vintages, while less intense events produce warmer and saltier versions (Yashayaev, 2007). Analysis of data available in the Labrador Sea from the 1960s (Yashayaev, 2007) indicate that CLSW formation was shallow and weak between the 1960s and the mid 1970s, between 1995 and 1999, and from 2001 to 2006. Convection was deepest between 1987 and 1994. Mixed layers reached 2400 m in 1993-1994, producing the coldest and freshest CLSW ever observed (Yashayaev, 2007). This extreme case was due to a succession of intense winters, each winter contributing to a weakening of the general stratification, allowing the subsequent winter to reach deeper, a process known as preconditioning (Lazier et al., 2002). Abrupt cooling episodes occurred also in 1971-1972 (Lazier, 1980), 1999-2000 and 2007-2008. The 1999-2000 event generated mixed layers that reached a depth of 1300 m. The 2007-2008 event reached depths of 1800 m (Vage et al., 2008b; Yashayaev & Loder, 2009). Pickart et al. (2002) report on winter convection during 1996-1997 and find mixed layers that reach depths of 1500 m. The interior product from that event, however, seems to have remained trapped in the Western Labrador Sea and was not exported to the subpolar region.

On interannual time scales, periods of intense mixing are modulated by the phasing of the North Atlantic Oscillation (Yashayaev, 2007). High NAO indices correspond to a stronger pressure difference between Iceland and the Azores (Hurrell, 1995). This translates into increased storminess in the subpolar region (Hurrell et al., 2006) and enhanced buoyancy forcing (cold air outbreaks from the American continent) in the subpolar North Atlantic (Myers & Donnelly, 2008). These conditions are favorable for the year-to-year weakening of the stratification and progressively deeper penetration of convection. Year-to-year variability in the surface buoyancy flux of the Labrador Sea region is not exclusively tied to the NAO, however (Sathiyamoorthy & Moore, 2002). For example, Vage et al. (2008b) and Yashayaev & Loder (2009) have recently observed deep convection to 1800 m and 1000 m (the deepest convective event since 1994) in the Labrador and Irminger Sea. This

convective event was not preceded by a series of harsh winters with associated increasing mixed layer in the traditional sense of inter-annual preconditioning.

The NAO index was low for the period 2001-2005, and was high in 2006 and 2008, yet convection was only observed in the second 2007-2008 winter. Vage et al. (2008b) suggest that deep convection arose in 2007-2008 from the interplay of different conditions of the climate system that were not present in 2006-2007 rather than from the year-to-year weakening of the mean stratification, as was the case for the 1987-1994 sequence. Air temperature was colder globally in 2007-2008, especially over North America, possibly due to a strong La Niña (Vage et al., 2008b; Yashayaev & Loder, 2009). The ice cover was also more developed in the Labrador Sea, allowing cold air to reach further into the Labrador Sea without ocean-induced warming (see Figure 8 for a typical impression of sea-ice cover in the Labrador Sea). The anomalously large ice-cover may have been the result of increased ice-export out of the Arctic. Arctic sea ice was especially low in the winter 2007-2008. Storm paths in the region also appear to have been very coherent in 2007-2008, many of them passing through the same region of the Labrador Sea. The storm paths were more erratic the previous winter. The 2006-2007 winter was also characterized by a reverse Greenland tip jet, wind anomalies blowing from the East into the Labrador Sea, rather than from the West into the Irminger Sea. While this atypical Greenland jet was not conducive to cold air outbursts, it may have contributed to the salinification of the Labrador Sea interior by promoting the import of saltier Irminger water (Yashayaev & Loder, 2009). The weaker winds North of Flemish Cap may also have influenced the path of the NAC meander characteristic in that region, allowing for a northward excursion of the NAC meander northwest of Flemish Cap, further contributing to the anomalously high salinity of the Labrador Sea. Conditions in the 2007-2008 winter were favorable for deep mixing as the Labrador Sea was anomalously salty and the air was generally cold.

While the concept of preconditioning in the Labrador Sea is often interpreted as that cumulative year-to-year weakening of the stratification made possible by long period and large-scale interannual climate conditions, other types of seasonal and local preconditioning, i.e. conditions favoring the development of deep mixed layers, also contribute to the formation of ULSW and CLSW (Clarke & Gascard, 1983; Straneo & Kawase, 1999). Local LSW preconditioning is associated with eddies, boundary current properties, and seasonal wind-induced recirculation cells. These processes act either to prolong the exposure of the water parcels to the surface buoyancy forcing, move isopycnals upwards closer to the surface, or change the thermohaline properties of the waters through inflow of salinity or removal of heat.

The formation of deep mixed layer is aided by the presence of cyclonic (counter-clockwise in the Northern Hemisphere) circulation cells in the Irminger and Labrador Sea (marked by magenta dashed arrows in Figure 5a). These recirculations cause the isopycnals to bend upwards at their center, bringing them closer to the mixed layer. The water inside the eddies is also trapped there and is thus exposed to concentrated surface cooling for longer periods. These eddies also play a critical role in bringing boundary current properties and IrSW towards the interior of the Labrador Sea (Khatiwala et al., 2002; Lilly & Rhines, 2002; Lilly et al., 2003). An eddy-induced overturning cells also develops in the Labrador Sea that contributes downwelling in the center of the Labrador Sea, convergent flows at the surface and divergent flows towards the boundaries at depth (Khatiwala & Visbeck, 2000).

Eddies not only play a role in the convective phase, but also in the restratification phase. In fact, solar heating in Spring and Summer only affects a thin upper layer that cannot account for the deep restratification that occurs after a deep convective event (Straneo, 2006). Restratification in the Labrador Sea after convection is mainly the result of lateral exchange with the boundary current waters, which are warmer than freshly convected waters in the interior. The restratification phase is thus characterized by a drift of the CLSW towards to the properties of the boundary current (Straneo, 2006). There exist two time-scales for restratification. The short time-scale is associated with the eddies that form as baroclinic instabilities in association with the convective chimney (Gascard & Clarke, 1983; Marshall & Schott, 1999). The longer time-scale corresponds to the inter-annual restratification process that occurs during successive non-convective years and to the slow continuous diffusion of heat.

Convection thus represents a balance between the heat lost at the surface due to cooling, and the heat gained in the ocean interior by convergence (Lazier et al., 2002). If lateral heat fluxes from the boundaries of the Labrador Sea to the interior dominate the surface heat loss or heat export out of the Labrador Sea, convection is not possible. Because the lateral eddy heat input is an ocean process that measures the integrated effect of eddies, it responds more slowly to perturbation. Variability of the formation of CLSW is thus more quickly responsive to atmospheric variability (Lazier et al., 2002).

The influence of freshwater near the surface. Because the surface layer of the Labrador Sea is so fresh, aside from a strong cooling, convection is stimulated by the presence of a salty water mass in the Labrador Sea (Clarke & Gascard, 1983). Some salt is provided to the Labrador Sea by the inflow of IrSW from the East. IrSW is not ULSW, it is best understood as a dense form of SPMW that forms in the Irminger Sea. IrSW is also the principal source of heat to the Labrador Sea. It is injected from the Irminger Sea below the West Greenland Current between 200 to 500 m above the continental slope. Salt is also injected at the southeastern corner of the Labrador Sea, from meanders of the NAC. Processes affecting the import of salt, or conversely the import of freshwater in the Labrador Sea, can greatly affect the convective activity in the Labrador Sea (Dickson et al., 1988; Belkin et al., 1998).

The freshwater that enters the Labrador Sea through ocean currents is ultimately from the Arctic, a region that is also the ultimate source of the Great Salinity Anomalies (Dickson et al., 1988; Hakkinen, 1993; Belkin et al., 1998), in agreement with isotopic data (Khatiwala et al., 1999). This does not mean that the flux of Arctic-origin water into the Labrador Sea controls

salinity variability of the Labrador Sea on all time-scales, however. For example, the seasonal salinity cycle in the Labrador Sea is predominantly governed by sea ice meltwater of Baffin Bay origin (Khatiwala et al., 2002). The seasonal sea-ice cycle and the sea-ice freshwater reservoir of the Hudson Bay is large but the volume flow to the Labrador Sea interior is small (Khatiwala et al., 2002). Freshwater outflow from the Hudson Bay (about 0.08 Sv, 34.8 psu equivalent) contributes about 50% to the freshwater transport of the Labrador Current, however (Straneo & Saucier, 2008). Most of the Hudson Bay outflow is in summer. A significant fraction of this water may be water of Baffin Bay origin that has recirculated through the Hudson Bay (Straneo & Saucier, 2008). Precipitation at most accounts for one third of the seasonal salinity cycle in the Labrador Sea interior (Lazier, 1980; Khatiwala et al., 2002).

Freshwater from the Arctic follows two routes to the Labrador Sea (Figure 5) for a combined freshwater transport of 0.3 Sv (Cuny et al., 2005a), relative to a salinity of 34.8. Arctic outflow is either from the Fram Strait (0.2 Sv) and into the East Greenland Current or through the Canadian Archipelago via the Lancaster and Jones Sounds and Nares Strait, the Baffin Bay (maximum depth 2400 m) and via the Davis Strait (sill depth 640 m, 0.1 Sv, Figure 5a). The importance of each route may vary in time (Belkin et al., 1998). Since both routes enter the Labrador Sea at different locations, their effects on Labrador Sea convection differ. Eddy-permitting simulations by Myers (2005) suggest that freshwater perturbations entering the Labrador Sea by the Davis Strait route do not tend to influence CLSW very much. The model of Myers (2005) indicates that the salinity of the Labrador Sea is mostly controlled by the Fram Strait route, in agreement with the observational estimate of Schmidt & Send (2007). Freshwater perturbations from the Fram Strait route influence IrSW, which is a necessary component of convection. Freshwater perturbations from the Davis Strait route are mostly constrained to the Labrador Current (Cuny et al., 2005a) and only interact weakly with the interior of the Labrador Basin. This also agrees with the $\delta^{18}O$ results of Khatiwala et al. (1999), who found that downstream of the Labrador Sea, southeast of Nova Scotia, the origin the freshwater there is most consistent with the Baffin Bay (Davis Strait route).

Export of Labrador Sea Water. Ventilated LSW is exported out of the Labrador Sea via three routes, represented by the darker blue arrows on Figure 5 (Talley & McCartney, 1982; Schmitz & McCartney, 1993; Faure & Speer, 2005): southward along the DWBC, eastward after entrainment with the NAC and across the Charlie-Gibbs Fracture Zone (Paillet et al., 1998), and northward into the Irminger Sea via the Irminger Current (Yashayaev et al., 2007). While the DWBC route (Figure 5) has been well documented from tracers (mainly CFC) (Weiss et al., 1985; Molinari et al., 1992, 1998; Smethie et al., 2000; Smethie & Fine, 2001; Kieke et al., 2009), the mechanisms that control the exchange between the Labrador Sea region and the DWBC in the subtropical region are not well understood (Lozier, 2010). The Gulf Stream acts as a potential vorticity barrier (Bower et al., 1985; Pickart & Smethie, 1993) that impairs cross-frontal exchange. The subpolar to subtropical exchange is influenced by the density of the water and hence the depth at which the exchange takes place, the eddy field, and local topography. As a general rule, the less dense and shallower layers do not cross over to the subtropics but tend to be re-entrained by the Gulf Stream and the NAC back into the subpolar gyre (Pickart & Smethie, 1993). Tracers fields are homogenous across the Gulf Stream on the deeper layers (i.e. mostly composed of the DSOW and ISOW), however, indicating *a priori* that water crosses the subpolar-subtropical boundary relatively unimpeded at depths (Pickart & Smethie, 1993).

While the CFC distribution in the North Atlantic emphasizes the DWBC tongue south of about 36°N (i.e. the separation latitude of the Gulf Stream at Cape Hateras), high CFC values can be found across the Atlantic north of the separation latitude (Weiss et al., 1985; Molinari et al., 1992; Pickart, 1992; Smethie, 1993; Rhein et al., 1995; Smethie et al., 2000) (Figure 11c). The importance of the interior spreading pathway for LSW (i.e. not associated with the DWBC, but driven by eddies) in the region to the North of the separation latitude but south of the Labrador Sea exit is in accord with the latest findings regarding the role of the recirculation cells (Figure 5, RG, Mann eddy) that are found in association with the Gulf Stream or topographic features, such as Orphan Knoll (Kieke et al., 2009), the Flemish Cap (Lavender et al., 2000) and the Grand Banks (Lozier, 1999; Lavender et al., 2000; Bower et al., 2009; Lozier, 2010; Bower et al., 2011). The dominance of the interior pathway for the southward export of LSW may be surprising at first but, in fact, the recirculation cells help explain the apparent aging and sharp dilution of the intermediate layers in the subtropical region. The mixing and entrainment process between freshly ventilated CLSW and ambient deep water of the ocean interior that is inherent to the recirculation cells contributes to the formation of the CFC minimum layer (between 2000 and 2500 m) that is systematically observed along the DWBC south of the Grand Banks. This minimum is particularly marked south of 36°N, and is located just below the CLSW core (Smethie, 1993; Smethie et al., 2000). The DSOW that constitutes the deep CFC maximum layer of the DWBC is believed to be affected less by the recirculations as these cells weaken with depth and because the DSOW may be more tightly steered by topography (Bower et al., 2011).

The role of Labrador Sea Water in the meridional overturning circulation and climate. Formation rates estimates for either ULSW, CLSW or the combined product, based on tracer or buoyancy budgets, vary greatly, between values of 1-10 Sv. While some of the variability between these estimates reflects temporal variability (Rhein et al., 2002; Myers & Donnelly, 2008), much of it reflects methodological differences (Pickart & Spall, 2007). Since some of these estimates assume all of the freshly ventilated LSW is exported from the Labrador Sea every year, the higher formation estimates are likely overestimates. Based on these published estimates (Rhein et al., 2002; Pickart & Spall, 2007; Myers & Donnelly, 2008), the long-term average is likely between 2-4 Sv. Cunningham et al. (2007) estimate the strength of the overturning at 26.5°N at 18.7±5.6 Sv.

Given that the dilution factor of LSW suggested by the CFC concentrations between the Labrador Sea and 26.5°N is about 10 (Smethie et al., 2000), this would indicate that LSW at most contributes 0.1-1 Sv (less than 5%) to the overturning at 26.5°N. This is consistent with the idea that most of LSW recirculates in the subpolar region (Straneo, 2006; Pickart & Spall, 2007) and with the results of Zhang (2010), who showed that high latitude overturning anomalies propagate at the advective speed to Gulf Stream separation latitude only. South of this latitude, propagation is achieved by Kelvin waves.

While convection is an efficient means of ventilating the deep ocean and removing heat from the surface water, the convection process is not an efficient means by which mass can be transferred to the deep ocean (Marshall & Schott, 1999). As such, convectively formed LSW does not contribute greatly to the mass transport at depth (Marotzke & Scott, 1999; Pickart & Spall, 2007). Significant mass transport can occur in association with convection, but only when convection occurs near steep topography (Spall & Pickart, 2001). Spall & Pickart (2001) and Boening et al. (1996) estimate that the net mass transport associated with LSW formation is about 1 Sv, a small fraction of the Atlantic overturning. LSW does not transfer large amounts of mass to depth but LSW formation provides a gate for tracers to penetrate the deep ocean and a mechanism to release heat to the atmosphere. This gate is particularly important for the capture of greenhouse gases, particularly anthropogenic carbon (Sabine et al., 2004; Steinfeldt et al., 2009).

It is likely that the convective activity of the Labrador Sea is more a diagnostic of climate change than a proximal cause for large climate shifts. As shown by Curry et al. (1998), and in a different context by Dickson et al. (1988), Labrador Sea convection responds to changes in atmospheric and oceanic conditions quite readily. It is not clear, however, if stoppage of LSW formation would greatly affect climate other than regionally. Assuming a formation rate of LSW between 1 and 10 Sv, and a temperature change between the surface and CLSW of about 2 °C, the heat removed by LSW formation is probably at most 0.1 PW, which corresponds to 10% of the northward heat transport of the upper ocean at 24°N (about 1PW, Hall & Bryden (1982)). Paleo-reconstruction of the intermediate water conditions during the last inter-glacial seem to indicate that LSW was not being formed at that time (Hillaire-Marcel et al., 2001). Yet, climate was only 2°C warmer, suggesting that LSW is relatively unimportant as a global driver of climate change.

LSW may influence the North Atlantic indirectly, however. LSW properties, which are modulated by convection, also affect the vertical distribution of density and horizontal density and horizontal pressure gradients (Curry et al., 1998). As such, LSW affects partially the dynamics of the DWBC and the northern recirculation gyre (Figure 5, NRG). It has been shown (Zhang & Vallis, 2007) that the properties of the DBWC affects the separation latitude of the Gulf Stream and indirectly the path of the NAC, what influences the northward heat transport to the North Atlantic (Yeager & Jochum, 2009). While the relevant DWBC properties for this process may be more those of DSOW, the partitioning between LSW and DSOW as to their effects on DWBC properties and Gulf Stream separation has not yet been assessed.

4.1.3. Southern Hemisphere

Overview. The salinity minimum extending equatorward from the Subantarctic Front (SAF) at depths between 500 to 1000 m characterizes AAIW, the intermediate water of the Southern Ocean. The presence of the salinity minimum has been known since the end of the 19^{th} century and the extent of that feature in the Atlantic was described in the 1930s (Deacon, 1933; Wüst, 1935; Deacon, 1937). Debate still exists regarding its formation mechanisms, its formation rates, and most importantly its role in the global overturning, however. While the salinity minimum is a sharp feature that is easily identifiable in oceanic sections, the salinity minimum does not follow a single isoneutral surface, both zonally and meridionally. At various locations around the Southern Ocean, AAIW properties are affected by basin-wide gyre recirculation, cross-frontal mixing, nonlinear mixing, topographic barriers and inter-basin exchange. Similarly to NPIW or LSW, AAIW is composed of multiple sublayers that are each influenced by various formation or ventilation mechanisms (Jacobs & Georgi, 1977; Molinelli, 1981; Talley, 1996).

Properties of the salinity minimum range in temperature from 2.8 to about 6°C and from 33.9 to 34.5 in salinity. AAIW is traditionally defined between $27.0 \leq \sigma_\theta \leq 27.4$ or $27.1 \leq \gamma_n \leq 27.5$, with σ_θ=27.25 (γ_n=27.3) marking the salinity minimum of the South Pacific. Above AAIW lies Subantarctic Mode Water (SAMW), characterized by a potential vorticity minimum. The densest outcrop north of the Subantarctic Front defines the top of AAIW. Below AAIW is UCDW, which is characterized by a local oxygen minimum. AAIW is the most extensive of all intermediate waters and penetrates well into the Northern Hemisphere, to 20°N in the Pacific and up to 60°N in the Atlantic (Tsuchiya, 1989; Tsuchiya et al., 1992; Talley, 1996). In the South Atlantic, an oxygen and CFC maximum can also be identified in the AAIW layer to about 25°S, although these maxima are located 50-100 m above the salinity minimum (Warner & Weiss, 1992; Talley, 1996). As Warner & Weiss (1992) suggest, this offset between the location of the CFC and salinity minimum reflects the different ventilation process affecting each layer, with the salinity minimum being affected by an AASW source and the CFC/oxygen maximum reflecting the influence of water from the South Pacific.

Isoneutral distribution of tracer properties. The global distributions of hydrographic properties on the γ_n=27.3 isoneutral are shown in Figure 10. The depth of the 27.3 isoneutral indicates that the circulation on that layer is mostly similar to that of the subtropical gyre. The 27.3 isoneutral is deeper (to about 1000 m) at the center and shallower towards the edges (Figure 10a) of the wind-drive gyres. This indicates that the circulation of the AAIW layer is dominantly wind driven (Schmid et al., 2000). The Brazil-Malvinas Confluence (38°S) is clearly visible on panel a. This boundary marks the northern limit of the direct propagation of fresh AAIW along the western boundary which is also visible for other tracers (Figure 10 b, c, d, f, g,

j). At the convergence, the bulk of the AAIW propagates eastward into the interior where it follows the interior subtropical gyre circulation of the wind drive gyren (Piola & Gordon, 1989; Maamaatuaiahutapu et al., 1992; Larque et al., 1997).

The AAIW layer is rich in gases, as shown by the oxygen, NO and CFC distributions (Figure 10b, f, c). These tracers also indicate the location of preferential ventilation in the Southeast Pacific and the Southwest Atlantic. Of interest are also the high oxygen tongues penetrating into the Northern Pacific and Atlantic on the western boundary, indicating the influence of AAIW in the Northern Hemisphere (Qu & Lindstrom, 2004; Tsuchiya, 1989). A lack of a zonal oxygen gradient at the equator indicates homogenization of properties in this region (Suga & Talley, 1995). ΔC_{gasex}, a relative measure of air-sea carbon disequilibrium, shows low values near the formation centers of AAIW. This is consistent with the relative undersaturation of this water mass with respect to other gases, such as oxygen and CFC (Russell & Dickson, 2003; Hartin et al., 2011). These low ΔC_{gasex} values reflect the influence of upwelled UCDW in the composition of AAIW. Were the precursor waters of AAIW uniquely of Subtropical origins, these would be well equilibrated.

The presence of low salinity AAIW and the competing high salinity intermediate waters from the RSOW and MSOW are evident in Figure 10d. Panels d and g indicate that AAIW is fresher and colder in the Atlantic than in the Pacific (Figure 10d, g). The difference in potential vorticity between the South Pacific and the South Atlantic, as was first recognized by McCartney & Talley (1982), can be seen in Figure 13g-i. Panel 13g shows that the thickness between 27.2 and 27.3 reaches 250 m in the Southeast Pacific, while it is less than 200 m in the South Atlantic (Figure 13h, i). Mixing across the Drake Passage and with waters from the Agulhas region in the South Atlantic explains the erosion of the low vorticity characteristic AAIW in the South Atlantic relative to freshly ventilated $AAIW_{PAC}$ in the Southeast Pacific.

AAIW is warmest and saltiest in the Indian Ocean, owing to the influence of RSOW on competing isopycnals (Figure 10d, g). As shown by Piola & Georgi (1982), the Kerguelen Plateau acts as a topographic barrier between waters of $AAIW_{PAC}$ origin flowing westward and waters of $AAIW_{ATL}$ origin flowing eastward. Fine (1993) used CFC data to demonstrate that the youngest, most recently ventilated intermediate waters in the Indian Ocean are due to $AAIW_{ATL}$ (Figure 10c). McCarthy & Talley (1999) calculated maps of potential vorticity on the γ_n=27.35 isoneutral for the Indian Ocean, showing higher potential vorticity values east of the Kerguelen Plateau, and lower values to the West. The isoneutral thickness plots shown in Figure 13f-h are too coarse to show this feature clearly.

Wong (2005) has emphasized the weak meridional salinity gradient in the Eastern Indian between 30 and 40°S (Figure 10d). This is indicative of a long mixing history. Wong (2005) proposed that this region would then be an interesting sentinel that filters short-term variability and would provide a clear picture of decadal climate change for the AAIW layer. The 27.4 maps show outcrops of that density in the Bellingshausen Sea (not shown). The 27.5 surfaces show an uninterrupted isoneutral connection from the Bellingshausen Sea to the Drake Passage and also reach close to the Antarctic coast on either side of the Kerguelen Plateau, suggesting that direct isoneutral supply of freshwater to the 27.5 level from the Antarctic upper layers is possible (not shown).

Nutrients (Figure 10 e and h) are relatively lower towards the southern outcrop, indicating the young age of the water, the influence of subtropical waters in the composition of AAIW, and most importantly their origin north of the Polar Front Zone, where biological production has depleted the mixed layer nutrients (Marinov et al., 2006). Regarding $N^\star$ (Figure 10i), the interesting signal is the low values in the North Pacific and Indian, indicative of denitrification, rather than the higher values towards the South. These denitrification regions are also characterized by a low ΔC_{gasex} (Figure 10l).

The low silicate and $Si^\star$ characteristic of AAIW is also clearly shown on panels j and k, consistent with Sarmiento et al. (2004b). The low silicate and negative $Si^\star$ reflect the fact that primary production in the Polar Frontal Zone is partly iron-limited. In these conditions, the silicate to nitrate ratio of diatoms increase preferentially lowering Si and explaining the silicate deficit.

On the formation of Antarctic Intermediate Water. The mechanisms that maintain the salinity minimum and that govern the vertical thickness of the AAIW layer are subject to some debate and ongoing research. In that regard, it is helpful to chronologically review the evolution of some hypotheses that have been proposed to explain AAIW formation and relevant findings. It was initially proposed that the salinity minimum associated with AAIW discussed by Wüst (1935) was forming circumpolarly in the Polar Frontal Zone (i.e. the Antarctic Convergence between the Subantarctic Front and the Polar Front, see Figure 7) by cross-frontal mixing between a water type with temperature 2.2°C and 33.8 psu, whose properties were assumed to be relatively uniform throughout the Southern Ocean, representing "pure AAIW", and warmer and saltier subtropical waters (Wüst, 1935; Sverdrup et al., 1942). Sinking would occur as a consequence of Northward Ekman transport and isopycnal sinking. The importance of AASW as a precursor to AAIW is obvious in the volumetric θ/S diagram of Figure 3a and d. This process, however, cannot be the unique ventilation mechanism. The density of the water at the base of the winter mixed layer in the Polar Front Zone of the Eastern South Atlantic and Western Indian Southern Ocean sectors is too light for direct isopycnal injection in the convergent region to be the direct source of the salinity minimum found in these basins. Furthermore, the Ekman downwelling implied by the more recent wind climatologies suggest that the induced downwelling is a small contribution at the AAIW outcrops (Sallée et al., 2010b).

An alternative to the Polar Front sinking and mixing model was proposed by McCartney (1977). Based on the similarity between the temperature and salinity properties of the AAIW found in the subsurface of the Drake Passage and the Scotia Sea and the SAMW properties in the Southeast Pacific, McCartney (1977) proposed to treat AAIW as the densest, freshest and coldest version of SAMW. This model implies formation of

AAIW by subduction principally in the Southeast Pacific. Interestingly, the relevance of the subduction process for AAIW formation is not expanded upon in the McCartney (1977) paper, it is just briefly mentioned as a direction for future research in the conclusions of the paper. The McCartney (1977) subduction model cannot by itself account for the fresher, colder and denser properties of the salinity minimum of the Southwest Atlantic, relative to its source in the Southeast Pacific, however.

In asking if mixing with a a cold fresh Antarctic source, as in the initial Wüst/Sverdrup model, could explain the Atlantic-Pacific difference, Gordon et al. (1977) investigated the characteristics of "isohaline" layers located between 100 and 500 m in the Scotia Sea, whose temperature and salinity properties tend towards those of the salinity minimum found downstream in the Argentine Basin. These isohaline layers are most easily visible north of the Subantarctic Front in the Scotia Sea. While Gordon et al. (1977) call them isohaline, these layers tend to have a salinity maximum at the top, a salinity minimum at the base and a weak temperature gradient exists within them, with the base being colder than their top. Gordon et al. (1977) interprets the top of the isohaline layer, characterized by the relatively greater salinity, to represent least contaminated SAMW (i.e. AAIW$_{PAC}$). The weak temperature and salinity gradients of the isohaline layer indicate subsurface mixing of cold water of Southern origin. Since air-sea buoyancy fluxes would act to cool and freshen the top of the isohaline layer further, not increase its temperature and salinity, air-sea fluxes cannot explain the presence of the subsurface temperature and salinity minimum. Gordon et al. (1977) concluded qualitatively that cross-frontal exchange of Antarctic Source waters is necessary to cool and freshen AAIW$_{PAC}$-type water in the Scotia Sea so as to transform it to AAIW$_{ATL}$-type. Using an extended database, Molinelli (1978) further investigated the origin of the isohaline structure discussed by Gordon et al. (1977). Molinelli (1978) concluded that the cold and fresh characteristics of the isohaline layer, as observed only in the Southeast Pacific east of 90°W, could be readily explained by isopycnal mixing between AASW in the PFZ, where AASW with densities between 27.2 $\leq \sigma_\theta \leq$27.3 appear to mix isopycnally with an SAMW water type characteristic of the Southeast Pacific across the Polar Front. Molinelli (1978) thus provided an argument consistent with the Sverdrup/Wüst mixing formation process, although highlighting the zonal localization of the formation, pointing out also the proximity of the fronts to the Antarctic zone in the Drake Passage area, a condition that favors spatial juxtaposition of the necessary water masses.

Using a set of meridional hydrographic sections around Antarctica, Molinelli (1981) showed the circumpolar variation of mass transport between isopycnal layers characteristic of AAIW. The evolution of the transport as a function of longitude picks out a few locations where transport is either increased, cooled or warmed, suggesting formation or alteration of AAIW at this longitude, or decreased, pointing to a transformation of AAIW to lighter densities. The results of Molinelli (1981) show clearly the importance of the Southeast Pacific as the dominant source region for the AAIW σ_θ interval. Molinelli (1981) also emphasizes the role of isopycnal cross-frontal mixing as an important mechanism that transforms AAIW. Maintenance of the Polar Front, where most of the mixing occurs, thus depends also on the maintenance of the water mass sources on either side of the front. Molinelli (1981)'s data show that the 27.2-27.3 isopycnal crosses the Polar Front in the Southeast Pacific and in the Drake Passage area, providing a conduit for cold and fresh Antarctic source waters, such as AASW, into the subsurface. These results complement McCartney (1977)'s subduction process and agree with the previous classical model of AAIW ventilation. They also agree with the interpretations of Gordon et al. (1977) and Molinelli (1978) with regards to the necessity of an Antarctic end member for the production of the isohaline layer found in the Southeast Pacific and Southwest Atlantic.

More support for the importance of the AASW precursor is provided by Naveira Garabato et al. (2009), who correlated patterns of hydrographic variability of the AAIW isopycnals in the Drake Passage with patterns of temperature and salinity variability in the surrounding regions. Naveira Garabato et al. (2009) demonstrated that Winter Waters (these turn into AASW as they are exported equatorward) of the Bellingshausen Sea are the likely source of the subsurface AAIW$_{ATL}$ variability. These results support the idea that cold and fresh waters of Antarctic origin contribute to the formation of AAIW$_{ATL}$ in the Drake Passage region and also show that localized perturbations in the Winter Waters of the Bellingshausen Sea, which are caused by wintertime heat flux and sea-ice variations, can transfer into the AAIW$_{ATL}$ layer. These changes in the wind patterns over the Bellingshausen Sea are mostly governed by ENSO or SAM. These changes seem to have little impact on the properties of upwelling UCDW, the precursor to WW, however (Sprintall, 2008).

Pacific to Atlantic differences. While Gordon et al. (1977) and Molinelli (1978) were able to show evidence that exchange with Antarctic source water were playing a role in the transformation of AAIW$_{PAC}$-type water into AAIW$_{ATL}$-type water, these authors did not provide a quantitative estimate of the transformation realized by this process. Quantification was first attempted by Georgi (1979), who budgeted the influence of mixing and air-sea fluxes on AAIW$_{PAC}$ as this water is being advected eastward. Georgi (1979) concluded that estimates pertaining to air-sea fluxes, eddy flux and hydrographic fine-structures are all too small to account for the full transformation of AAIW$_{PAC}$ into AAIW$_{ATL}$. Uncertainties associated with these calculation were high but confidence is also provided by the fact that the same conclusion was reached by Piola & Georgi (1981). Piola & Georgi (1981) used seasonally resolved hydrographic data in the Drake Passage region to estimate the magnitude seasonal cycle of air-sea fluxes necessary to account for the hydrographic data. The buoyancy fluxes obtained by air-sea exchange alone are too small to account for the full transformation of AAIW$_{PAC}$ into AAIW$_{ATL}$ by a factor two, suggesting the existence of another mechanism or location where cooling and freshening of AAIW$_{PAC}$ must occur.

Using hydrographic data from the northern Scotia Sea and the Argentine Basin, Piola & Gordon (1989) analyzed the de-

tails of the transformation of the AAIW layer in the Southwestern Atlantic. Piola & Gordon (1989) identified three sub-layers, all of which experience cooling and freshening relative to the Pacific. The upper warmer low-salinity layer north of the SAF ($AAIW_{PAC}$) is transformed into a denser, colder and denser version at Burdwood Bank (a topographic feature east of the tip of South America on the north Scotia Ridge), where it is affected by air-sea interaction. The deeper, denser and colder low salinity layer, i.e. the layer that has already been modified by AASW in the Drake Passage (i.e. the isohaline layer of the Drake Passage), is not affected by surface fluxes but is further influenced by isopycnal mixing with Antarctic source water east of Burdwood Bank. Both layers ultimately flow northward entrained by the Falkland-Malvinas Current. Below both layers, owing to the cyclonic protrusion that is the Falkland-Malvinas recirculation, isopycnal mixing further injects Antarctic-source cold and low salinity water into the Southwest Atlantic on the 27.5 isoneutral.

Zonal differences in AAIW properties. Other regions where AAIW transformation occur, although to a lesser degree than in the Drake Passage, are associated with the Agulhas region, the Kerguelen Plateau and the Tasman Sea (Molinelli, 1981; Thompson & Edwards, 1981; Piola & Georgi, 1982; Hamilton, 1990; Park & Gamberoni, 1997; Griesel et al., 2010). These regions of transformation of the AAIW layer typically involve the confluence of a warm and salty poleward western boundary current or topographically induced northward meandering of the ACC. These conditions results in the spatial juxtaposition of warm salty waters, or old recirculating AAIW, with cold fresh waters, conditions favorable for the development of cross-frontal mixing, cabbeling or double diffusion. Meridional mixing is particularly important in the Southern Ocean as eddy fluxes are thought to largely compensate the northward Ekman transport (Sallée et al., 2010a,b). Eddy mixing is also believed to play a role in weakening the summer stratification below the mixed layer, preconditioning the water column for deep winter mixing (Lachkar et al., 2009; Sloyan et al., 2010) in a manner reminiscent to the role of eddies in the Labrador Sea, by returning heat and salt southward after a winter deepening of the mixed layer. The role of interannual preconditioning has not yet been assessed in the Southern Ocean.

The way eddies are parameterized, or resolved, in model simulations affects the mechanisms by which these models form AAIW and the distribution of AAIW in the models. A suite of modeling experiments by Lachkar et al. (2009), using models with various resolution and parameterizations, show that in non-eddying models with the Gent-McWilliams (GM) parameterization of eddies (Gent & McWilliams, 1990), formation of AAIW is rather circumpolar and homogenous. Eddy resolving simulations show AAIW formation that is patchier and is overall thinner than in non-eddying models. Owing to the zonal variations in wind stress, these simulations show that the effects of eddies are strongest in the Indian Ocean, intermediate in the Atlantic and weakest in the Pacific. Representations of AAIW in models vary greatly from models to models, however. Reasons range from the way formation of deep and bottom waters is captured in the models (England, 1992), which affect the penetration depth of AAIW, model resolution and associated mixing parameterization (Sorensen et al., 2001; Schouten & Matano, 2006; Sen Gupta & England, 2007; Lachkar et al., 2009), buoyancy, meltwater rates and wind forcing (Saenko et al., 2003a; Santoso & England, 2004; Sloyan & Kamenkovich, 2007; Sen Gupta et al., 2009).

Formation and ventilation rates. Net formation estimates of newly ventilated AAIW are rather uncertain and available estimates are difficult to compare as they are produced from different methods and are reported for different density intervals. Using the kinematic method to estimate subduction in conjunction with ARGO data, Sallée et al. (2010b) estimated the global net formation of AAIW (actually a net meridional northward flow across the Polar Front) to be 12 Sv. This is about one third of the estimate provided by Sloyan & Rintoul (2001) using an inverse model that uses a set of WOCE sections in the Southern Ocean south of 30°S. The reason for this large discrepancy is not clear. Hartin et al. (2011) estimated the formation of $AAIW_{PAC}$ that remains in the Pacific as 5.8±1.7 Sv based on the CFC inventory in the South Pacific. This is a lower estimate as it neglects the transport out of the Pacific along the ACC. An estimate for the total transport of AAIW at 77°W is estimated to be 19.8±2 Sv (Hartin et al., 2011). Assuming all of it is newly formed $AAIW_{PAC}$, an upper bound for the total production of $AAIW_{PAC}$ would be about 26 Sv. Since AAIW also recirculates within the ACC and a recirculation cell associated with the Chilean coast exist, this upper bound is likely too large. Talley (2003) gave the meridional AAIW export in each ocean basin at about 30°S, proposing values of 5.2 Sv for the South Atlantic, 4.8 Sv for the South Pacific (in rough agreement with Hartin et al. (2011)), and a net southward flow of -7.9 Sv out of the Indian Ocean. The net southward flow in the Indian Ocean indicates convergence into the AAIW layer from strong diapycnal fluxes in the Northern Indian basin. You (2002b) estimated a northward export of AAIW in of the South Atlantic of 4.26 Sv, in agreement with the adjusted geostrophic transport estimates of Talley (2003). You (2002b) further quantified the fraction coming from the Drake Passage and the fraction coming from the Agulhas Current using a linear mixing model and assuming no local formation in the South Atlantic. His results showed 2.7 Sv originating from the Drake Passage and 1.56 Sv from the Indian Ocean. The relative importance of each route for the return pathway of the meridional overturning circulation to the North Atlantic has yet to be fully understood, however (Gordon et al., 1992; Döös, 1995; Beal et al., 2011). Zonally averaged export estimates for the AAIW layer are also provided by Talley (2008): 5.2 Sv for the South Atlantic, 2.5 Sv for the South Pacific and -10.1 Sv for the Indian.

As this paragraph has shown, the formation rates for AAIW are quite uncertain. Values around 4-5 Sv seem appropriate to describe the AAIW flow into the South Atlantic. The uncertainty range remains substantial in the Indian and Pacific. Overall, the formation rate of AAIW is poorly known.

On the role of AAIW for the meridional overturning circulation and climate. As a pathway that returns freshwater to the Atlantic (Broecker et al., 1990), AAIW affects the net freshwater balance of the Atlantic. The net freshwater flux in or out of the South Atlantic is believed to play an important role for the stability of the Meridional Overturning Circulation (Rahmstorf, 1996; Saenko et al., 2003b; de Vries & Weber, 2005; Hawkins et al., 2011). Variations in the properties and rate of production of AAIW have been seen in the paleo-record and are thought to play an important role in governing the overturning regime shifts between glacial and interglacial periods (Keeling & Stephens, 2001; Waelbroeck et al., 2011). Paleo-reconstruction of oceanic conditions agree that major changes have occurred at intermediate depths during glacial periods, both in the Northern and Southern Hemispheres (Ninnemann & Charles, 1997; Rickaby & Elderfield, 2005; Pahnke & Zahn, 2005; Jung et al., 2010; Thornalley, D.J.R. and Barker, S. and Broecker W.S. and Elderfield H. and McCave I.N., 2011; Waelbroeck et al., 2011). Pahnke & Zahn (2005) presented sediment data from the Southwest Pacific suggesting that changes in the production rate of AAIW act on basin-wide salt budgets and the large-scale meridional density gradients, thus affecting meridional overturning stability in the North Atlantic. Other paleo-proxies are consistent with a strong presence of a Southern sourced intermediate water in the North Atlantic (Rickaby & Elderfield, 2005; Thornalley, D.J.R. and Barker, S. and Broecker W.S. and Elderfield H. and McCave I.N., 2011).

An hypothesis proposing that variations in the thermohaline properties of AAIW can induce glacial-interglacial fluctuations in the meridional overturning circulation was formulated by Keeling & Stephens (2001). The main aspect of this hypothesis are that 1) the overturning circulation is driven by Southern Ocean wind-induced upwelling and not by low-latitude diapycnal mixing (Toggweiler & Samuels, 1998) but does not require a meridional shift in the position or magnitude of the winds, 2) the main source of AAIW is UCDW that upwells from below the sill depth of the Drake Passage, 3) the stability of the meridional overturning is governed by a salinity feedback similar to that captured by the model of Stommel (1961) although applied to the Southern Ocean, where the net freshwater transport in or out of the Southern Ocean is governed by the low to high latitude transfer of moisture by evaporation and precipitations and the development of sea-ice and brine.

The Keeling & Stephens (2001) hypothesis argues that the stable modern warm state is characterized by a fresh Southern Ocean upper layer (AASW) that feeds production of AAIW and returns freshwater to the North Atlantic. During glacial cold states, on the other hand, growth of sea-ice in the Southern Ocean increases the salinity of the AASW layer and AABW through brine-rejection, resulting in an AAIW water mass whose density competes with that of NADW. Sea ice also prevents the outgassing of carbon dioxide, helping to reduce atmospheric CO_2 levels during glacial periods (Stephens & Keeling, 2000). At the point when NADW is not dense enough to penetrate below AAIW, it is also not able to cross the Drake Passage as it lies above the sill depth of the Drake Passage and as such stops contributing to the upwelling in the Southern Ocean. Boyle & Keigwin (1987) refer to this type of NADW as Glacial North Atlantic Intermediate Water (GNAIW). Keeling & Stephens (2001) suggest that GNAIW would behave as an Atlantic analogue of present-day NPIW.

Model perturbations in the thermohaline properties in the mode and intermediate layers of the South Atlantic have been shown to affect North Atlantic climate directly. In order to probe the sensitivity of the climate system simulated by the HadCM3 coupled climate model, Graham et al. (2011) perturbed the density layers between $27.7 \leq \sigma_\theta \leq 29.4$ (encompassing the salinity minimum in that model) between 10 and 20°S in the South Atlantic with salinity-compensated temperature perturbations of ±1°C in this density range, and smaller perturbations of ±0.5°C in the neighboring model layers. Graham et al. (2011) used salinity compensated perturbations to minimize effects due to changing the interior density structure of the simulated ocean and better trace the effect of changing thermohaline properties. While much of the water in these intermediate layers recirculates at depth (about one third in these simulations), the perturbations propagated at advective speeds along the western boundary until the NAC, the Labrador Sea and the GIN Seas, where some intermediate water was entrained into the mixed layer and some recirculated at intermediate depth in the Northern Atlantic. Surprisingly, both the hot and the cold perturbations provoked a decrease in the meridional circulations. The hot perturbation yielded an increase in the Northward heat transport into the North Atlantic, directly affecting the stratification of convective regions. The cold perturbation, however increased the freshwater transport but also cooled the subpolar region, affecting the circulation of the Subpolar gyre and thus affecting the heat and salt balance of the convective regions. Both types of perturbations significantly altered the SST patterns of the North Atlantic and climate in continental regions bordering the North Atlantic. If representative of the real world, the experiment of Graham et al. (2011) would suggest that the modern AAIW may correspond to a high-state with regards to the meridional overturning. These simulations show that variability in the thermohaline properties of AAIW are able to induce climate variability in the Northern Hemisphere.

Variability. As was shown by Iudicone et al. (2007), the export of $AAIW_{PAC}$ into the Pacific is diagnostically related to the basin scale meridional pressure gradient, which is mechanistically related to the thermal wind balance in the Southeastern Pacific that supports the northward flow of intermediate water (the exchange window). As such, and because AAIW circulation largely follows the gyre circulation, perturbations in the export of AAIW may not necessarily be caused by local events over the formation regions, but are also subject to remote forcing. Furthermore, since AAIW has to cross the equator to penetrate into the North Atlantic (Suga & Talley, 1995), tropical and equatorial phenomenon affecting the subtropical cells (Hazeleger & Drijfhout, 2006) may also play a role in dictating the potential impact of AAIW perturbations on the Northern Hemisphere.

One interesting difference between the processes influencing the formation and characteristics of intermediate water masses

like LSW, NPIW or AAIW is the geographical extent limiting their formation region. LSW formation is limited to the Labrador Sea and NPIW formation is mostly associated with the Okhostk Sea and the MWR of the Northwestern Pacific. Both regions are geographically limited, close to the western boundary and very sensitive to the position of the storm track. As such, these regions are extremely vulnerable to local and zonal anomalies (Seager et al., 2002; Li & Battisti, 2008). The Asian monsoon or the North Atlantic Oscillation affect the storm track path, storm frequencies and magnitude. The Labrador Sea is also sensitive to freshwater disturbances originating from either the Arctic or high-salinity eddies stemming from the North Atlantic Current. On the other hand, while there is still debate about the relative importance of the various mechanisms affecting AAIW ventilation (mainly circumpolar Ekman convergence, localized South East Pacific convection and subsurface diapycnal mixing), one might expect that this diversity in formation mechanisms and the mixing and recirculation of this water mass in the Southern Hemisphere would render AAIW relatively more robust to local perturbations. In that sense, regional zonal perturbations and perturbations on short time scales might be a lot less effective in greatly affecting AAIW characteristics and influencing climate than large-scale meridional shifts in the winds or continuous changes in buoyancy as induced by anthropogenic climate change. This is not to say that natural modes of climate variability, such as ENSO or SAM do not affect AAIW formation, however (Sallée et al., 2010a), just that it is unclear how or if this natural variability propagates to the North Atlantic, affects the overturning or interacts with other modes of variability at lower latitudes (Hickey & Weaver, 2004). As stated above, large changes have occurred at intermediate depth in all basins. The causes for these changes, i.e. changes in the source characteristics, changes in the production rates, ventilation pathways, decreased competition with other water masses on shared isopycnals, have yet to be elucidated, however.

4.2. High salinity intermediate waters

Warm and extremely saline waters (MSOW, RSOW, PGW) flow out of net evaporative marginal seas (Mediterranean Sea, Arabian Sea, Persian Gulf) across relatively shallow and narrow straits (Gibraltar, Bab el-Mandeb, Hormuz). These outflows sink and stabilize on isopycnals at intermediate depths in the North Atlantic and Indian Oceans and constitute the world's high salinity intermediate waters. Their presence in the North Atlantic and Indian Ocean can be easily detected on isoneutral maps of salinity (see for example Figure 10d). Spreading of these high-salinity water masses in the ocean interior is not simply a passive process, as was mostly the case with low-salinity intermediate waters. A significant fraction of the export of the high-salinity intermediate water occurs through the propagation and destruction of subsurface mesoscale eddies that have diameters of order 100 km and are able to propagate faster than the mean flow. As such, the tongues of elevated salinity typical of the high-salinity intermediate water masses do not reflect the mean circulation on these isopycnals (Talley et al., 2011).

4.2.1. Mediterranean Sea Overflow Water

Overview. The Mediterranean Sea can be thought of being stratified in three main layers (Baringer & Price, 1999; Candela, 2001). Relatively fresh modified Atlantic Water enters the Mediterranean Sea through the Strait of Gibraltar from the North Atlantic and occupies the top 150 m. Owing to the strong evaporation over the basin, of order 0.5 m/yr, the salinity of that layer is greatly increased in the Mediterranean Sea relative to its characteristics at the Gibraltar inflow. The intermediate layer (roughly 150-800 m) is composed of Levantine Intermediate Water (LIW). LIW forms by shallow convection in the eastern Mediterranean region and is the warmest and saltiest water found in the subsurface (13.1-13.2°C and 38.5 psu). Below that is western Mediterranean Deep Water (WMDW), which is colder and fresher (12.8-12.9°C and 38.42-38.45 psu). It forms by episodic deep convection in the Gulf of Lions and to a lesser extent in the Adriatic Sea. LIW participates in the production of WMDW in a manner similar to the role of IrSW in the Labrador Sea, by preconditioning the subsurface.

The Gibraltar Strait is about 15 km wide at its narrowest and is at most 300 m deep (at the Camarinal Sill South), implying that a substantial fraction of the water that exits the Mediterranean Sea is from the intermediate layers of the Mediterranean (Millot et al., 2006). The outflowing layer is very thin relative to the sill depth. It is only of order 50 m at the sill (Iorga & Lozier, 1999b). Properties of the overflow are typically around 13°C and 38.4 psu ($\sigma_\theta \approx$28.95), but the exact composition and properties of the overflow layer has been shown to evolve somewhat in time, with variations up to 0.5°C and 0.1 psu (Millot et al., 2006). The salinity in the Mediterranean has been increasing in recent decades and is projected to increase another 0.13 psu, largely in response to the diversion of river water for irrigation in Russia and Egypt (Candela, 2001).

High frequency variability in the source properties of MSOW appears to have relatively little influence on the MSOW layer found in the North Atlantic (Lozier & Sindlinger, 2009). Bozec et al. (2011), using a high resolution model of the North Atlantic investigated the effect of atmospheric variability as the driver of property changes of MSOW in the North Atlantic. The modeling results indicate that most of the MSOW variability in the eastern North Atlantic over the last 50 years is driven by large scale patterns of variability (NAO) rather than changes in the characteristics of Mediterranean seawater source or NACW source characteristics.

The currents across the Strait of Gibraltar are quite variable. Currents are dominated by the tides (about 70%). Large-scale atmospheric perturbations in the Mediterranean Sea roughly account for another 10% of the currents' variability and variations in the Mediterranean to Atlantic Waters pressure gradient, in a hydraulic manner similar to DSOW, explain another 20% (Candela, 2001). Local effects near Gibraltar, particularly local wind patterns, can also be an important source of variability (Menemenlis et al., 2007). Modern net outflow estimates of Mediterranean Water into the North Atlantic at Gibraltar hover between 0.5-1 Sv (Baringer & Price, 1997). Overflow transports show a seasonal cycle, with an amplitude of about 0.2 Sv,

and a minimum in early summer, and interannual variability of order 0.1 Sv.

Overflow and characteristics in the Gulf of Cadiz. Upon passing the Strait of Gibraltar, MSOW initially follows a gravity driven boundary current along the northern continental slope of the Gulf of Cadiz. Neutral buoyancy is achieved by Cape St. Vincent (The southwestern corner of the Iberian Peninsula). At that point the transport has nearly doubled (Baringer & Price, 1997) owing to entrainment of fresher and colder North Atlantic Central Waters (NACW, 11.4-12.5°C, 35.6-35.7 psu). Most of the mixing and entrainment occurs within 50 km of Gibraltar. By that point, salinity has decreased to 36.6 psu. Baringer & Price (1997) investigated the evolution of the thermohaline properties of MSOW from the Strait of Gibraltar to Cape St. Vincent in association with velocity measurements. These analyses show that the entrainment and mixing process are both nearly isothermal as temperature does not change very much from Gibraltar until MSOW achieves neutral buoyancy. Temperature only decreases slightly from about 13 to 12°C, while salinity changes from over 38 to about 35.5 psu.

MSOW splits into three distinct cores between Gibraltar and Cape St. Vincent. The two shallowest cores tend to merge back into a single entity but the deep core remains independent. The remaining two MSOW cores settle on the 27.5 and 27.8 isopycnals although the influence of MSOW can be seen throughout the water column between at least 27.2 and 28.0. The formation of the cores seems to be set early on in the Gulf of Cadiz (by 7°10'W Iorga & Lozier (1999a); Ambar & Howe (1979)). By the time the cores exit the Gulf of Cadiz, the shallow inshore core lies at about 700-800 m and the deeper southern core is at 1000-1200 m (Ambar & Howe, 1979; Baringer & Price, 1997, 1999; Ambar et al., 2002). The shallower core is warmer whereas the lower core is better defined by a salinity maximum (Ambar et al., 2002). The cores form through mixing with different water masses. That mixing process is possibly affected by shear and topography that involves NACW in the upper layers and waters originating from the South along the African continental slope in the deeper portion (550-650 m) (Madelain, 1970; Ambar & Howe, 1979; Iorga & Lozier, 1999a; Baringer & Price, 1997, 1999; Iorga & Lozier, 1999a).

Cape St. Vincent is characterized by a very sharp steepening of the topography, as well as by a sudden northward turn of the continental shelf off the southwestern corner of Portugal. Regions where a boundary current encounters sharp deepening in topography, such as is the case south of the Grand Banks, are regions where recirculation cells can be generated through vortex stretching (Zhang & Vallis, 2007). Evidence for such a recirculation in the interior west of Cape St. Vincent can be found in the data (Lozier et al., 1995; Iorga & Lozier, 1999a,b). This recirculation helps maintain a reservoir of MSOW in the Targus Abyssal Plain, a small basin located westward of Cape St Vincent near the coast of Portugal (Iorga & Lozier, 1999b; Bower et al., 2002b). The complex topography in the Gulf of Cadiz also generates a southward cyclonic recirculation cell there (Figure 5a, Iorga & Lozier (1999a)).

Cape St. Vincent is also a branching point for the spread of MSOW (Figure 5a). The upper core is more likely to follow the continental boundary northward than the lower core, which tends to spread westward (Zenk & Armi, 1990; Daniault et al., 1994). MSOW propagates both along a northward route along the continental slope of Portugal and a westward route across the interior of the Atlantic (Bower et al., 2002b). The northward route can be traced at least to 50°N (Iorga & Lozier, 1999a; Lozier & Stewart, 2008). Lozier & Stewart (2008) find that the northward spreading extent of MSOW is linked to the dynamics of the subpolar gyre. When the NAO is in a positive phase, the subpolar front moves eastward and blocks the intrusion of MSOW past the Porcupine Bank. During low NAO phases, the subpolar front moves westward and MSOW penetrates past the Porcupine Bank. Additional evidence for this process is provided by the anti-correlation between the salinity anomalies present in the Rockall Trough on LSW and MSOW density intervals.

Meddies. The exact partitioning between these routes is not clear but it is estimated that Meddies, sub-mesoscale coherent anticyclonic vortices characterized by a warm and salty core propagating about about 1000 m depth (Richardson et al., 2000), transport about 25% of the salinity flux that escapes through the Gibraltar Strait and 50% of the zonal salinity flux in the interior of the Atlantic at these depth and latitudes. Meddies form with diameters of about 9 km but quickly grow to 20-150 km in diameter, with typical thicknesses of 650 m (Richardson et al., 2000; Talley et al., 2011). Their lifetime is about 2-3 years. Richardson et al. (2000) estimated that about 17 Meddies form each year and that there is an average of 29 Meddies at any given time in the North Atlantic. Meddies propagate westward about five times faster than the mean flow with translation speeds near 0.08 m/s (Bower et al., 1995). Meddies originate in the region off Cape St. Vincent where topography steepens sharply and turns northward abruptly. Meddies may contain water from either the lower core or both cores.

Meddies interact with seamounts in the region west of the Gulf of Cadiz (Richardson et al., 2000). Shallow topographic features there steer the propagating Meddies southward (Bower et al., 1995). Meddy-seamount collisions also induce substantial mixing and deposition of warm and salty Meddy water locally. As was pointed out by Bezbodorov & Ovsyany (1991), Meddies transport oxygen into the oxygen minimum layer of the North Atlantic. Richardson et al. (2000) estimate that major collisions between Meddies and seamounts occur on average every 1.7 years.

Changes in the dynamical control of the Mediterranean Undercurrent (i.e. the name given to the MSOW outflow in the Gulf of Cadiz) can be seen at the Portimão Canyon, just south of Portugal, southeast of Cape St Vincent (Bower et al., 2002b), but the formation mechanisms as well the processes that control the frequency with which Meddies are spun off are not totally clear. Proposed mechanisms include shear, baroclinic or boundary layer instability, geostrophic adjustment, temporal variability of the Mediterranean Undercurrent or interactions with the Azores Current. Westward non-Meddy spreading of MSOW has also been shown to occur (Bower et al., 2002b), but this

appears to be limited to the East of 20°W as this water recirculates in the Eastern North Atlantic (Iorga & Lozier, 1999a,b). Far-field propagation of MSOW is mostly driven by Meddies (Maze et al., 1997).

Influence on the North Atlantic. As Figures 9, 10 and 11 indicate, while the influence of MSOW on the North Atlantic is very clear in the distribution of salinity, MSOW does not form a thick, low PV, layer (Figure 13). Talley et al. (2011) warn that the salt tongue, as mainly formed from westward propagating Meddies, does not follow the large-scale circulation. The MSOW contributes at most 30% to the salinity enhancement of the North Atlantic. The high salinity characteristic of the Atlantic is mostly the consequence of subtropical evaporation. McCartney & Mauritzen (2001) also reject the idea that MSOW feeds the warm inflow to the Nordic Seas. This conclusion minimizes the potential influence of MSOW on climate.

In spite of MSOW being injected in the North Atlantic along rather narrow cores, through only a 50 m thick outflow, its high salinity and warm temperatures in a background of colder and fresher waters, imply large vertical temperature and salinity gradients at its upper and lower interfaces, where differential mixing of heat and salt have an effect on the the density structure. Double diffusive convection below the MSOW salinity maximum contributes to downward salt transport, in addition to the background turbulent mixing (Daniault et al., 1994). The value of the density ratio $R_\rho = \alpha\frac{\partial T}{\partial z}/\beta\frac{\partial S}{\partial z}$, a diagnostic of non-linear mixing processes (Schmitt, 1994), near the Iberian Peninsula in the temperature range 5-8°C at the base of the salinity maximum is about 1.2-1.3. This is indicative of active salt fingers (Daniault et al., 1994; Schmitt, 1994). Daniault et al. (1994) point out, however, that the most favorable conditions to double diffusion are north of 40°N, where it is not only the properties of MSOW that promote double diffusion, but also the presence of a fresh LSW layer underneath at these northern latitudes. Arhan (1987) argue that the salt-fingering double diffusive flux below the salinity maximum, which is of similar magnitude as the surface Ekman flux, induces a northward buoyancy driven flow in the Eastern North Atlantic. The importance of this effects diminishes northward as isopycnals shoal and are increasingly affected by the wind-induced circulation, however.

It was mentioned earlier in the LSW discussion (and see Figure 11) that MSOW nutrient properties were similar to that of the background Atlantic and as such could not be used as tracers of MSOW influence. While is is true on the large scale, this is not the case at finer scales near the outflow (Ambar et al., 2002; Cabecadas et al., 2002). The Mediterranean Sea is extremely oligotrophic and MSOW has a signature low nutrient concentration.

While the influence of MSOW as a source of salt to the North Atlantic is not believed to be critical for the maintenance of high latitude convection in the GIN seas (McCartney & Mauritzen, 2001), sea level drops of order 120 m between glacial and interglacial periods have constricted the magnitude of the Gibraltar outflow during glacial periods. Analyses of the sediment composition patterns (foraminiferal assemblage, δ^{18}O of planktonic foraminifera, grain size, sand deposition, erosion) in the Gulf of Cadiz (Baringer & Price, 1999; Ambar et al., 2002) suggest nonetheless that a net evaporation increase over the Mediterranean Basin and sea-level rise (allowing for deeper and saltier MSOW ouflow) during the last deglaciation contributed to a 0.5 psu increase in the upper 2000 m of the North Atlantic between 17.5 and 14.6 thousand years ago (Rogerson et al., 2006). These data also indicate that the Mediterranean Undercurrent was deeper during the Last Glacial Maximum. Rogerson et al. (2006) propose that the shoaling and intensification of the MSOW plume (15-14.5 thousand years ago) may have contributed to the large scale preconditioning of the North Atlantic towards conditions more favorable for convective overturn and has favored resumption of present-day convection patterns in the Labrador Sea region. As such, the shoaling of the MSOW plume may have played a role in the re-establishment of the modern stratification from the Glacial North Atlantic Intermediate Water and AAIW pair to the traditional NADW/AAIW pair.

Gravity driven overflows are important phenomenon that inject dense waters to the deep ocean and influence overturning circulation (Price & Baringer, 1994; Legg et al., 2009). Overflows are particularly difficult to parameterize in global climate models, however (Price & Baringer, 1994; Hallberg, 2000; Papadakis et al., 2003; Legg et al., 2006, 2009). Owing to these limitations, while it is known that other overflows, such as DSOW play an important role, it is challenging to assess with confidence the influence of MSOW on the global overturning circulation and climate in models. Existing coarse model simulations and the analysis of McCartney & Mauritzen (2001) would suggest, however, that the influence of MSOW on the meridional circulation and on climate is small. The hypothesis proposed by Rogerson et al. (2006) with regard to the role of MSOW in the centennial-to-millennial variability in the North Atlantic warrants further quantification, however.

4.2.2. Red Sea and Persian Gulf overflows

Overview. The formation of RSOW and PGOW share many traits with that of MSOW. All are formed from entrainment by a gravity current that exits an highly evaporative basin across a shallow sill. Furthermore, all overflows propagate as undercurrents that pass through a Gulf with complex topography (Gulf of Cadiz for MSOW, Gulf of Aden for RSOW and Gulf of Oman for PGOW) on their way to the open ocean.

One difference between MSOW and RSOW/PGOW is that the Mediterranean Sea is located on the eastern boundary of the Atlantic, while the Red Sea and the Persian Gulf are on the western boundary. This affects the way these water masses spread in the interior of the basins. Also, the Bab-el-Mandeb Strait (about 13°N) and Straits of Hormuz (about 26°N) are also located much closer to the equator than the Strait of Gibraltar (about 35.7°N). This implies that the Coriolis frequency (f) is about 3 times larger for MSOW ($8.9{\cdot}10^{-5}$ s^{-1}) than it is for RSOW ($3.1{\cdot}10^{-5}$ s^{-1}) at the latitude of their respective straits. The effect of rotation is thus more important for MSOW than for RSOW (inertial circles have a smaller radius towards the poles). The deformation radius at depth will of course also de-

pend also on the stratification. In fact, the low-latitude position of the Bab-el-Mandeb and Hormuz straits coupled with the low outflow transport across them make these outflows dynamically closer to frictional density currents weakly impacted by rotation, than geostrophic boundary currents (Bower et al., 2000).

Overflow and formation characteristics. The annual mean outflow through the Bab-el-Mandeb Strait (160 m deep at the Hanish sill, 18 km wide) is 0.37 Sv. Seasonality, modulated by the monsoon, is important, however. July-September outflows are as low as 0.05 Sv but winter February transports peak at 0.7 Sv Murray & Johns (1997); Beal et al. (2000). The thickness of the outflowing layer oscillates seasonally between 50 and 100 m. The water in the Red Sea below 80 m is rather homogenous, with a temperature of 22° and a salinity of 40.5 psu. In consequence, outflow properties tend to be very stable and converge towards these values. The salinity of RSOW at the strait is almost 2 psu more than the Mediterranean Water passing Gibraltar. Net evaporation rates in the Red Sea and Persian Gulf can exceed 2 m/yr (Ahmad & Sultan, 1991; Bower et al., 2000), about 4 times the mean evaporation of the Mediterranean Sea. Because the transport through the strait varies temporally, the equilibration density, the degree of entrainment and the final properties of the RSOW layer also vary. Neutral buoyancy is reached about 40 km from the strait, with mean equilibrium properties of about 18.1°C and 37.5 psu, corresponding to an average dilution factor of about 2.5 during the strong winter outflow. The dilution factor is more important (about 6) during the low summer outflow, which also results in a RSOW product that is cooler than during winter. Taking into account the dilution factors of the outflow and the measured outflow transports at the strait yield RSOW production rates between 0.3 Sv and 1.75 Sv.

Owing to the complex topography in the Gulf of Aden, the outflow follows two main pathways, mainly through the Northern and the Southern Channels, resulting in various amounts of entrainment and a layering of the final RSOW product. Waters flowing through the Northern Channel (close to the Yemeni coast) mix less with ambient waters and their final product is saltier and denser (σ_θ ≈27.5) than the water exiting through the Southern Channel (close to Djibouti), which is steeper and broader than its northern counterpart (Bower et al., 2000; Peters et al., 2005; Peters & Johns, 2005; Matt & Johns, 2007). As a consequence of these two pathways, RSOW tends to form two interior cores, a shallow one near 600 m, which is warmer (≈18°C, σ_θ =27.2) and derives from the Southern Channel, and a deeper one, about 1.52°C cooler, near 100-1200 m with σ_θ =27.65 that originates from the Northern Channel (Bower et al., 2000, 2005; Saafani & Shenoi, 2007). Both the Southern and the Northern Channel flow into the 1800 m deep Tadjura Rift, a canyon located at the western edge of the Gulf of Aden. Neither the Northern nor Southern outflow is dense enough to reach the bottom of the Rift, however (Bower et al., 2005).

Characteristics of a continuous undercurrent, as can be found in the Gulf of Cadiz downstream of Gibraltar, cease to exist in the Tadjura Rift. The current is replaced by mesoscale eddies throughout the Gulf of Aden (Bower et al., 2002a). The reason for a lack of an undercurrent are unclear but likely involve temporal variability in the overflow transport and boundary detachment of the jets leaving the channels, which may not be able to reattach (Bower et al., 2005). It is known that RSOW forms lenses. Some of these lenses constitute coherent vortices, called "Reddies", which are able to travel far from their origins (Shapiro & Meschanov, 1991; Meschanov & Shapiro, 1998; Bower et al., 2002a). The formation mechanisms of Reddies is not well-understood (Shapiro & Meschanov, 1991), but the topographic influence of the Tadjura Rift and the deep-reaching mesoscale eddies described by Bower et al. (2002a) in the Gulf of Aden are likely to play a role (Bower et al., 2005). Propagation of Reddies is mostly eastward and seems to follow the frontal zone that separates RSOW and background Indian Ocean water (Shapiro & Meschanov, 1991). Reddies are slightly thinner than Meddies, about 200 m thick, but otherwise share similar properties with regard to their density anomalies and diameters (Meschanov & Shapiro, 1998). Reddies propagate at a slightly shallower depth than Meddies, however, at around 700 m (Meschanov & Shapiro, 1998). A census by Shapiro & Meschanov (1991) revealed the presence of seven Reddies on average in the Indian Ocean, as determined from data from 1935-1981.

Interleaving structures are found extensively in the RSOW layer throughout the Indian Ocean and in consequence the depth of the salinity maximum can vary substantially from station to station and in time at fixed stations (Beal et al., 2000). This makes the precise tracing of a particular salinity maximum layer extremely challenging. The high salinity layer of RSOW and the monsoonal variability that can be observed in RSOW properties in the Arabian Sea can be traced to the Agulhas (Grundlingh, 1985; Beal et al., 2000), however. Variability on the isopycnals representative of the RSOW and salinity are much weaker in the Bay of Bengal, suggesting limited penetration of RSOW east of the Indian sub-continent (Beal et al., 2000). Spreading of RSOW is mostly southward along the continental boundary, with a preferred pathway through the Mozambique Channel. As was the case with MSOW, the conditions at the base of the high salinity layer are conducive to double-diffusive mixing (You, 1996, 2000, 2002a). These dianeutral fluxes extend the influence of the high salinity RSOW to depths over 2000 m and densities close to γ_n=28.0 in the Arabian Sea.

In comparison to the Red Sea, the Persian Gulf is extremely shallow. The maximum depth of the Red Sea reaches 2000 m, but the deepest part of the Persian Gulf is merely 160 m deep, with an average depth of only 35 m (Swift & Bower, 2003). The transport out of the Persian Gulf is about 0.2 Sv (Ahmad & Sultan, 1991), about half that out of the Red Sea, although the water properties at the Strait of Hormuz (80 m deep, 57 km wide, with a narrower central channel) are saltier and warmer than the waters from Bab-el-Mandeb. Salinities as high as 57 psu have been measured in the Persian Gulf (Bower et al., 2000). Unlike RSOW, the overflow transport through the Strait of Hormuz does not experience much seasonal variation (Swift & Bower, 2003). A seasonal cycle exists with regards to the temperature of the overflow, however, with values ranging from 19 to

25°C. This seasonal cycle occurs in the Persian Gulf because of the very shallow depths there relative to the Red Sea (Swift & Bower, 2003). The average winter and summer properties of the overflow at the strait are 20.4°C, 39.6 psu in winter and 24.2°C, 39.4 psu in summer (Bower et al., 2000). PGOW typically occupies the layer between 200 and 350 m along σ_θ=26.5 in the Arabian Sea. Similarly to RSOW, hydrographic stations downstream of the overflow show significant spatial and temporal T/S variability.

5. Central waters

5.1. Overview

Central waters are represented by long quasi-linear branches stemming from the intermediate waters on a θ/S diagram (Figure 1, 2, 3). Mode waters are the building blocks of central waters. Mode waters tend to form in restricted locations and inherit special properties that can be used to evaluate their influence. Most notably, they can be identified because they contrast with the background stratification of the pycnocline.

Karstensen & Quadfasel (2002a) estimate the global ventilation rate for the permanent thermocline of the World Ocean to be about 160 Sv. That is, the flow of water that enters the pycnocline is roughly of similar magnitude as the transport of the ACC at the Drake Passage. This is about 5-6 times the rate of deep and bottom water formation. Given the volume of the ocean between 200 and 800 m, this gives a globally average residence time of about 40 years.

The term Central Water is used to represent the whole volumetric ridge or mixing line that connects intermediate waters to the shallow salinity maximum (Subtropical Underwater, STUW) on a θ/S diagram (Talley et al., 2011), as can be seen in Figures 1, 2 and 3. Central Waters may be influenced by, or contain, multiple types of mode waters. Central Waters are the waters of the main pycnocline under each gyre. They are maintained both by subduction (Luyten et al., 1983) and by vertical mixing processes, including salt fingering (Suga et al., 2008; Toyama & Suga, 2011). Because they constitute the pycnocline, the ocean region of strongest vertical gradients, the properties of Central Waters are defined broadly and it doesn't make sense to describe them in terms of a water type. It is more effective to describe them in terms of their constitutive mode waters when possible, or simply in θ/S space, where they can be clearly identified.

Mode waters are important components of of the marine biogeochemical system in that they play a role in exporting nutrients from higher latitudes to lower latitudes and control the supply of nutrients in the oligotrophic subtropical gyres (Palter et al., 2005; Krémeur et al., 2009). They also store significant portions of the anthropogenic carbon inventory (Sabine et al., 2004). Furthermore, owing to their residence times (1-60 years, Suga et al. (2008)), thermocline waters are not only able to store climate perturbations but they also can transport temperature anomalies and affect regional climate patterns downstream with a delay (Gu & Philander, 1997).

5.2. Potential vorticity

As one of the defining characteristics of mode waters is their low potential vorticity, it is helpful to review the processes that can induce low vorticity layers in the ocean. An expression for PV in the context of thermocline ventilation is given by Williams (1991) (Equation (1), see also Oka & Qiu (2011)):

$$PV = \frac{f}{\rho_o} \frac{\left(\frac{\partial \rho_m}{\partial t} + \mathbf{u}_b \cdot \nabla \rho_m\right)}{\left(w_b + \frac{\partial h}{\partial t} + \mathbf{u}_b \cdot \nabla h\right)} \quad (1)$$

where f is the Coriolis term (planetary vorticity), ρ_o is a reference density, ρ_m is the density of the mixed layer, h is the mixed layer depth and $\mathbf{u}_b$ and w_b are the horizontal and vertical velocities at the base of the mixed layer. Low PV layers can be generated either when the numerator of Equation (1) is low or the denominator is high.

In the denominator, which corresponds to the negative of the subduction rate (Williams, 1991), w_b is referred to as the vertical pumping term and is often estimated practically by the vertical Ekman velocity, which can be calculated from wind stress data, and may include a correction for the β-effect on the meridional geostrophic velocity (Huang & Russell, 1994; Huang & Qiu, 1998; Qiu & Huang, 1995). As can be seen from the schematic in Figure 14, the Ekman layer usually only consists of a thin layer near the surface, whereas the subduction involves the much deeper mixed layer. The term $\mathbf{u}_b \cdot \nabla h$ is called the lateral induction term and represents the injection of water below the mixed layer by horizontal advection across the sloping base of the mixed layer. Note that this term can be positive or negative, depending on whether the velocity field advects a water parcel in or out of the mixed layer. Lateral injection is the dominant process that drives formation of WSTMW and SAMW (Qu et al., 2008), essentially mode waters that form in association with a strong current. $\frac{\partial h}{\partial t}$ captures the temporal evolution of the mixed layer depth, which is deeper in winter and shallower in summer. The seasonal evolution of the mixed layer depth does not follow a sinusoidal trajectory, however. While the deepening phase may be gradual from fall to winter, the restratification tends to be abrupt, usually occurring in early Spring. This abruptness increases the efficiency of the subduction process as thick layers are suddenly trapped below the mixed layer. All the terms in Equation 1 vary in time, including the velocities, which is why calculations of subduction rate are difficult as they must be performed in a Lagrangian framework (Huang & Russell, 1994).

The numerator of Equation 1 captures the evolution of vertical stratification: the vertical density contrast between the mixed layer and a parcel that has been injected below it. This vertical density contrast depends firstly on the evolution of the mixed layer density in response to changing buoyancy fluxes ($\frac{\partial \rho_m}{\partial t}$). The stratification also depends on the evolution of the difference in density between the parcel that subducts and the overlying mixed layer density as the parcel advects beneath the mixed layer. Assuming the interior is adiabatic, the density of the subducting parcel does not change and so the vertical density contrast due to advection is only a function of the horizontal density gradient in the mixed layer ($\mathbf{u}_b \cdot \nabla \rho_m$). The implication

for this second term is that low PV layers in the interior can be created if the horizontal mixed layer density gradient is weak in the direction of flow. This is the dominant formation mechanism for subtropical mode waters found on the eastern side of ocean basins (Ladd & Thompson, 2000; Oka & Qiu, 2011), as well as for the Central Mode Water of the North Pacific (Suga et al., 2004), which is a type-III water mass as per the classification of Hanawa & Talley (2001) (see section on "Types of mode waters" below for an explanation for mode water types) and could be renamed North Pacific HDSTMW to avoid confusion with regard to the use of "central" for this water mass.

It is important to note that the velocities in Equation 1 represent absolute velocities. These are often reduced to Ekman and geostrophic velocities owing to pragmatic limitations, but eddy-induced recirculations also contribute to the subduction process. Nishikawa et al. (2010) used an eddy-resolving simulation of the North Pacific and found that in fact, eddies can account for a significant fraction (nearly half) of the total subduction of STMW near the Kuroshio, in agreement with observational results relying on ARGO floats and satellite altimetry (Kouketsu et al., 2011). The role of eddies in the formation of SAMW has also been highlighted in the Southern Ocean (Sallée et al., 2008).

An alternative method to the kinematic approach (denominator of Equation 1) is the thermodynamic approach, pioneered by Walin (1982) but subsequently modified to include the effects of eddies (Marshall, 1997; Marshall & Schott, 1999). In the thermodynamic framework, water flux through the base of the mixed layer is assumed to be driven by diapycnal convergence in the mixed layer and vertical Ekman pumping. Diapycnal fluxes are caused by heating and cooling at the surface and by evaporation and precipitation, or by eddies in the mixed layer (see Figure 14). A mass budget between layers of constant density implies by continuity the magnitude of the flow at the base of the mixed layer. This technique is Eulerian and so simpler computationally than the Lagrangian kinematic approach. Buoyancy flux data are, however, very uncertain, and the effect of eddies is difficult to quantify in practice. The role of eddies is, in theory, implicit in the Lagrangian kinematic framework (although it can be parameterized in practice), but this requires knowledge of the absolute velocity as a function of time, data which are not available. So far, kinematic subduction calculations have relied on smooth low resolution geostrophic velocity fields instead. It is customary to define results from the kinematic approach as the "subduction rates", whereas results from the thermodynamic approach are usually called "formation rates".

5.2.1. Mixed layer depth

A map of the global distribution of the mixed layer depth is shown in Figure 15a. Aside from the deep mixed layer that can be seen in the high latitude convective regions, deep mixed layers are systematically located in the vicinity of western boundary currents and most strongly north of the subantarctic ACC front (Orsi et al., 1995). The seasonal amplitude of the mixed layer depths is strongest where mixed layer depth are deepest (compare Figure 15 a and b). Contours of neutral density are shown in Figure 15a on the surface of deepest mixed layer at the time of deepest mixed layer. Note how the density contours are close to one-another on the western side of the basin, while the horizontal density gradients are weaker on the eastern side (Figure 15a). The strong density gradients indicate swift boundary currents, implying large values of $\mathbf{u}_b$ and a strong contribution by the denominator in Equation 1. As can be seen in the numerator of Equation 1, however, low PV values can also be generated in regions of weak density gradient and weak flows.

5.2.2. Isoneutral thicknesses

The global distribution of Mode Waters can be inferred from Figures 12 and 13 showing the progression of water thickness between isoneutral layers from γ_n=25.1 to γ_n=27.4 in increments of 0.1 kg/m^3. Since the density increment in constant, these maps present essentially a measure of $\left(\frac{\partial \rho}{\partial z}\right)^{-1}$. The presence of Mode Waters in the subtropical gyres is clearly visible from γ_n=25.1 to γ_n=26.8. The presence of thick layers towards the eastern side of the basins, particularly in the Pacific, is visible in panels 12a to e. Indication of the formation and presence of STUW in the North Atlantic can be seen on Figure 12e to j by the development of a relatively thick layer from the eastern outcrop at about 20°N. The eastward density progression from the Atlantic to the Southeast Pacific characteristic of SAMW formation (McCartney, 1977) is clearly visible in Figures 12 and 13, from about γ_n=25.7 to 27.3. The presence of Subpolar Mode Water in the North Atlantic and it's counterclockwise progression around the subpolar gyre maybe traced in Figures 12c and 13n from γ_n=26.8 to 28.0, with the very thick and extensive layers in panels 13m-n marking the ultimate transformation of SPMW into LSW.

One peculiar feature in Figure 12i-o and Figure 13a-c is the development of thick layers in the eastern equatorial Pacific, from γ_n=26.0, with the thickness anomaly apparently propagating westward with increasing density following the northward and southward edges of the shadow zones. This feature does not outcrop and it cannot be considered a mode water. Its easternmost signature is associated with the Costa Rica Dome (Hofmann et al., 1981).

Mode water spreading from sites of subduction is achieved chiefly through entrainment along the anticyclonic wind-driven gyres (McCartney & Talley, 1982). As mentioned above, spreading of mode waters can be influenced by strong local recirculation cells and large eddies, however.

5.3. Types of mode waters

Based on their own literature survey and the authors' extensive experience on the topic, Hanawa & Talley (2001) propose the following fundamental unifying characteristics for mode waters:

- They form a volumetric mode.
- They tend to have horizontally and vertically homogenous properties (e.g. ρ, θ, S, O_2).

- They can be identified by their characteristically low vertical density gradient, or equivalently low Brunt-Vaisala frequency or potential vorticity (PV, practically, this is isopycnic $PV = -\frac{f}{\rho}\frac{\partial \rho}{\partial z}$, with f the Coriolis parameter and ρ the potential density). PV minimum core layers are commonly used to trace the spreading of mode waters of various forms.

- Their formation areas are associated with permanent fronts, always on the low-density side of the fronts. For example, Subtropical Mode Waters are associated with every separated western boundary current in the subtropical gyres.

- Their formation and maintenance are associated with wintertime convective deepening of the mixed layer due to buoyancy loss in geographically limited regions and springtime restratification. The water that is trapped below the Spring mixed layer and advected out of reach of the next winter's deep mixing forms the Mode Water. This process is known as subduction. An illustration of the process is shown in Figure 14. The dominant driving force or dynamics for the advective displacement of the water differs for the various Mode Waters.

Using these constraints, Hanawa & Talley (2001) investigated the similarities and differences of waters having these characteristics and developed a systematic classification scheme for Mode Waters by typifying them as per their formation mechanisms into a few types. The classification system proposed by Hanawa & Talley (2001) is summarized in Table 3 and illustrated in Figure 16. The different types of mode waters are described below.

5.3.1. Western Subtropical Mode Waters (WSTMW)

The term "Mode Water" was first introduced by Masuzawa (1969) in reference to the STMW in the North Pacific that forms southward of the Kuroshio extension. Worthington (1959) used the term Eighteen Degree Water (EDW) in reference to the STMW that forms south of the Gulf Stream in the North Atlantic. Both form at roughly similar latitudes which explain why their temperatures are both close to the canonical 16-18°C (Figure 17). Since this class of mode water forms in association with the western boundary currents, the name Western Subtropical Mode Water (WSTMW) is proposed here (Table 3).

WSTMW formation is modulated by outbreaks of cold continental air in winter (Kelly et al., 2010). Dense mixed layers form on the equatorward side of the western boundary currents because this is the side of the current with salty surface waters. The poleward side is typically too fresh for the cooling to be sufficient to form deep mixed layers on that side of the current. Owing to the strong influence of the air-sea heat flux, interannual perturbations of the storm tracks can affect the latitude, frequency and intensity of the cold air outbreaks that reach the formation region (Kelly et al., 2010). In consequence, large-scale modes of climate variability, such as the NAO (Joyce & Robbins, 1996), El Niño (Holbrook & Maharaj, 2008), the PDO (Qu & Chen, 2009; Davis et al., 2011; Xie et al., 2011) and the East Asian Monsoon (Taneda et al., 2000; Hanawa & Kamada, 2001) have a signature on the formation characteristics of WSTMW.

Hanawa & Kamada (2001) showed, by analyzing a 40 year record of WSTMW temperature from the North Pacific, that the western boundary current transport, in this case the Kuroshio, can also influence the properties of WSTMW on decadal timescales. In contrast, the effects of the East Asian Monsoon in the North Pacific were shown to operate on shorter inter-annual time-scales. A similar decoupling in time scales associated with particular perturbations was observed in the South Pacific. There, variations in the transport of the East Australia Current operate on longer time scales than local atmospheric perturbations over the subduction region (Tsubouchi et al., 2007). Western boundary current transports are controlled by the trade winds over the whole basin. Local heat flux perturbations over the subduction regions near the Western Boundary detachment latitude are caused by meridional or zonal displacement of the mean boundary between the trade wind regime and the mid-latitude cyclones. These types of perturbations induce rapid responses in the WSTMW properties. The response to perturbations of the whole trade wind systems driving the basin-scale subpolar dynamics, however, are likely to take longer for the full adjustment of the system, however. These types of perturbations are associated with the spin-up or spin-down of the entire gyre (Sutton & Roemmich, 2011), which explains why their effect on the WSTMW formation properties operate on the decadal scale.

WSTMWs are found in all gyres, including in the Southern Hemisphere (Roemmich & Cornuelle, 1992; Provost et al., 1999; Tsubouchi et al., 2007; Holbrook & Maharaj, 2008). There, they are found in association with the East Australia Current, the Brazil Current and the Agulhas Current, although WSTMWs are not as well developed in the South as they are in the North Atlantic and North Pacific. One reason why the subtropical mode waters of the Southern Hemisphere are less developed is because land masses located westward of the formation regions are smaller and do not reach as far poleward in the South. As such, continental air bursts in winter are not as cold or as intense in the southern subtropics.

Another reason why WSTMWs in the North are more prominent than in the South is because of the strong recirculation cells that exist equatorward of the western boundary currents in the North. Some of these recirculation features can be seen in Figure 5 (Worthington gyre, Mann eddy). The equivalent feature exists in the North Pacific, where it is known as the Kuroshio Countercurrent (Suga & Hanawa, 1995) or the Subtropical Counter Current (Xie et al., 2011). Suga & Hanawa (1995) showed that the recirculations can split into two anticyclonic gyres and affect the spreading of WSTMW into the basin. This affects the residence time of WSTMW, which can range from a few months to a year depending on the dynamical regime of the Kuroshio system (Suga & Hanawa, 1995). Thick recirculating subsurface pycnostads precondition the water column for deep convection by decreasing stratification. The weakness of recirculation cells associated with the western boundary currents in the Southern Hemisphere and the less intense win-

ter cooling result in weaker pycnostads being produced in the South.

Because the volumes of STMWs produced in each subtropical gyre of the Southern Hemisphere are smaller than in the North, temporal and spatial variability in a given STMW class is larger in the South than in the North (Roemmich & Cornuelle, 1992). This results in the layering of the WSTMW mode. The layering of STMWs in the South is also due to the lack of coherence of the western boundary current upon separation from the coast in the Southern Ocean. For example, the East Australia Current splits into multiple filaments almost instantaneously upon separation (Ridgway & Dunn, 2003). Layers associated with filaments of the separated boundary current were also observed in the North Atlantic (Harvey & Arhan, 1988). Temporal and spatial variability typically produce two or three main classes of WSTMW (Roemmich & Cornuelle, 1992; Provost et al., 1999; Tsubouchi et al., 2007).These layers are only detectable with high resolution data sets and close to their origins; however.

Layers within the main WSTMW mode also exist in the northern regimes, where it is common to see the densest (freshest and coldest) modes of WSTMW located slightly to the East and not next to the coast. The particular location of the densest mode can vary (Suga & Hanawa, 1995; Oka & Suga, 2003; Joyce, 2011) as it depends on the North-South angle of the western boundary current after separation, which affects the heat flux, the background temperature of the water, the degree of dilution with fresher subpolar waters, and the distance from the coast. Uehara et al. (2003) also point out that WSTMW formation in the North Pacific can be modulated by mesoscale eddies (preferential formation inside anticyclonic eddies), adding to the spatial and temporal variability of WSTMW formation.

Maze et al. (2009) estimated the formation of WSTMW in the North Atlantic using the thermodynamic approach of Walin (1982) and proposed net annual values between 3-5 Sv. Forget et al. (2011) investigated the seasonal cycle of WSTMW in the North Atlantic (i.e. EDW) using a similar method as Maze et al. (2009) and also calculated the volume budget of the water mass as a function of time. The results of Forget et al. (2011) reinforce the idea of the importance of seasonality for the formation of WSTMW as their result shows that the seasonal amplitude is about 6 times larger than the annual net production of WSTMW. This means that destruction (obduction, see Figure 14) of the water mass, which occurs eastward of its formation region in the North Atlantic, is a significant process that cannot be neglected, in accord with earlier studies that used the kinematic approach to estimate water mass transformation (Qiu & Huang, 1995).

WSTMW account for an estimated 3-10% of the global oceanic uptake of anthropogenic carbon. This fraction is rather uncertain, however, because the residence time of the WSTMW is relatively short, the total volume of WSTMW relatively small and because both formation and destruction of these water masses are both subject to interannual variability. These waters do not represent a long-term sink of carbon and contribute to the interannual variability of the oceanic carbon uptake (Bates et al., 2002).

5.3.2. Eastern Subtropical Mode Waters (ESTMW)

The density of ESTMW compares with the density of WSTMW. ESTMWs are found in the subtropical region equatorward of zonal tropical fronts, such as the Azores Current in the North Atlantic (Kase et al., 1985; Rudnick & Luyten, 1996; Volkov & Fu, 2010), the Kuroshio Extension front in the North Pacific, the St. Helena Front in the South Atlantic (Juliano & Alves, 2007) and more generally the subtropical front in the Southern Hemisphere (Wong & Johnson, 2003). Their influence eastward is limited by the eastern boundary currents (Canary, California and Peru Currents).

As Figures 12a-d (North Pacific and South Pacific) and 13a-c (North Atlantic) show, their volumetric importance is much less than WSTMW. This is supported by Siedler et al. (1987), who resolved the seasonal cycle of Madeira Mode Water, the ESTMW of the North Atlantic. This particular specimen of ESTMW is bounded by the density layer 26.5< σ_θ <26.8 and has a temperature of about 18°C, comparable to its WSTWM counterpart. Siedler et al. (1987) found that this water mass almost totally disappears as a volumetric mode due to mixing after about 6 months. The location where formation of this water mass occurs can be readily identified in Figure 15a and b as the local deep mixed layer region southwest of Gibraltar.

The ESTMW of the North Pacific was characterized by Hautala & Roemmich (1998). ESTMW in that basin is located on isopycnals between 24< σ_θ <25.4 and is found east of Hawaii. It forms at the subtropical-subpolar boundary between 25-30°N. It is a relatively shallow feature. Its potential vorticity minimum sits at just over 100 m and has a broad temperature range (16-22°C). Its formation area can be easily identified in Figure 15a as the local deep mixed layer region in the Eastern North Pacific, surrounded by a meander of the γ_n=25 isoneutral contour. Figure 15b shows that the seasonal amplitude of the mixed layer depth also shows a local maximum at that spot. This water mass is reminiscent of the Winter Waters that are formed around Antarctica due to winter cooling. Winter Waters are perennial features, but are most easily observable when the water surface cap is on in Summer.

A hinted at earlier, the low PV of ESTMW is largely due to the small surface density gradient (term $\mathbf{u}_b \cdot \nabla\rho_m$ in the numerator in Equation 1). The large spacing between isoneutral contours on the deepest mixed layer surface is readily visible in Figure 15a. The weak density gradient is partly caused by a low salinity tongue propagating southwestward off North America (Hosoda et al., 2001).

The reasons for the deep mixed layer maximum associated with ESTMW in the North Pacific are not clear: this feature looks rather anomalous in the middle of the open ocean and is not associated with any strong current system. Ladd & Thompson (2000) showed that evaporation and winds alone are incapable of producing the deep mixed layers at that location. One key aspect is that the restratification in summer is relatively weak in this area. As such, the summer seasonal pycnocline is readily eroded in winter, even if the winter there is not particularly harsh (Ladd & Thompson, 2000). Toyoda et al. (2004)

explain the weak summer stratification by a northward Ekman transport of salt towards the region and the strong presence of stratus clouds which lowers insolation. This is a form of preconditioning, although it is not due to the presence of an advected subsurface feature but to the peculiarity of the seasonal cycle in the region.

It is worth speculating about the fate of the ESTMW in response to increasing anthropogenic atmospheric CO_2. As the climate warms, summer stratification is predicted to increase. It is conceivable that the summer warming, and possibly freshening, may not need to be very different for the winter conditions to not be able to produce the deep mixed layer conducive to ESTMW formation. For this reason, it would seem that monitoring the evolution of these water masses (a simple mooring in the center of the ESTMW deep mixed layer region would probably suffice), could provide an interesting early warning system for climate monitoring studies. Given the difficulty of climate models to reproduce the mixed layer depth, it is not clear if a model-based proof of concept study for this hypothesis is feasible at this time. Nonetheless, forced ocean-only simulations by Hosoda et al. (2001) and Toyoda et al. (2004) are encouraging.

Wong & Johnson (2003) describe the most prominent of all ESTMWs, the specimen from the South Pacific (Figure 15 and 12a-d). These authors estimate a total subduction rate of 8.7 Sv for this water mass and a residence time of 4 years. This is much longer than all other ESTMW. Here again, weak surface density gradients created by the compensating temperature and salinity distributions, are present. The wide area over which the surface density gradient is weak explains the large formation rate. ESTMW in the South Pacific propagates far enough to contribute to the South Equatorial Current. Owing to its connection to the tropics, Wong & Johnson (2003) speculate that ESTMW could modulate ENSO dynamics by propagating equatorward wind and buoyancy perturbations from over the formation region. This proposal has yet to be formally tested.

In spite of their relatively low volumes and limited influence, ESTMWs are interesting entities that depend, for their formation, on a fragile balance between the compensating effects of the surface distribution of temperature and salinity on density. This fragility is also why they are interesting as they can be used as a warning system for climate change and also because they can be susceptible to and export atmospheric perturbations towards the equatorial region, the engine of ENSO variability. In that sense, it is possible that regional perturbations could be amplified through global ENSO teleconnections.

5.3.3. High Density Subtropical Mode Waters (HDSTMW)

The third class of mode waters identified by Hanawa & Talley (2001) are called here High Density Suptropical Mode Waters (HDSTMW). They are termed "High Density" because they are denser than either WSTMW or ESTMW, but remain subtropical in that they are formed equatorward of the subarctic or subantarctic fronts. HDSTMW form between the subtropical and subpolar fronts. Subantarctic Mode Water (SAMW) is the best example and most prominent of this type of mode water. The presence of type-III water (Table 3) has also been reported in the North Pacific, where it is often named Central Mode Water (CMW, Nakamura (1996) and Suga et al. (1997)). Renaming it HDSTMW avoids the confusion with respect to the use of the term "central water". In the North Atlantic, a form of HDSTMW is found equatorward of the NAC in the Eastern Atlantic and has been called Eastern North Atlantic Water (ENAW, Harvey (1982)). It should not be confused with ESTMW, which is Madeira Mode Water in the North Atlantic.

HDSTMWs constitute the bulk of the central waters in all basins. As shown by Suga et al. (2008) in the North Pacific, HDSTMW havs the longest residence time of all types of subtropical mode waters in the North Pacific (20-60 years). Because of their relative volume and their longer turnover times, they are the mode waters that are potentially the most interesting ones with regards to anthropogenic carbon uptake and storage. The bulk of study efforts go into WSTMW, however. WSTMW are often regarded as the "archetypical" mode water because the pycnostad associated with this mode water type is the most easily identifiable. The influence of WSTMW, however, is limited to the region around western boundary currents owing to the strong recirculation cells in these locations. Furthermore, as Bates et al. (2002) show, these waters only provide a short-term sink for carbon.

North Atlantic. Harvey (1982) was the first to describe the HDSTMW of the North Atlantic and to identify its rough formation area equatorward of the NAC. The identification of the NAC as a northern boundary for the mode waters found in the region was also noted by Pollard & Pu (1985). The formation mechanism is described in Pollard et al. (1996). Prior to the paper of Hanawa & Talley (2001), it was customary to treat this water mass as a type of SPMW, so care should be applied when reading older literature about the hydrography of the Eastern North Atlantic (i.e. Paillet & Arhan (1996)). HDSTMW can be seen in Figure 13e-f in the North Atlantic. It has a temperature between 11 and 14°C, a salinity between 35.5 and 36 psu for a density $27 < \gamma_n < 27.2$.

As can be seen on the schematic in Figure 5a and the sea surface dynamic topography in Figure 5b, the region west of France and Portugal, bounded to the North by the NAC and to the south by the Azores front appears to be somewhat separate from both the subpolar and the subtropical gyre. Pollard et al. (1996) call this region an "intergyre zone". It is still part of the subtropical circulation, however. As the spacing between mean dynamic topography contours indicates, the mean circulation is rather sluggish there. There is a latitude (about 47°N, west of Cap Finistère, in Brittany, France) where dynamic topography contours diverge, flowing either northward or southward (Figure 5b). In spite of the weak southward transport, Figure 15 clearly shows that mixed layer depths decrease southward in the direction of flow. Waters of the deep mixed layer region that follow the southward branch at 47°N are thus facing a positive mixed layer depth gradient favorable for lateral induction. Isoneutral density contours in Figure 15a further show that downstream density gradients (i.e. meridional density gradients) are weak there, implying that the density advection term in the numerator of Equation 1 also contributes to the formation

of a low PV layer in the Eastern Atlantic.

As the sea surface salinity map shows (Figure 18), this region is also characterized by a relatively high salinity for its latitude, and the temperature (Figure 17) is lower than that around 37°N, the latitude of formation of WSTMW. The net effect being that the density of HDSTMW is greater than WSTMW or ESTMW. There is, however, a strong tendency for density compensation along the path of the NAC, or along the path of detached western boundary currents in general. So even if the density of HDSTMW in higher than that of WSTMW in the North Atlantic and North Pacific, the difference is attenuated by the compensation process. The degree of density compensation is captured on θ/S diagrams by the slope of the Central Water lines (Figure 3). A shallow slope indicates a strong compensation effect.

North Pacific. HDSTMW in the Pacific is visible in Figure 12fo, in the central North Pacific, east of WSTMW. The separation between these two types becomes apparent in Panel 12f. It appears to be the most voluminous type of mode water in the North Pacific. The spreading of WSTMW is constrained by the strong recirculation cells associated with the western boundary current, limiting the influence of that water mass on the basin scale (Suga et al., 1997). HDSTMW is the largest contributor to the central waters of the North Pacific subtropical gyre (Toyama & Suga, 2011).

Pacific HDSTMW has a temperature between 10-13°, a salinity between 34 and 34.5 psu with a main core bounded by 26.0< γ_n <26.6 (Suga et al., 2004). It was first characterized by Nakamura (1996) who named it Central Mode Water (CMW). It forms between the Kuroshio Extension (its southern boundary) and the Kuroshio Bifurcation (its Northern Boundary) fronts. The mixed layers in the formation region of HDSTMW are deeper there than anywhere else in the North Pacific, reaching 200 m (Figure 15), explaining its volumetric importance. Eastward propagation of thick mixed layers in a band of elevated heat loss along the North Pacific Current at the subpolar-subtropical boundary contributes to the upstream preconditioning that weakens downstream stratification and allows increasingly thick mixed layers eastward (Suga et al., 1997). As can be seen in Figure 15a, isoneutral contours start to diverge where the thick mixed layer patch suddenly stops.

Suga et al. (2004) questioned the importance of lateral injection as the dominant subduction process. As can be seen in Figure 12f-o, the bulk of the HDSTMW is found west of 200°E, the longitude where deep mixed layers between the two Kuroshio fronts shoal. Furthermore, as can bee seen in Figure 15a, isoneutral contours on the surface of deepest mixed layer are nearly zonal, aligned with the dominant eastward velocities in the deep mixed layer region of the central North Pacific. As such, the Lagrangian density gradient (i.e. the density gradient calculated along the stream path of a water parcel) is weak. Suga et al. (2008) performed a Lagrangian subduction calculation and confirmed the suggestion of Suga et al. (2004) that in fact, the dominant formation mechanism for Pacific HDSTMW is the small density advection rate (numerator term in Equation 1).

Shifts in the thermohaline properties (increase in temperature and salinity, decrease in density) of Pacific HDSTMW were recorded in 1988/1989 (Suga et al., 2003). These shifts are thought to be linked to a weakening of the Aleutian Low. A weaker Aleutian Low yields weaker westerlies and changes the SST distribution owing to the spin-down and a corresponding widening of the subtropical gyre. Variability, both spatial and temporal, can induce a layering of the HDSTMW mode. Such a layering can be seen in the North Pacific with a light and a dense class of HDSTMW (Mecking & Warner, 2001; Oka & Suga, 2005).

Southern Ocean. SAMW is volumetrically the most important of all mode waters and it extends throughout the Southern Hemisphere. It is classified as HDSTMW as it forms between the subtropical front and the subantarctic front (Figure 15b). The gradual densification and southward spiraling progression from the Atlantic to the Southeast Pacific described by McCartney (1977) can be seen in Figure 13o and 13a-g. The deep mixed layers associated with the formation of SAMW are also very clear in Figure 15. The lightest SAMW mode is found in the South Atlantic, where the subantarctic front is most equatorward. The temperature and salinity for the lightest type of SAMW is about 15° and 35.5 psu (Figure 3). The densest type, essentially AAIW$_{PAC}$ (see intermediate water section) has a temperature of nearly 5°C and a salinity of 34.2 psu. Neutral density for SAMW is 26.5< γ_n <27.3.

While Figures 13 and 15 may provide a sense of circumpolar continuity in the SAMW formation process, detailed estimates of the formation (Sallée et al., 2006, 2008, 2010b) and subduction rates (Karstensen & Quadfasel, 2002a; Qu et al., 2008) and close inspection of hydrographic sections for the distribution of PV and CFC in the Southern Ocean (Herraiz-Borreguero & Rintoul, 2011; Hartin et al., 2011) show that SAMW isoneutrals are ventilated most intensely at 6-7 "hotspot" locations on the circumpolar path. The major regions of formation are in the Southeastern Indian Ocean and Pacific, where the deepest mixed layers are found (Figure 15). Influential topographic features are located at the Kerguelen and the Campbell Plateau at 70-80°E and 170°E and at 140-150°W where the mid-ocean ridge turns equatorward.

Formation rates in the South Pacific converge to an average of 10-15 Sv, as estimated from CFC data (Qu et al., 2008; Hartin et al., 2011). Another 20-30 Sv is formed in the Indian Ocean (Sloyan & Rintoul, 2001; Karstensen & Quadfasel, 2002b,a) and 9-10 Sv in the South Atlantic (Karstensen & Quadfasel, 2002a). Formation rates from different studies (Macdonald et al., 2009; Qu et al., 2008; Karstensen & Quadfasel, 2002b; Sloyan & Kamenkovich, 2007) are difficult to compare as they often use different layer boundaries, do not always provide separate estimates for SAMW and AAIW, and the different techniques measure different properties (ventilation, subduction, transport, export). Overall, however, studies concur in giving a sense that formation is smallest in the South Atlantic, largest in the Indian and intermediate in the Pacific.

Kinematic Lagrangian subduction calculations (Karstensen & Quadfasel, 2002a; Qu et al., 2008) indicate that the lateral induction term dominates the vertical pumping term (see Equa-

tion 1). The importance of the induction term arises from topographically steered meanders of the ACC. When the ACC crosses the mid-ocean ridges or shallow topography, the current is displaced equatorward to maintain the vorticity constraint. Downstream of the topographic feature, the ACC returns poleward. These meanders (not resolved in Figure 15b) cross the deep mixed layer band thus alternating through regions of positive and negative mixed layer depth meridional gradients. Since the total transport of the subantarctic front and other ACC filaments accounts for a large fraction of the total ACC 135 Sv transport (measured at the Drake Passage), subantarctic front meanders can contribute large SAMW fluxes. Note that a meander returning poleward can induce similarly large obduction rates into the mixed layers.

Since the location of ACC meanders are largely fixed by topography, variability in the formation rate and properties of SAMW are mostly caused by buoyancy effects on the development of the mixed layer or by the winds, by affecting Ekman transport. Investigating an observed cooling and freshening of the SAMW layer South of Australia, Rintoul & England (2002) concluded that air-sea heat and freshwater fluxes were insufficient to account for the magnitude of the changes and for the density compensating nature of the observed thermohaline variations of the SAMW layer. Rintoul & England (2002) used a climate model to show that cooling and freshening events of appropriate magnitude can be caused by variability in the Southern Ocean wind stress. Their diagnostics indicate that the cause is increased meridional Ekman transport of colder and fresher waters across the subantarctic front into the deep mixed layer regions. The importance of winds as a leading agent for change is also suggested by Sallée et al. (2010a). Sallée et al. (2010a) analyzed deep mixed layers variability using ARGO data and showed zonally asymmetric wind perturbations caused by the Southern Annular Mode (SAM), the dominant mode of interannual variability in the Southern Ocean, affected the heat budget of the mixed layer.

Investigating observational variability of the SAMW and AAIW layers in the Drake Passage, Naveira Garabato et al (2009) found that interannual SAMW variability in the Southeast Pacific appears to be mostly controlled by ENSO-modulated variations in air-sea heat flux and evaporation. Constructive interference between ENSO and SAM in 1998 resulted in an Ekman dominance of SAMW formation due to the strong shifts in the winds, however, consistent with earlier work by Rintoul & England (2002) South of Australia.

The role of Southern Ocean eddies is a controversial topic. Eddies are thought to play a role in the physical controls of the ACC current system, the thermohaline circulation, tracer transports, biological effects and air-sea exchange. With regard to the influence of eddies on SAMW characteristics, Sallée et al. (2008) evaluated their influence by performing a heat budget calculation for the mixed layer waters in the Southern Ocean, considering the effects of surface heating, and vertical and horizontal diffusion by eddies. In this case, Sallée et al. (2008) approximated the eddy flux using the GM parameterization of Gent et al. (1995) applied to ARGO data.

The results of Sallée et al. (2008) highlight two main points. While the role of eddies for the heat budget of the waters in the mixed layers vanishes when integrating zonally, locally, they can be very important and can enhance the stratification, attenuating the development of deep mixed layers in certain regions. Secondly, regions where the eddy heat flux is large are systematically located southward of the poleward flowing western boundary currents. These currents inject not only heat but also salt. In that sense, the distance of the Southeast Pacific from the subtropical influence of a western boundary current contributes to the coldness and freshness of the waters that form AAIW_{PAC}. The influence of the western boundary currents on the development of deep mixed layers is apparent in Figure 15, where mixed layers are shallow in the Agulhas region and Southeast of New Zealand.

Finally, owing to their global importance for carbon and heat uptake, their near equilibration with atmospheric gases and their residence times of order a few decades, it is important for climate models to accurately simulate HDSTMW, particularly in the Southern Ocean. The current generation of climate models, however, generally produce SAMW layers that are too thin, too light and of limited equatorward extent (Sloyan & Kamenkovich, 2007). Their small volumes may influence their sensitivity to variability and their vulnerability in climate change simulations. The difficulty of climate models to simulate mixed layer dynamics correctly is a bottleneck for improved mode waters simulations (Boé et al., 2009b; Carman & McClean, 2011).

5.3.4. Subpolar Mode Waters (SPMW)

Waters identifiable as SPMW are found in association with the subpolar gyres or, in the Southern Ocean, equatorward of the Polar Front. Water masses that could be classified as SPMW have been observed in the North Atlantic, where they were first defined (McCartney & Talley, 1982). In the Southern Ocean, the densest form of mode water in the Southeast Pacific forming between the subantarctic and subpolar front that contributes Pacific-type AAIW (McCartney, 1977) can be classified in this group. Pacific-type AAIW will not be discussed further here; see the earlier discussion on low-salinity intermediate water for details about this water mass.

A water mass known as Dichothermal Water (DTW) has been identified in the North Pacific subpolar region. This water mass is a local subsurface temperature minimum found in the western subpolar gyre and in the adjacent Okhostk and Bering Seas at a rather uniform depth of about 80-140 m throughout the subpolar North Pacific with a density of about σ_θ=26.6 (Ueno & Yasuda, 2003). Dichothermal Waters are here tentatively classified as SPMW in the North Pacific. Dichothermal Water are part of the so-called "mesothermal structure", which is composed of two layers: the Dichothermal Water, and the waters below that form a local temperature maximum, the Mesothermal Water (MTW) (Uda, 1963; Favorite et al., 1976; Miura et al., 2002; Endoh et al., 2004; Ueno & Yasuda, 2005).

Just as with SPMW in the Atlantic, DTW is high in oxygen and is well ventilated. Deep mixed layers do not form in the subpolar North Pacific because of the strong halocline there, explaining the limited vertical reach of SPWM in that

basin compared to the >500 m reach of SPMW in the North Atlantic. This strong halocline also explains why waters in the mixed layer can be colder than waters below it and result in a subsurface temperature minimum. A similar situation was seen around Antarctica with respect to the formation of Winter Waters. Figure 15 shows that the deepest mixed layers in the subpolar North Pacific are found in the western Bering Sea. Miura et al. (2002) postulated that this is also the most likely site of formation for the dichothermal SPMW of the North Pacific. DTW are transported into the North Pacific by the Kamchatka Current. Model results confirm this hypothesis (Miura et al., 2003), but another source, which is local to the North Pacific, south of the Bering Sea, has since been suggested. This second source forms seasonally, east of the Kamchatka Peninsula (Ueno & Yasuda, 2005; Ueno et al., 2007). Because it is so shallow, its volume so small and its residence time short (of order of a few months to a year), the temperature minimum layer is prone to signifiant sub-annual to interannual variability, driven by variation in the degree of winter surface cooling (Masuda et al., 2006).

In the North Atlantic, the name SPMW stops being used for densities higher than σ_θ=27.75. Westward (or above that density level), names such as Irminger Sea Water and Labrador Sea water are preferred. These latter water masses form convectively and were discussed earlier in the section on low salinity intermediate water. The focus here is on waters lighter than $\sigma_\theta \leq$27.75. The deep mixed layer (up to 500 m thick) associated with the formation of SPMW in the North Atlantic is also clearly visible in Figure 15. Both Panels 15a and b show a relative minimum (a saddle point) in the depth of the mixed layer along Greenland just south of the Denmark Strait Overflow. This separation corresponds to the σ_θ=27.75 level, illustrating the boundary between intermediate and mode waters. To the southeast, the separation between HDSTMW (i.e. ENAW) and SPMW is not clear, although Talley et al. (2011) suggest that SPMW starts where the North Atlantic Current bifurcates northeastward near the British Isles (see Figure 5). This corresponds roughly with the 11° isotherm (Figure 17). The lower temperature of SPMW correspond to the upper temperatures of LSW, about 4.5°C (see Figure 3b). Salinities range between 35 and 35.5 psu.

SPMW in the North Atlantic was described by McCartney & Talley (1982), although its formation and distribution has recently been reassessed by Brambilla & Talley (2008) and Brambilla et al. (2008). These latter studies emphasize the role of topography (Rockall Plateau and Reykjanes Ridge) and of the local circulation in the Rockall Trough, Iceland Basin and the Irminger Basin. As shown schematically in Figure 5a, branches of the NAC are found in each one of these basins, where each filament is steered by the ridges separating each basin and flows cyclonically, being bounded northward by the GIN straits. These filaments of the NAC are known as the Iceland-Faroe Front in the Iceland Basin and the subarctic front in the Irminger Basin (Brambilla & Talley, 2008). Brambilla & Talley (2008) show that a sequence of SPMW layers exists in each one of these basins, refining the assessment of McCartney & Talley (1982) with regard to a continuous densification along the subpolar gyre. SPMW from the Rockall Trough and and Iceland Basin may enter the Nordic Seas. This is indicated in Figure 3b by the dotted magenta arrow labeled with the Norwegian Atlantic Current (NwAC) and the East/West Spitsbergen Currents (E/WSC). The effects of topography can be inferred in Figure 13k and l by the elongated shape of the thick layers SPMW layers. The broad-scale counter-clockwise evolution and densification process (cooling and freshening) characteristic of North Atlantic SPMW formation (McCartney & Talley, 1982) is evident in the isoneutral thickness sequence shown in Figure 13d-n.

Subsurface export of SPMW below the mixed layer, while still a consequence of subduction, is slightly different than traditional WSTMW subduction. SPMW interacts with the Nordic Seas overflow and it is thus subducted partly through this entrainment process (Brambilla et al., 2008). SPMW thus directly impacts NADW properties. Brambilla et al. (2008) estimate the average air-sea buoyancy diapycnal formation rate of SPMW to be about 14±6.5 Sv, with a peak to nearly 30 Sv at a density of σ_θ=27.35. Isopycnal subduction contributes an additional 7-15 Sv.

Increasingly deep mixed layers (Figure 15) along the subpolar gyre are facilitated by a sequential preconditioning process, a process that is rather similar to that which explains the southeastward progression of the mixed layers in the Southern Ocean (McCartney, 1977). Since the direction of flow is northward, waters from the mixed layers move towards locations with colder surface conditions, which are conducive to convective overturn. This deep mixing is facilitated by the fact that inflowing waters (from the South) are already weakly stratified.

SPMW variability, in terms of property changes, volume or formation rates, is dominated by the NAO (Dickson et al., 1996; Sarafanov, 2009). In the low NAO phase, the subpolar gyre contracts westward and SPMW become warmer and saltier owning to the enhanced influence of the NAC subtropical waters (Bersch, 2002; Hakkinen & Rhines, 2004; Hatun et al., 2005). SMPW cools and freshens during high NAO phases. The bulk of these adjustments results from changes in the circulation field and not from the changes in the air-sea buoyancy fluxes (Thierry et al., 2008).

The resolution of North Atlantic SPMW in CMIP3 climate models suffers from significant biases, mostly in the salinity (Carman & McClean, 2011). These models have a difficult time producing SPMW in their actual observed locations, i.e. the Rockall Trough, the Iceland Basin and in the Irminger Basin. Carman & McClean (2011) point out that some models form waters of SPMW characteristics too far southward, at the location of HDSTMW, southwest of the British Isles. These deficiencies result in significant biases in the properties of Atlantic Waters that feed into the Nordic Seas and also affects the salinity of NADW. The SPMW biases are most likely caused by errors in the winds over the North Atlantic, which affects the dynamics of the subpolar gyre, i.e. the gate keeper for salt transport into the Nordic Seas. Since ocean temperatures can significantly affect the wind patterns in that region, it is not directly obvious how improvements in the SPMW properties and their northward export can be achieved. It is expected, however that

improved parameterizations of the GIN overflows, which can influence the path of the Gulf Stream (Zhang & Vallis, 2007), would greatly improve the CMIP3 simulations, including the North Atlantic wind field.

As Hanawa & Talley (2001) point out, the Ross and Weddell Sea gyres are also wind driven gyres, similar to the subpolar gyres with respect to the sense of rotation and to the low sea-surface height at their centers. Further research is necessary to evaluate if a form of SPMW forms in these gyres. One could imagine that this is in fact the case and that these waters do help in weakening the stratification to enhance convective mixing over the continental shelves of the Ross and Weddell seas, in a process that is essentially similar to the progression of SPMW around the subpolar gyre of the North Atlantic, which culminates with the formation of LSW. Owing to the similarity of the formation process of Winter Waters with the formation of the dichothermal waters in the North Pacific, it is perhaps justifiable to classify Winter Waters as a class of SPMW for the Antarctic.

5.3.5. High Salinity Subtropical Underwaters (HSSUW)

HSSUW (Table 3) marks the shallow subsurface salinity maximum of the subtropical gyre (O'Connor et al., 2002, 2005). These waters are often referred to as Subtropical Underwaters (STUW), Tropical Waters or Salinity Maximum Waters (Blanke et al., 2002) in the literature. Types of HSSUW are found in all gyres. It owes its salinity maximum both to the high evaporation rates that provides the high salinity source, but also to the fact that HSSUW subduct underneath fresher waters, highlighting their higher salinities in the subsurface.

Their temperatures are consistently around 20°C, indicating some consistency with regards to their latitudes of origin. Their salinities vary according to the characteristic salinities of the ocean basins and particular gyre systems. The saltiest are found in the North Atlantic and the freshest in the North Pacific. These waters can be readily identified by their salinity maximum on the θ/S diagram (Figure 3). Their volumes are very small and their thickness is at most of order a few tens of meters. They are the lightest waters that are discussed here. The densest variety is found in the North Atlantic and peaks at σ_θ=26.0 (see Figure 12i). The zonal location of the surface salinity maximum varies in each basin (Figure 18). It is centrally located in the North and South Pacific, but it is slightly offset towards the eastern side of the North Atlantic and towards the western side of the South Atlantic. In the Indian Ocean, it is located towards the East.

O'Connor et al. (2002) calculated the subduction rate of HSSUW in the North and South Pacific to be 4-5 Sv and 6-7 SV respectively. An alternative method using CFCs reaches a similar conclusion, with a larger formation rate in the south than in the north. Using the same techniques, O'Connor et al. (2005) estimate subduction rates in the North Atlantic (2 Sv) and in the Indian Ocean (1 Sv). These are much smaller than in the Pacific.

O'Connor et al. (2005) also performed a decomposition of the subduction equation (denominator in Equation 1) into its constituent terms for the HSSUW of each gyre. Their results show that vertical Ekman pumping is typically the dominant term, in contrast with all other types of mode waters, where decompositions of the subduction calculation showed this term to contribute only small fluxes. Lateral induction is shown to be negligible in the gyres of the Northern Hemisphere. Lateral induction is about 30% of the magnitude of the vertical Ekman pumping term in the South Pacific so both contribute to the formation of HSSUW in that basin. This term is, however, large and negative in the Indian Ocean, indicating that it contributes to entrainment of high salinity water into the mixed layer instead of detrainment into the ocean interior. O'Connor et al. (2005) explain that this is a reflection of the poleward location of the high evaporation region in the Indian Ocean. Formation of HSSUW in the Indian Ocean is driven by vertical pumping.

The relevance of HSSUW on the larger scale is in that they export high salinity around the subtropical gyres in what is referred to as the "salt river" (Qu et al., 2011). HSSUW participate in the circulation of the subtropical cells (Blanke et al., 2002; Zhang et al., 2003; Hazeleger & Drijfhout, 2006). In spite of their low volumes, they can influence the properties of the upward branch of the Atlantic meridional overturning (Zhang et al., 2003) and ultimately convective overturning in the North Atlantic (Latif et al., 2000). Using a Lagrangian analysis, Blanke et al. (2006) estimate that as much as 60% of the waters that participate in the northward meridional overturning transport between 45°S and 47°N has been influenced by at least one of the HSSUW types in the Atlantic. The net salinity change of a water parcel moving northward in the Atlantic represents essentially a balance between the effects of salinification by mixing with HSSUW and freshening in the ITCZ equatorial region. The net salinification can be seen on the θ/S diagram by the salinity offset between the central waters mixing line of the South Atlantic and the North Atlantic (Blanke et al., 2006).

6. Synthesis and conclusion

The intent in writing this review was to provide, in a single document, a full account of the main water masses of the ocean. Information about water masses is spread widely in the literature and I believe that there is some value in gathering all this information into a compendium. A large fraction of the information presented here can be found in the recently published book by Talley et al. (2011), although the material there is organized very differently, by ocean basins. I chose here to organize the material going from high latitudes to the tropics, or from the deep and bottom waters to the mode waters, as this naturally pulls together the water masses that have a comparable role in the ocean-climate system.

While each water mass is described in quite a bit of detail, there are many aspect that have not been discussed here. One notable omission is a discussion of paleo-hydrographic reconstruction. The text above is also not very good in providing an assessment of water mass transport. Summarizing transports and formation rates is a very difficult task as it is not always clear how the different measures should be compared.

A summary table of the water masses with water type definitions for each one was purposefully left out. The reason is that

while it is helpful to use water masses as practical construct to communicate about the ocean or to define a system of study, the particular division of the water masses that will be most helpful depends on the problem under evaluation. For example, a water type definition of NADW would be of value in the global context, but as was made clear in the discussion about NADW, NADW itself is constructed by a convoluted mixing process involving many precursor water masses and even includes mixing with an old, aged, recirculating version of itself. People interested in using the concept of water type and linear mixing models would thus be better off finding their own definitions. Definitions based on isoneutral layers are avoided also, for similar reasons. As the volumetric θ/S presented here shows (Figure 3), the ocean is a continuum and hard water mass boundaries do not usually exist on very large scales. Hard density boundaries only exist across fronts or across clearly defined basins separated by topography.

Volumetric θ/S diagrams calculated from the CMIP3 set of global climate models were presented to illustrate the difficulty these models have in representing water masses accurately. These volumetric θ/S diagrams show, however, that many of the models are able to capture the large scale stratification. That is, models have bottom waters, deep waters, intermediate salinity minima and central waters. As was indicated on a few occasions, water mass formation is sometimes impacted by very small bathymetric features, such as Maud Rise in the Weddell Sea, or Orphan Knoll in the Labrador Sea. Models presented here do not include small topographic features such as these. It was also shown that overflows and entrainment at the overflows can depend strongly on the local topography, e.g. the presence of sharp canyons. Improvement in the representation of the overflow process will doubtlessly result in greatly improved simulations. Mode and intermediate water formation are critically dependent on the winds and on the ability of models to model the mixed layer, which, as was the case for ESTMW of the North Pacific, can also depend on peculiarities of the seasonal cycle of buoyancy flux. As water mass formation often requires cold winter air bursts, small zonal or meridional shifts in the winds can have a dramatic impact on the formation characteristics of these water masses.

Many of the details presented above may seem excessive considering the state of climate models today. It is possible, however, that some of the local details presented above may become relevant in the upcoming model inter-comparison exercises with the new generation of global climate models (CMIP5) as these models benefit from improved resolution and parameterizations.

7. Acknowledgements

I would like to thank support from the UK GEOTRACES project and the Oxford James Martin School by means of a James Martin postdoctoral fellowship, in addition to years of financial support and guidance from J. L. Sarmiento, who was my mentor while I was a graduate student in his group, when I started writing this review.

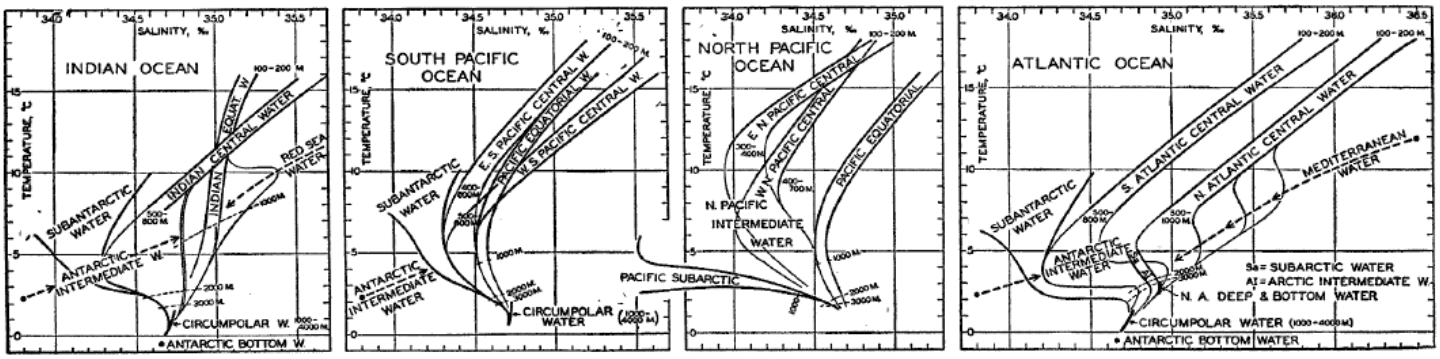

Figure 1: θ/S relationships of the principal water masses of the world proposed by Sverdrup et al. (1942). Figure reproduced from Sverdrup et al. (1942).

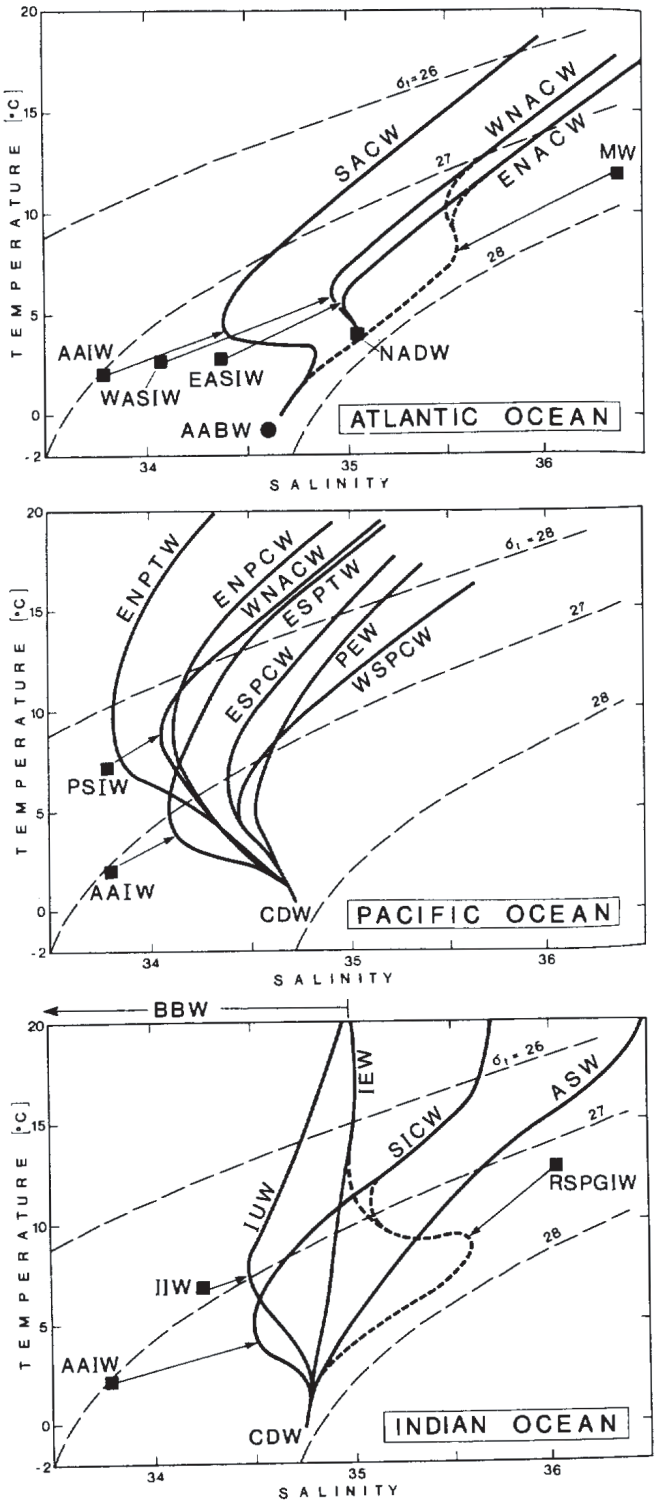

Figure 2: θ/S relationships of the principal water masses of the world proposed by Emery & Meincke (1986). Figure reproduced from Emery & Meincke (1986). Nomenclature for central waters (CW): leading "E/W" for East/West followed by the "N/S" for North/South, "A/I/P" for Atlantic, Indian, Pacific. E/WASIW: Eastern/Western Atlantic Subarctic Intermediate Water, MW: Mediterranean Water, PSIW: Pacific Subarctic Intermediate Water, PEW: Pacific Equatorial Water, IEW: Indian Equatorial Water, ASW: Arabian Sea Water, IUW: Indonesian Upper Water, IIW: Indonesian Intermediate Water, RSPGIW: Red Sea and Persian Gulf Intermediate Water.

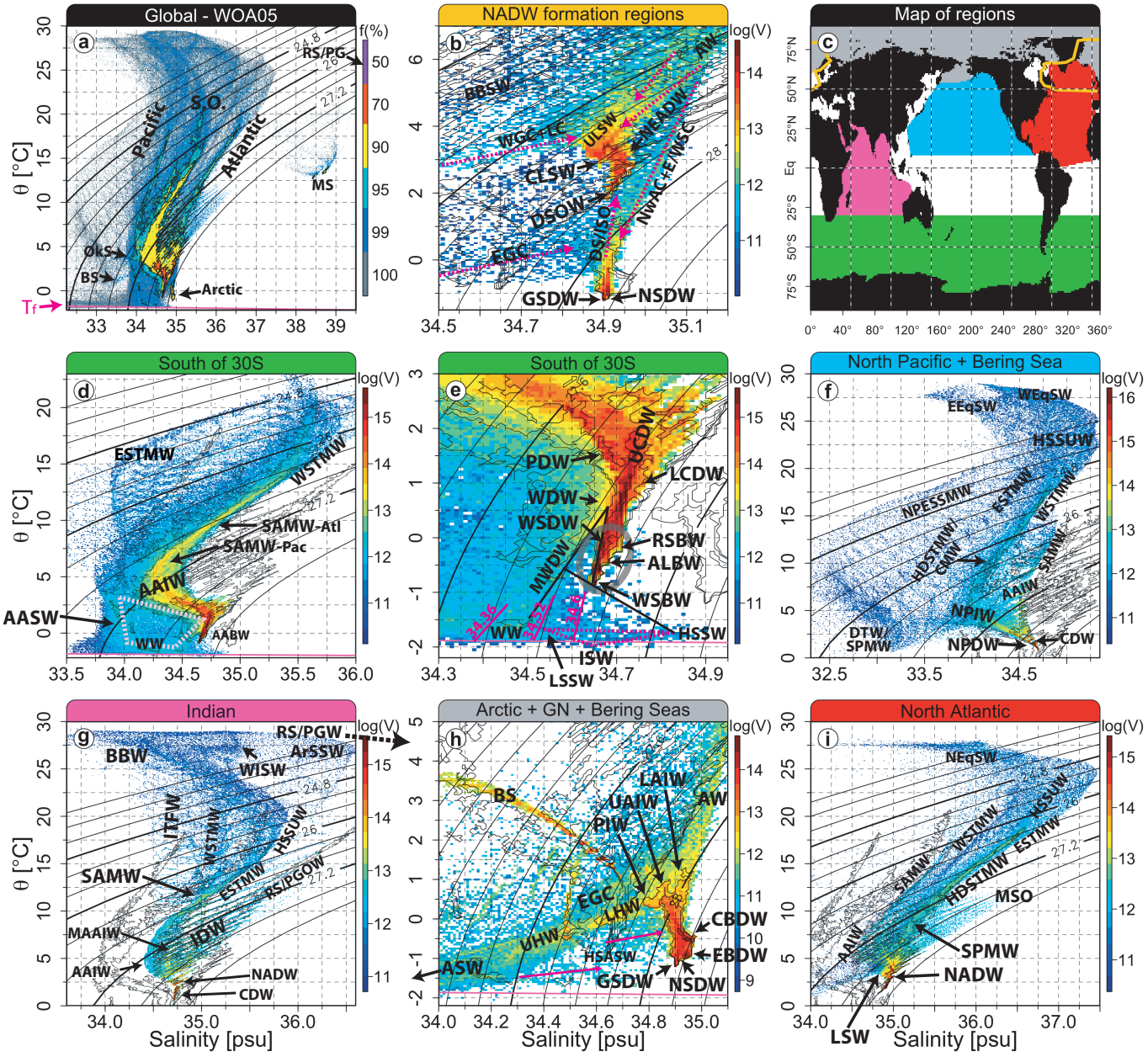

Figure 3: Annotated volumetric θ/S diagrams generated from the annual $1^o \times 1^o$ WOA05 climatology. a) Global domain, b-i) specific diagrams from regions shown in c). The color scale in panel a) is designed to show the fractional cumulative volumetric distribution, ranked from the θ/S bin with largest volume to that of lowest volume. For instance, all colors up to yellow (i.e. purple, orange, yellow) together account for 90% of the global ocean volume. Other panels show the base-10 logarithm of the volume in each θ/S bin. Water mass annotations (Table 2) are indicative of θ/S regions where each water mass is dominant. Label locations should not be interpreted as "end-member" properties. σ_θ isopycnals are shown for reference. The freezing point of seawater (T_f) is shown as a nearly horizontal magenta line and is reproduced in multiple panels. Magenta arrows and black/pink line segments suggest dominant mixing interactions. In panel a), MS=Mediterranean Sea, S.O.=Southern Ocean, Oks=Okhotsk Sea, BS=Bering Sea. Dashed lines/arrows indicate approximate mixing lines and/or flow direction.

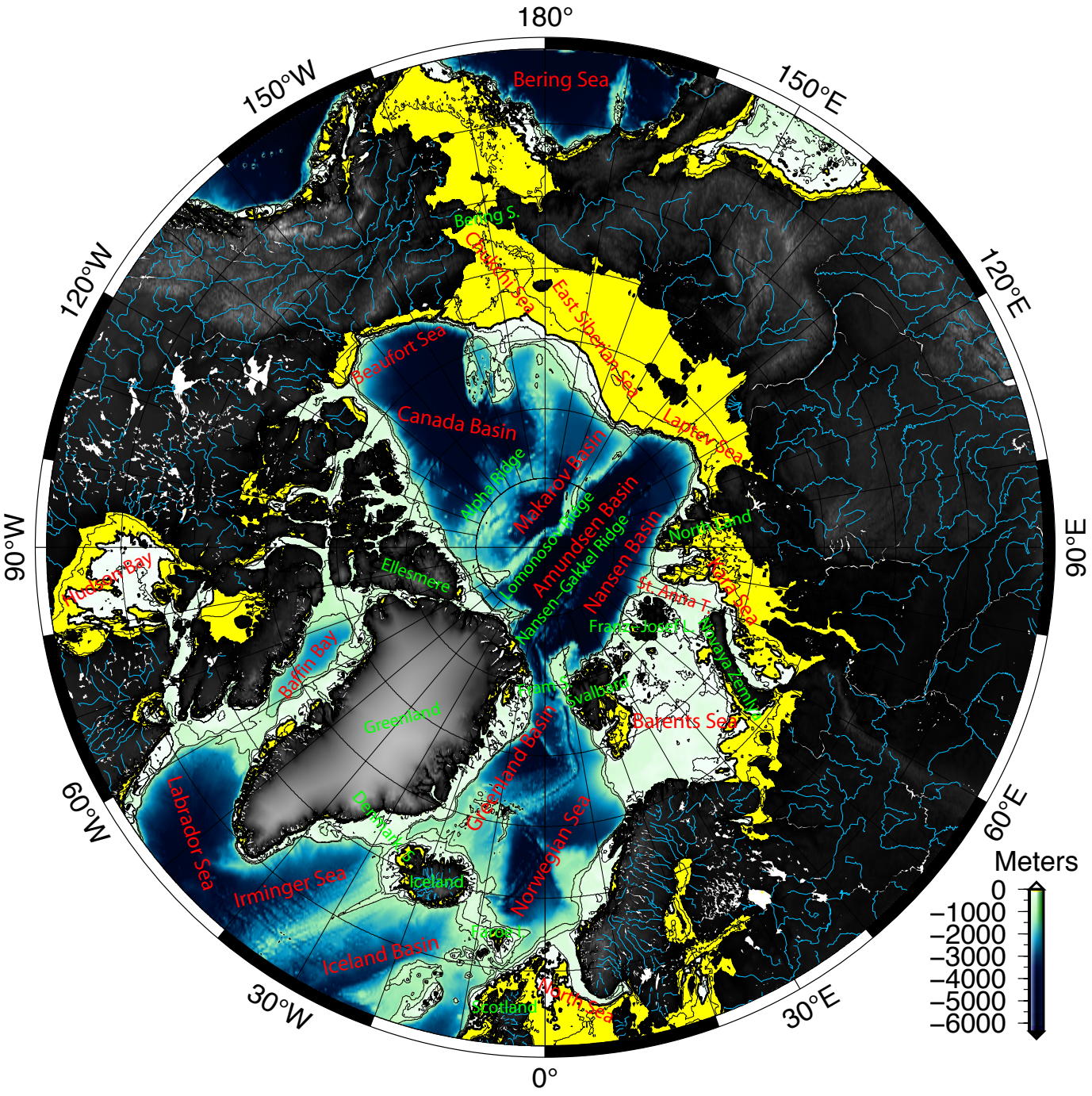

Figure 4: Topographic map of the Arctic region highlighting the names of relevant hydrographic basins in red and other features in green. Black contours are drawn at 50 m, 200 m, 500 m and 1000 m. Shelf regions shallower than 120 m are shaded yellow.

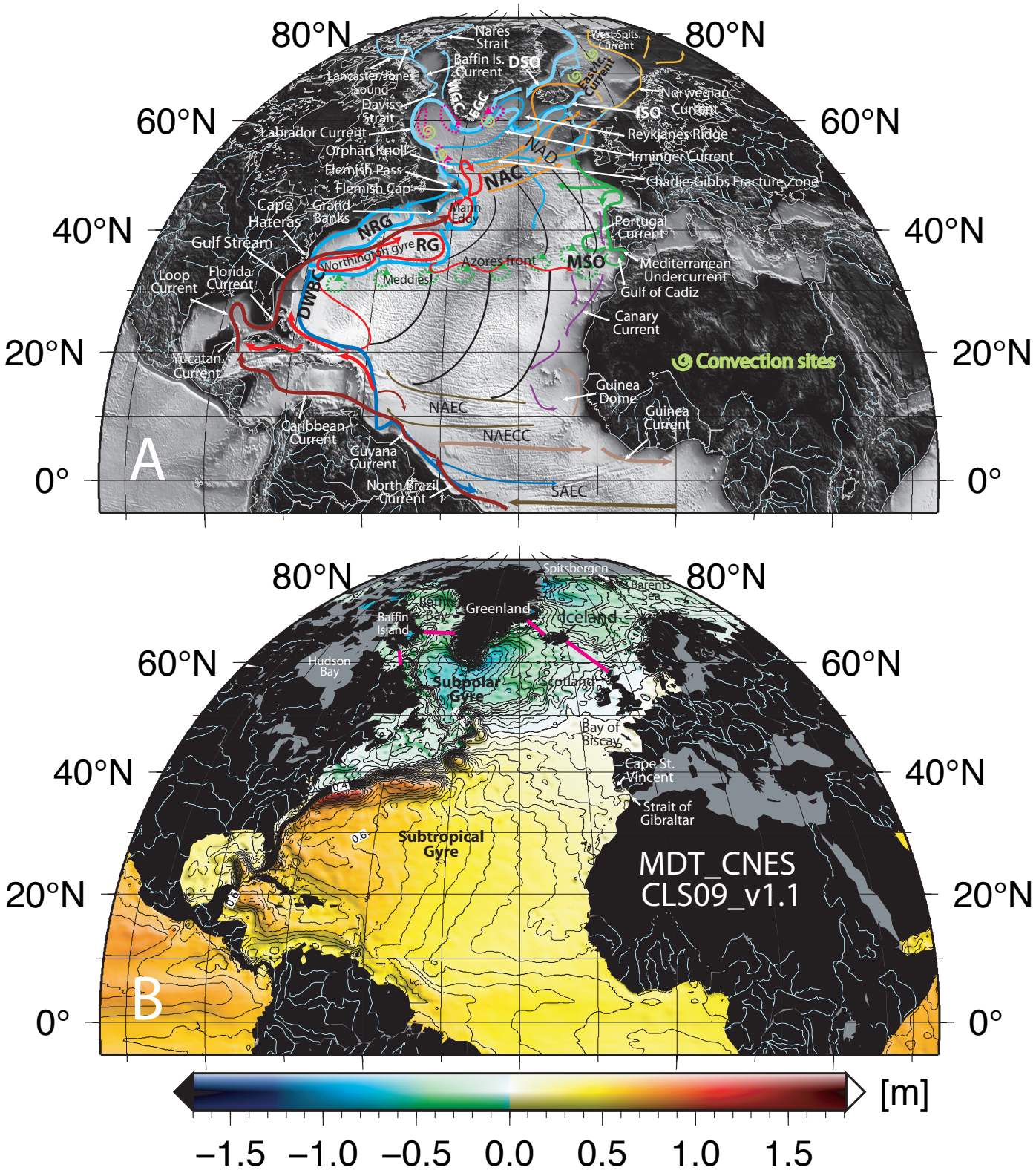

Figure 5: a) Schematic circulation of the North Atlantic. DSO: Denmark Strait Overflow, ISO: Iceland-Scotland Overflow, WGC: West Greenland Current, EGC: East Greenland Current, NAD: North Atlantic Drift, NAC: North Atlantic Current, NRG: Northern Recirculation Gyre, DWBC: Deep Western Boundary Current, NAEC: North Atlantic Equatorial Current, SAEC: South Atlantic Equatorial Current, NAECC: North Atlantic Equatorial Counter Current. Colors are subjective and are only used to group similar circulation features for cosmetic reasons into upper (reds), intermediate (orange, green, light blue) and deep (blues) circulations. b) Climatological combined mean dynamic topography (MDT CNES-CLS09 v1.1) for the period 1993-1999 (Rio et al., 2009).

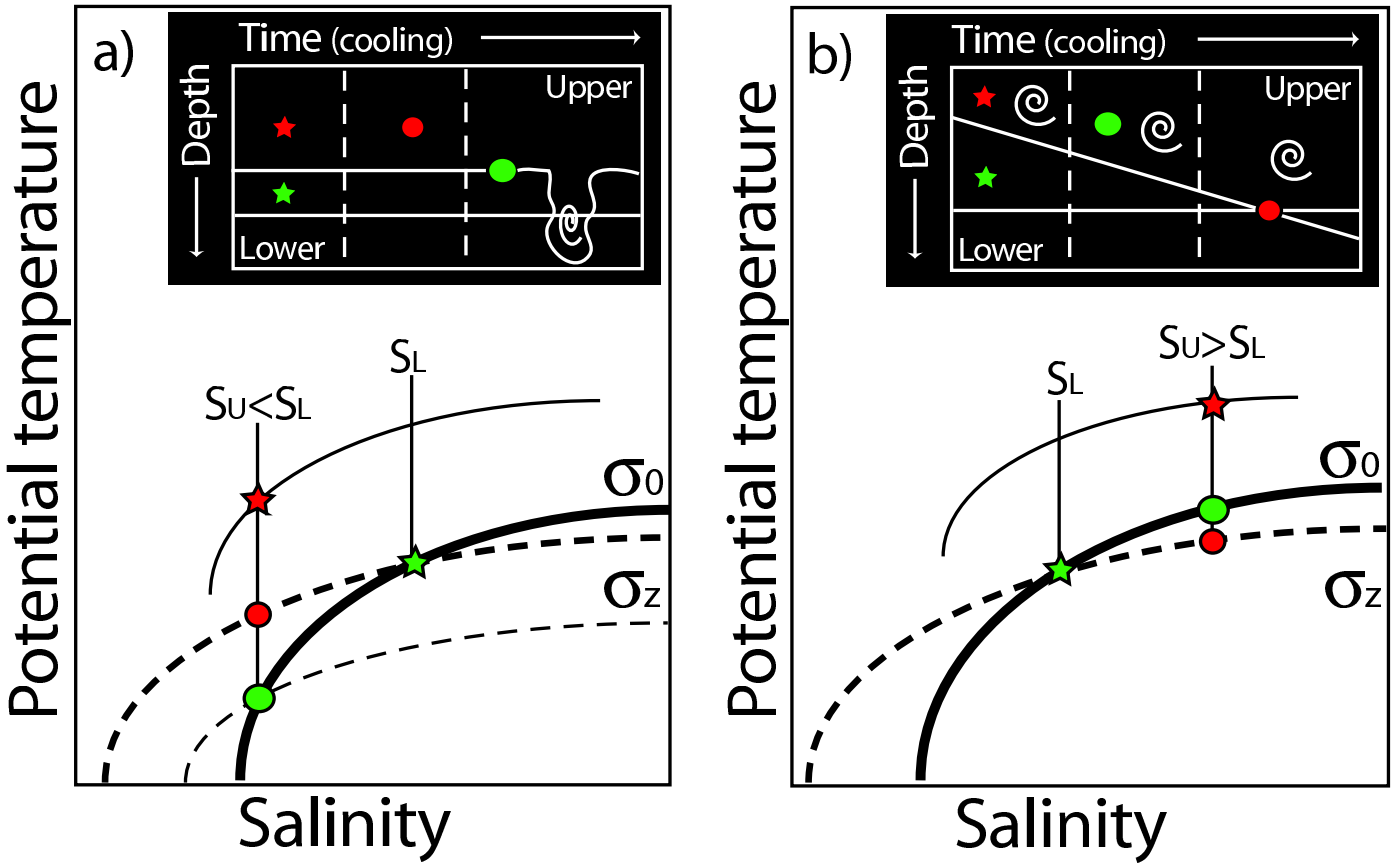

Figure 6: Schematic illustrating the controlling influence of the subsurface water mass (S_L) on the convective ability of the upper water mass (S_U) for cases a) when the upper layer (red star) is fresher than the layer underneath (green star) and b) when the upper layer (red star) is saltier than the layer underneath (green star). In a), as the upper layer cools (red point), because of the nonlinearity of the equation of state of seawater, the water at the surface can have a density evaluated at depth (σ_z) that is denser than if that density were evaluated at the surface (σ_0). Further cooling is necessary for the upper water to match the density of the subsurface water (green point). At this point, convective overturn occurs without further cooling since the density of the upper water is already denser than the density of the deeper layer. In b), the density of the upper water column, even evaluated at depth, is always lighter than (green point) or as dense as (red point) the water underneath. Constant cooling is required to deepen mixing. Adapted from (Aagaard & Carmack, 1989).

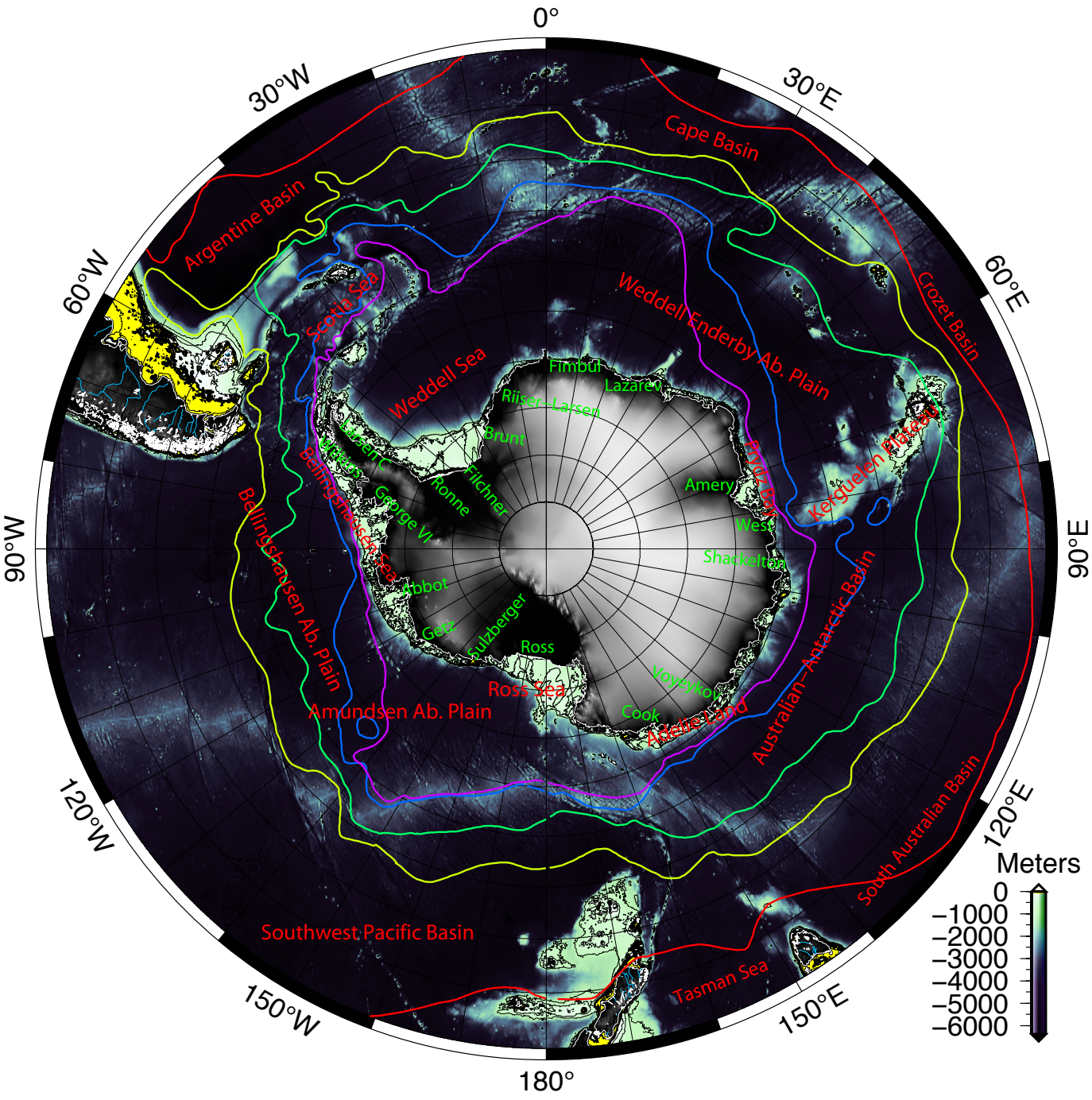

Figure 7: Topographic map of the Antarctic region highlighting the names of relevant hydrographic basins (red), the largest ice shelves (green) and the mean position of the Southern Ocean fronts after Orsi et al. (1995): Subtropical front (red), Subantarctic front (yellow), Polar front (green), Southern ACC front (violet) and southern Boundary of the ACC front (magenta). Black contours are drawn at 100m, 200m and 1000m.

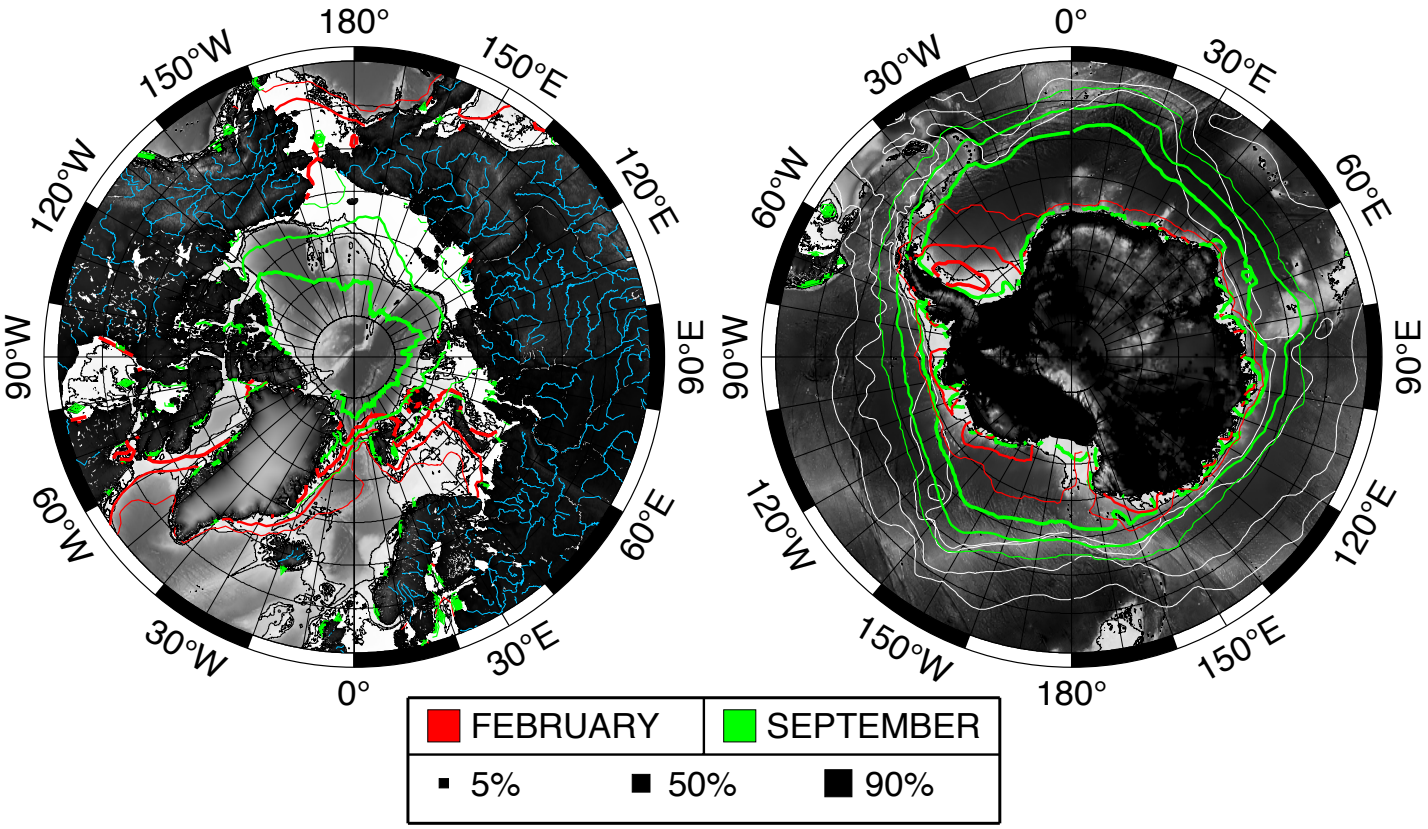

Figure 8: Climatological sea-ice concentration isolines (Reynolds et al., 2002) during the months of January (red) and July (green) in the Arctic (left) and Antarctic (right) regions. The thick, medium and thin lines represent the 90%, 50% and 5% sea-ice concentrations isolines, respectively. Thin white lines show the mean location of the main Southern Ocean fronts.

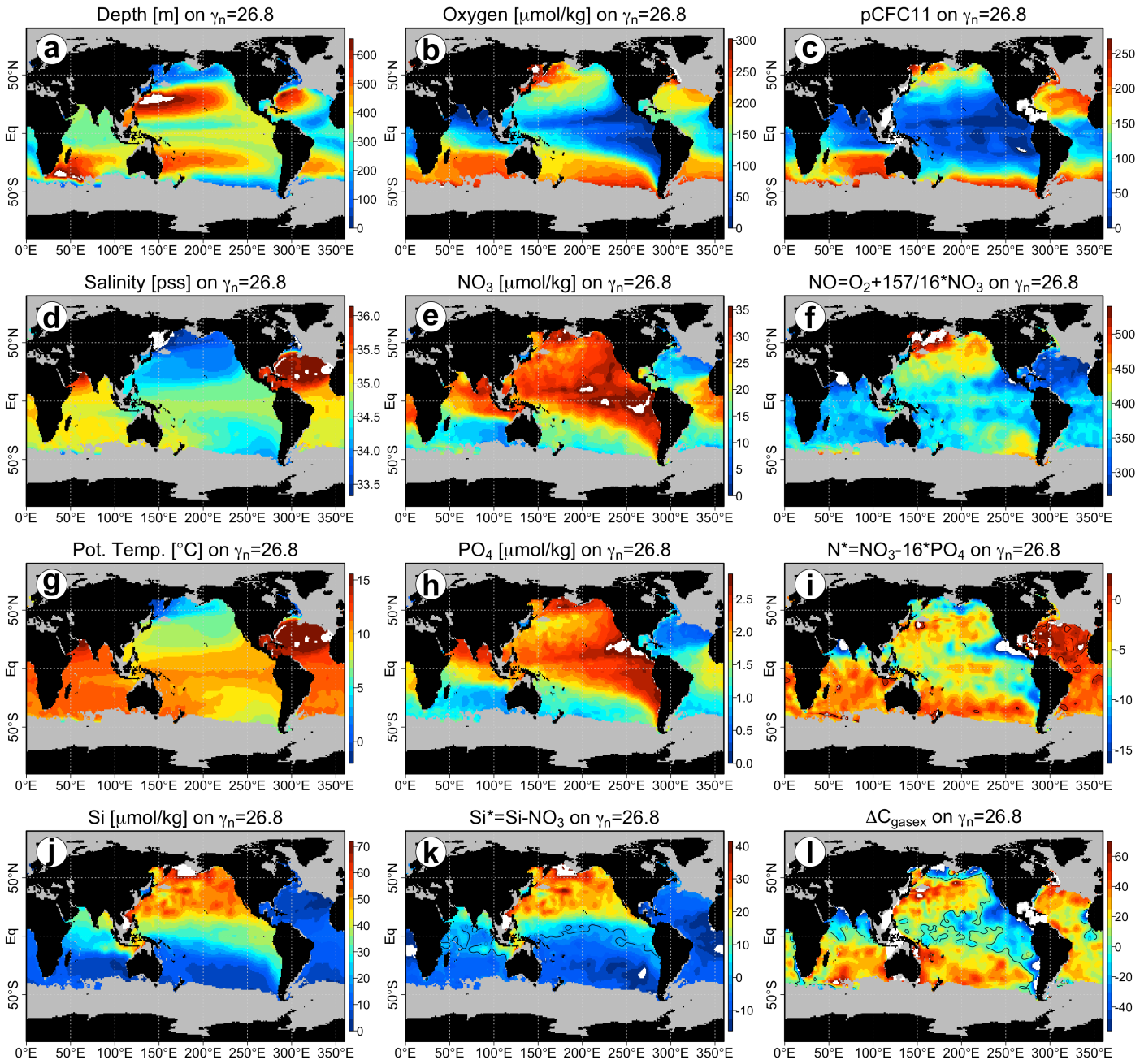

Figure 9: Global maps of hydrographic properties on the γ_n = 26.8 isoneutral from the gridded annual mean WOA05 climatology and GLODAP. Surfaces are trimmed at their winter outcrops (grey shading), as defined by the deepest observed mixed layer depths at each grid point as given by the monthly climatology of de Boyer Montegut et al. (2004). pCFC11 is in patm.

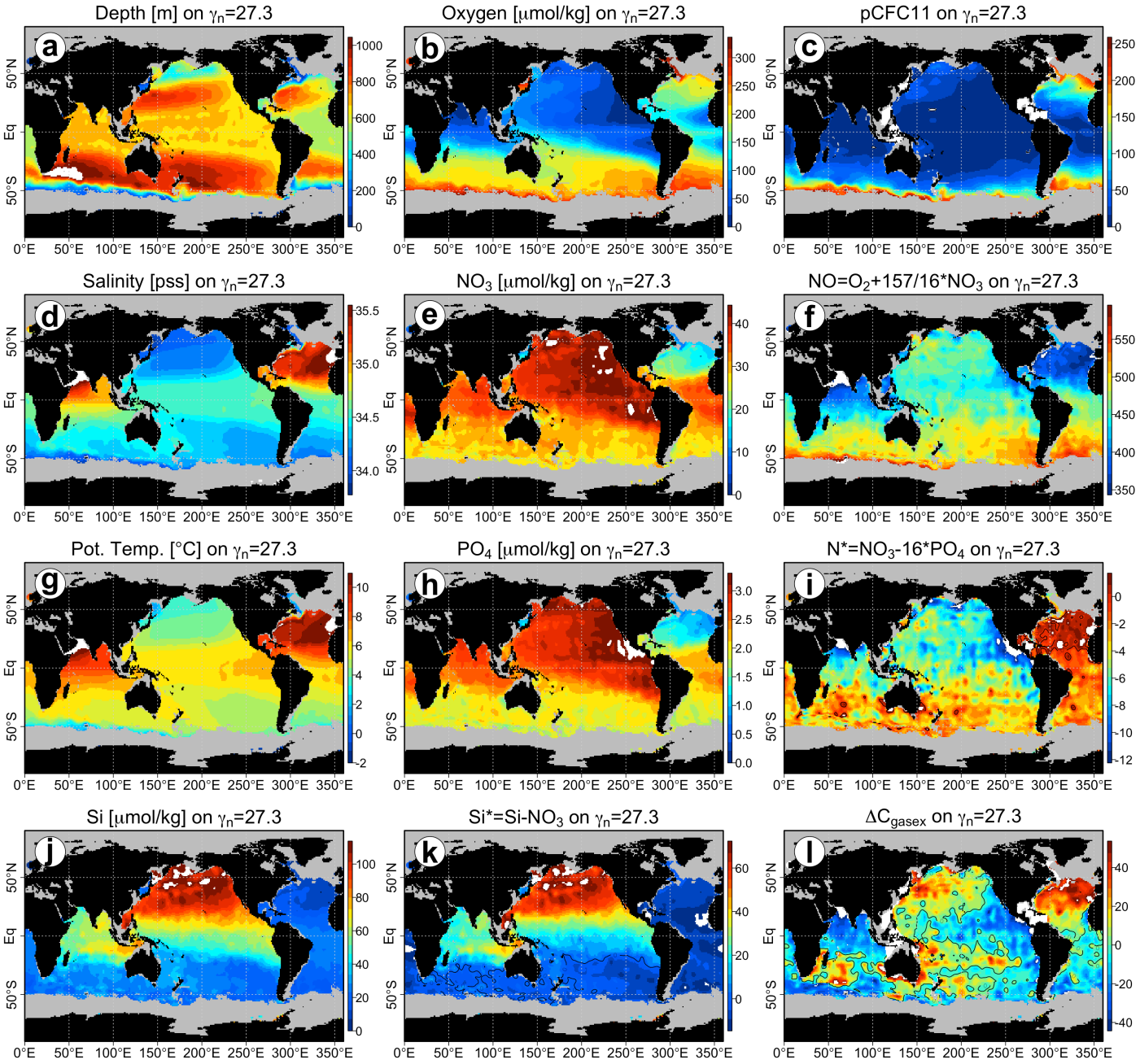

Figure 10: Global maps of hydrographic properties on the γ_n = 27.3 isoneutral from the gridded annual mean WOA05 climatology and GLODAP. Surfaces are trimmed at their winter outcrops (grey shading), as defined by the deepest observed mixed layer depths at each grid point as given by the monthly climatology of de Boyer Montegut et al. (2004). pCFC11 is in patm.

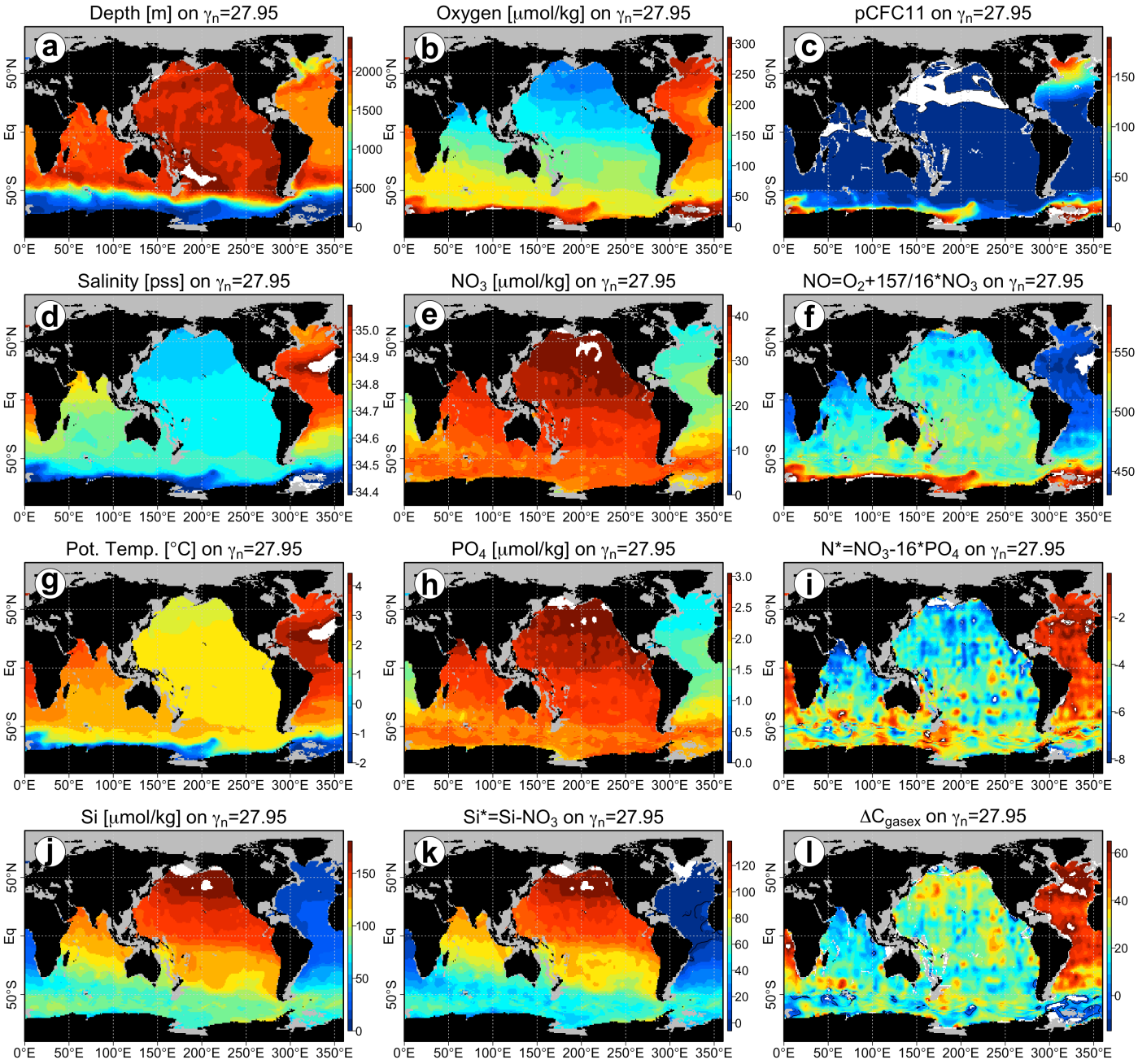

Figure 11: Global maps of hydrographic properties on the γ_n = 27.95 isoneutral from the gridded annual mean WOA05 climatology and GLODAP. Surfaces are trimmed at their winter outcrops (grey shading), as defined by the deepest observed mixed layer depths at each grid point as given by the monthly climatology of de Boyer Montegut et al. (2004). pCFC11 is in patm.

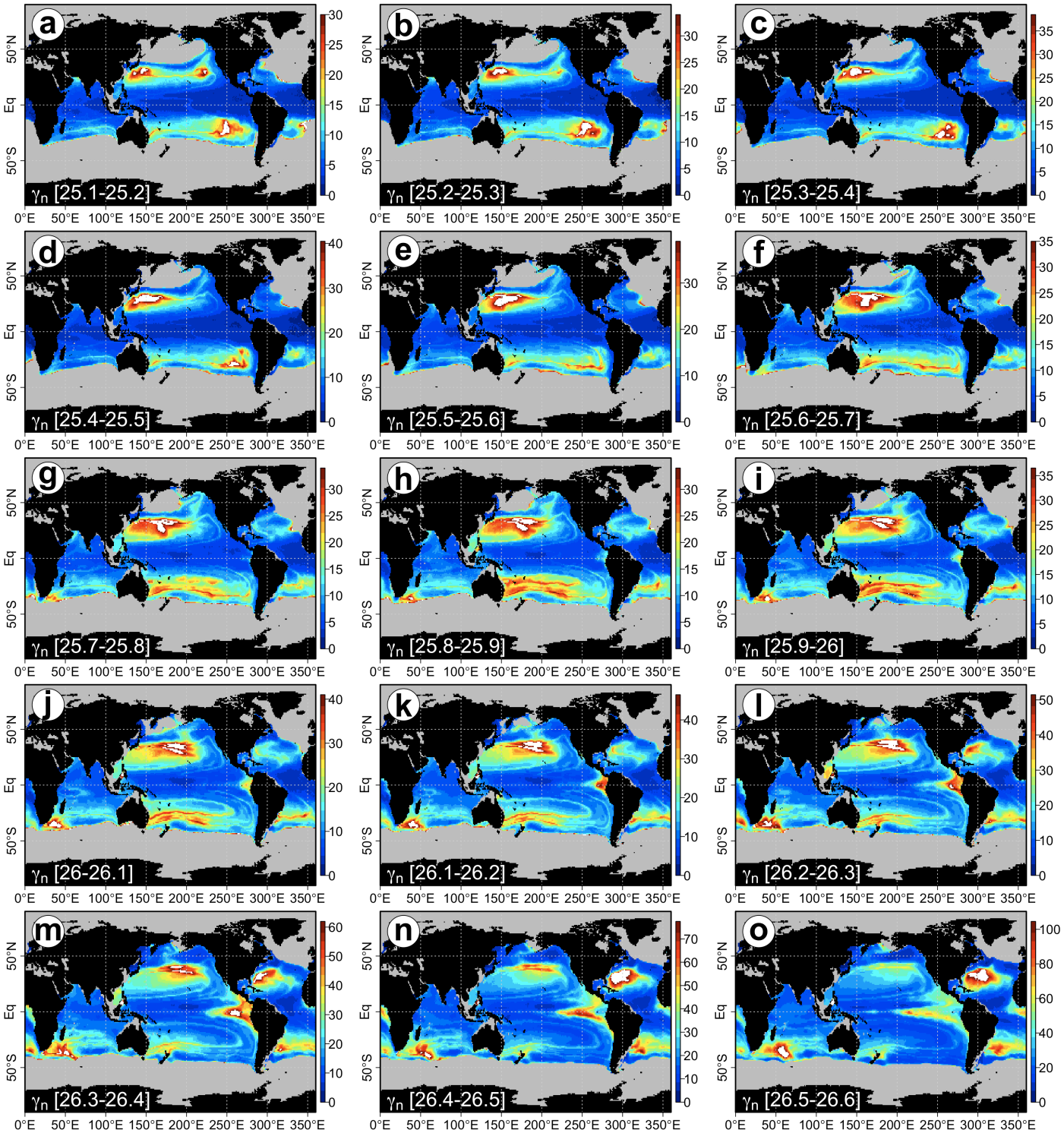

Figure 12: Water thicknesses [m] contained between isoneutral surfaces computed from the annual WOA05 climatology for the interval $25.1 \leq \gamma_n \leq 26.6$.

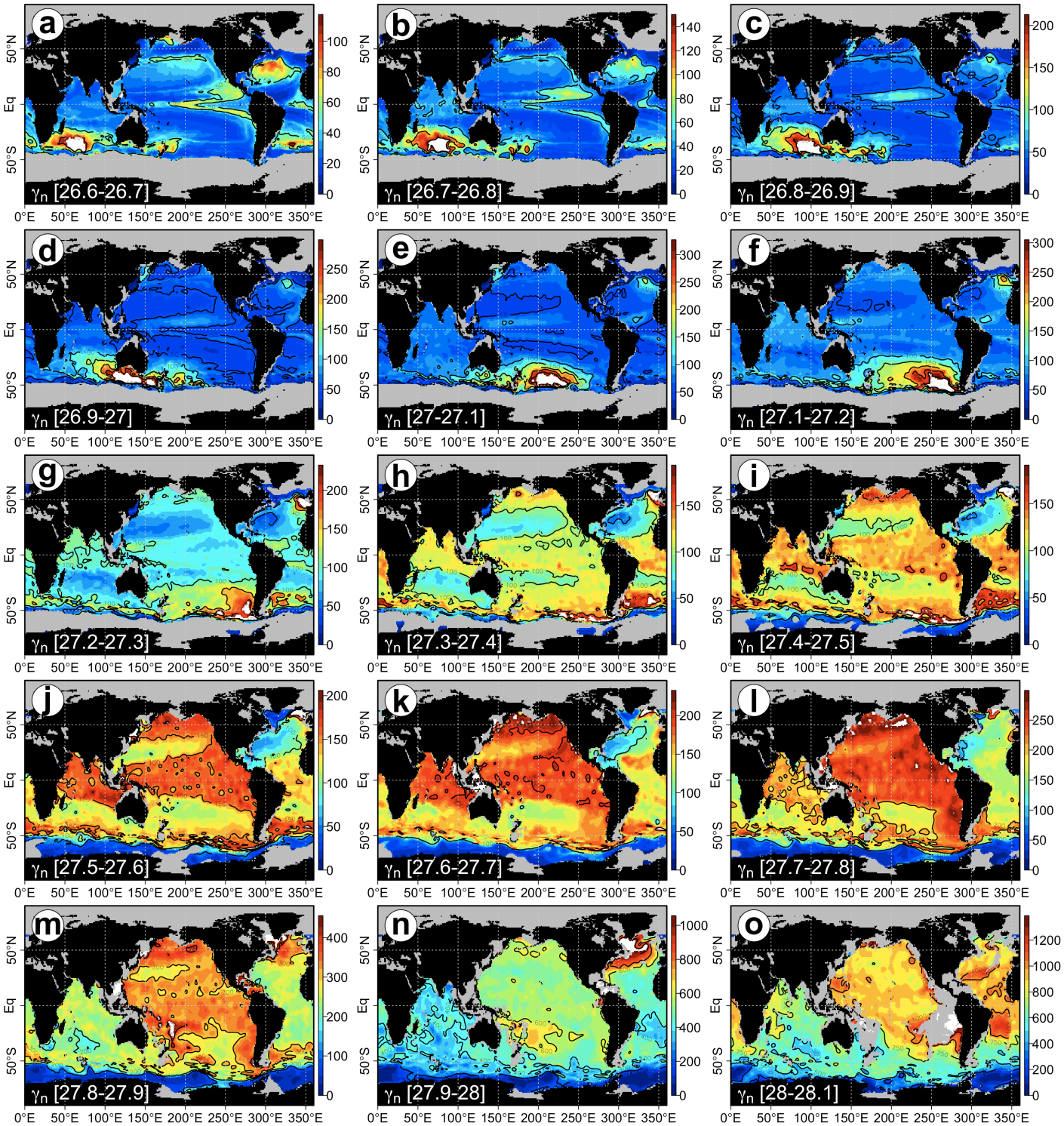

Figure 13: Water thicknesses [m] contained between isoneutral surfaces computed from the annual WOA05 climatology for the interval $26.6 \leq \gamma_n \leq 28.1$.

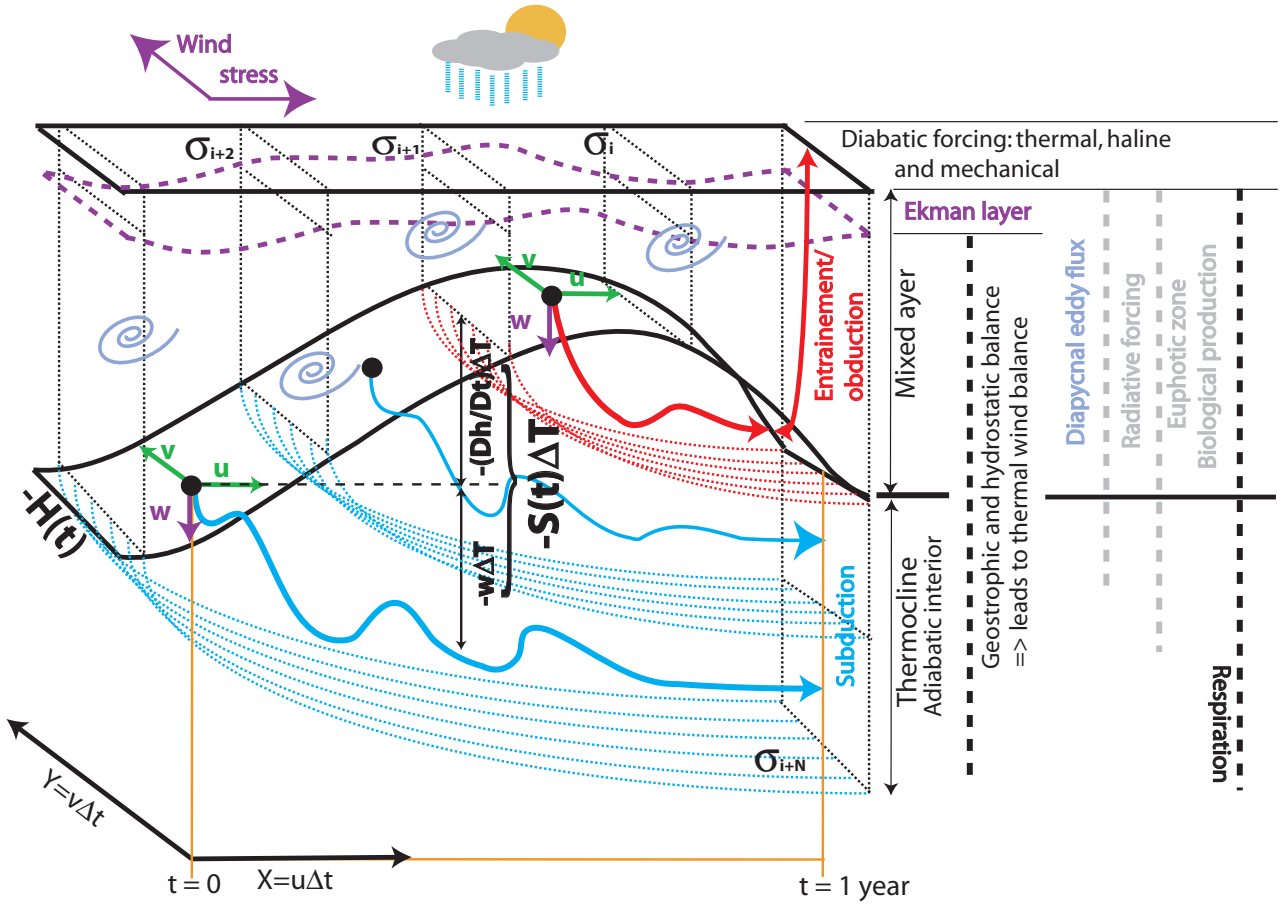

Figure 14: Illustration of the subduction/obduction processes responsible for the ventilation of the thermocline and the formation of mode waters. Following a water parcel of a given density (σ_i), subduction represents the annually integrated balance between the net sinking relative to its position when it first crosses the bottom of the mixed layer (H) and relative to the motion of the layer marking the bottom depth of the mixed layer. A parcel that is seen to reenter the mixed layer, either due to advection into a region of deeper mixed layer or because of mixed layer deepening in winter is said to be entrained back into the mixed layer. This is the obduction process, shown in red. The Ekman layer is typically shallower than the mixed layer. Eddies (shown as spirals) can also contribute to net motion across the mixed layer base.

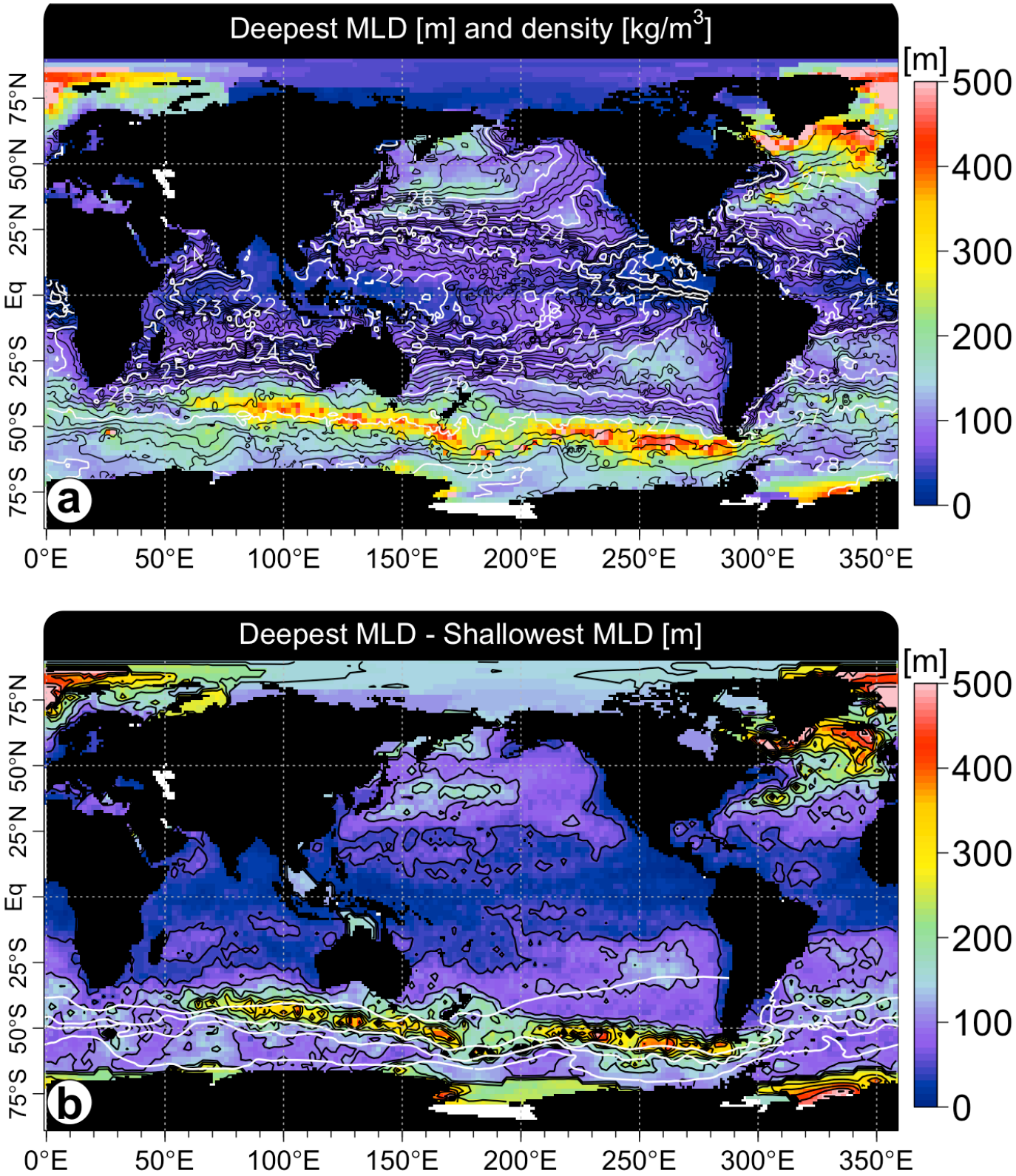

Figure 15: a) Depth of the deepest mixed layer defined independently at every grid point by the density criterion method (de Boyer Montegut et al., 2004). Contours show the neutral density of each grid cell calculated from monthly WOA05 temperature and salinity fields on the surface of deepest mixed layer depth. Contour interval is 0.2 kg/m^3 for black lines, 1 kg/m^3 for white lines. b) Maximum seasonal amplitude of the mixed layer depth, defined independently at each grid point from the mixed layer depth climatology of de Boyer Montegut et al. (2004). White contours in the Southern Ocean show the main fronts of the ACC as defined by Orsi et al. (1995).

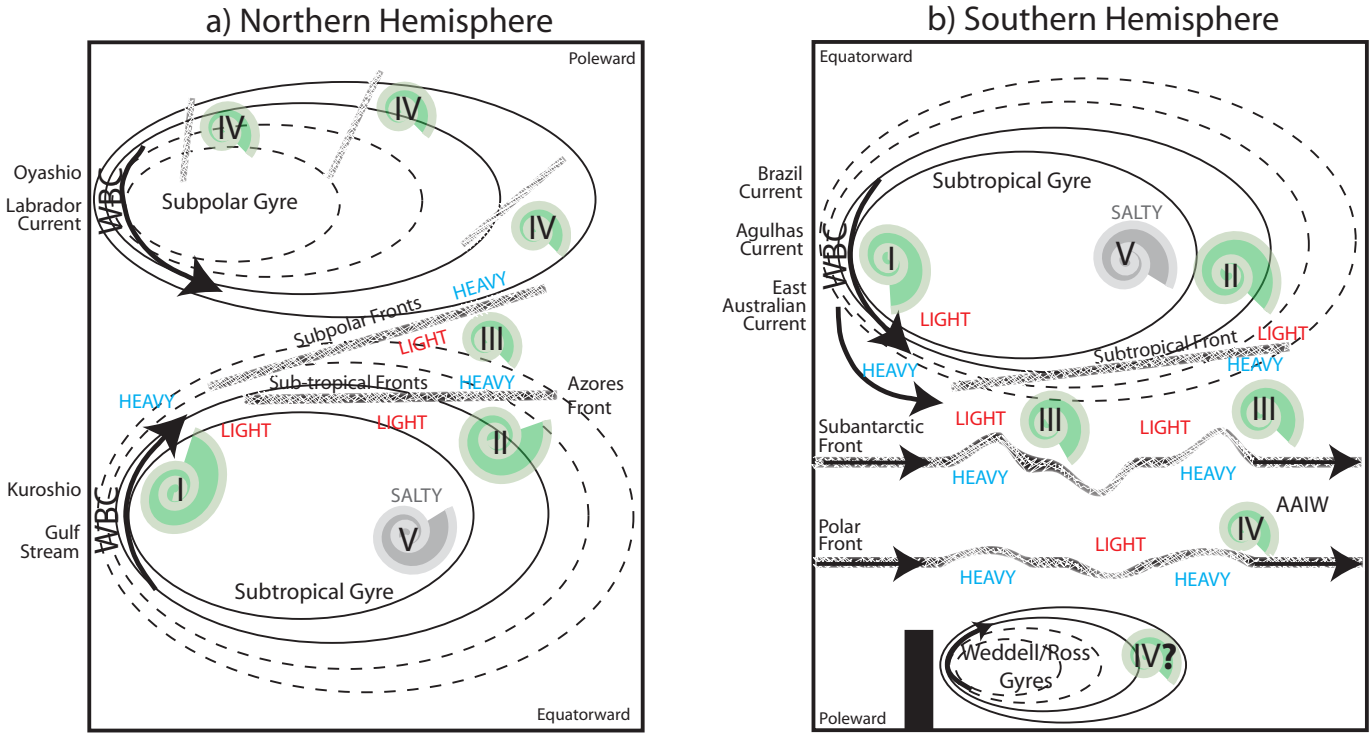

Figure 16: Cartoon summarizing the different types of mode waters constituting the main thermocline of the world ocean. Solid and dashed contour are indicative of the sea surface height or thermocline thickness trends, where solid lines indicate relatively higher SSH (deeper pycnocline) and dashed lines indicate relatively lower SSH (shallower pycnocline). Descriptions of the different types of mode waters (I-V) are provided in Table 3. Relative density across fronts are indicated by the words “light” (less dense) and “heavy” (more dense). Fronts are indicated by hatched line segments.

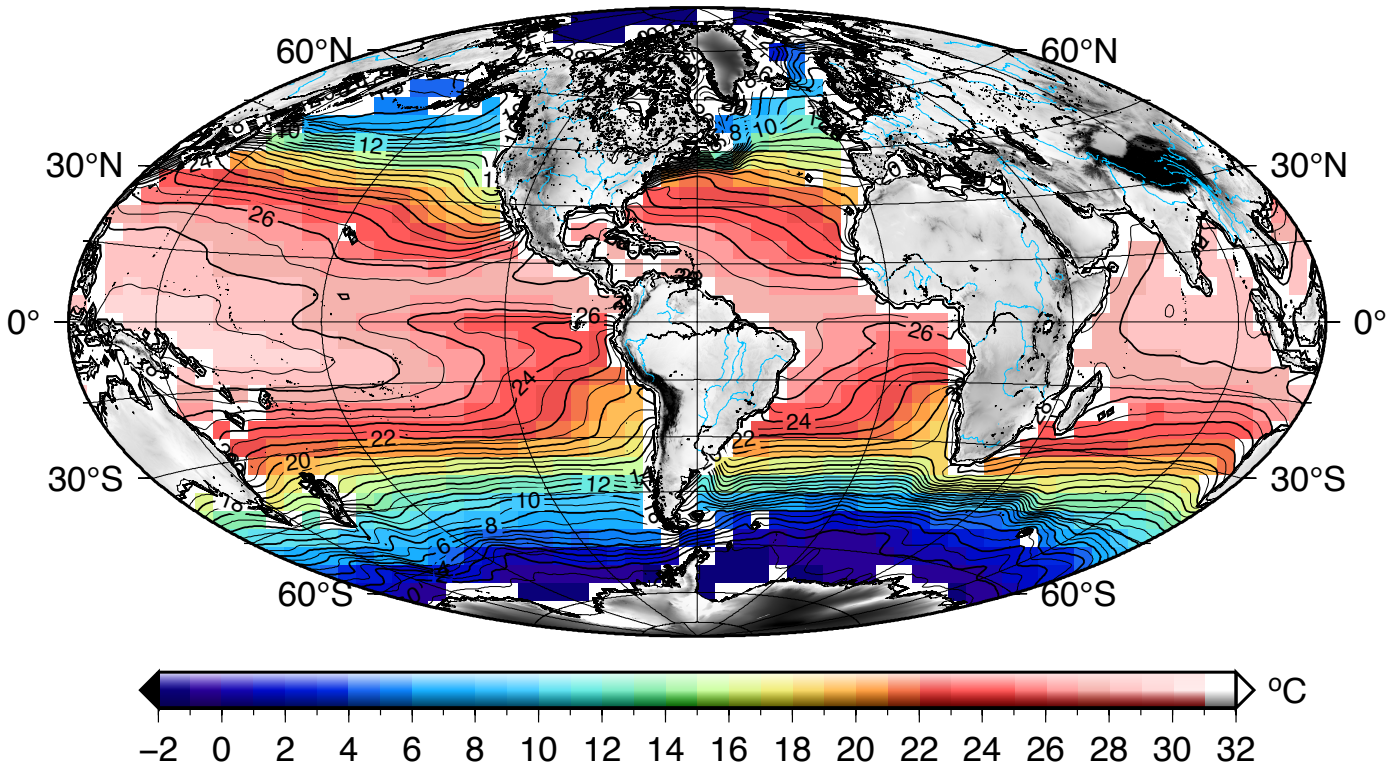

Figure 17: Annual mean sea surface temperature from WOA05.

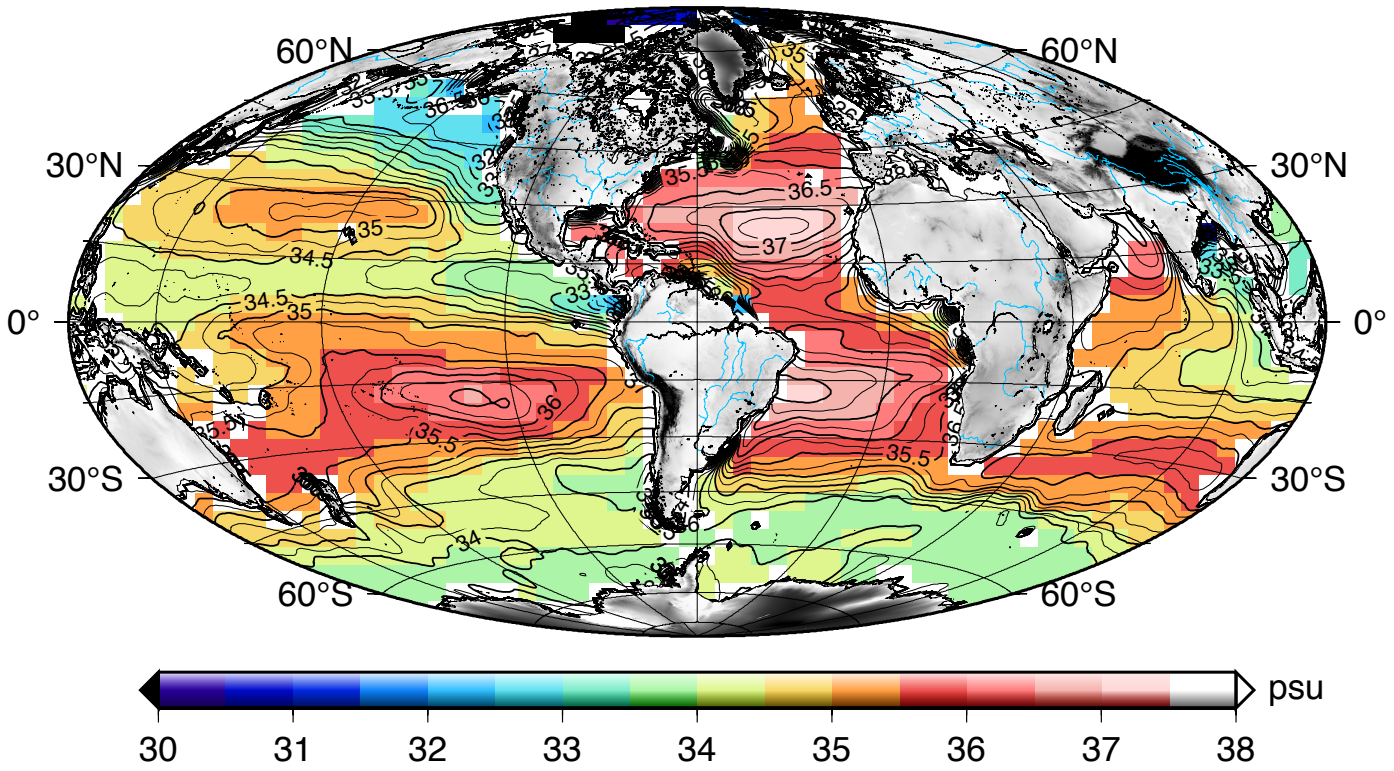

Figure 18: Annual mean sea surface salinity from WOA05.

Table 1: List of acronyms. Main currents and miscellaneous.

Acronym	Full Name	Acronym	Full Name
Currents and Fronts			
ACC	Antarctic Circumpolar Current	NwAC	Norwegian Atlantic Current
ASF	Antarctic Slope Front	WBC(s)	Western Boundary Current(s)
DS/ISO	Denmark Strait/Iceland-Scotland Overflow	WGC	West Greenland Current
DWBC	Deep Western Boundary Current	SAF	Subantarctic/Subarctic Front
E/WSC	Eastern/Western Spitzbergen Current	PFZ	Polar Frontal Zone
EGC	East Greenland Current	NAD	North Atlantic Drift
LC	Labrador Current	N/SAEC	North/South Atlantic Equatorial Current
NAC	North Atlantic Current	NAECC	North Atlantic Equatorial Counter Current
Miscellaneous			
AD	Antarctic Dipole	MWR	Mixed Water Region
ARGO	Array for Real-time Geostrophic Oceanography	NAO	North Atlantic Oscillations
BS	Bering Sea	NRG	Northern Recirculating Gyre
CFC	Chlorofluorocarbon	Oks	Okhotsk Sea
CMIP	Coupled Model Inter-comparison Project	PDO	Pacific Decadal Oscillation
ENSO	El Niño Southern Oscillation	PV	Potential Vorticity
GCM	General Circulation Model	SALH	Silicic Acid Leakage Hypothesis
GIN	Greenland, Iceland, Norwegian Seas	SAM	Southern Annular Mode
GISS	Goddard Institute for Space Studies	S_{crit}	Critical Salinity
GLODAP	Global Ocean Data Analysis Project	S.O.	Southern Ocean
IPCC	Intergovernmental Panel on Climate Change	THC	Thermohaline Circulation
ITCZ	Inter-Tropical Convergence Zone	TSD	Transpolar Drift
MLD	Mixed Layer Depth	TTD	Transit Time Distributions
MOC	Meridional Overturning Circulation	WOA05	World Ocean Atlas 2005
MS	Mediterranean Sea	WOCE	World Ocean Circulation Experiment

Table 2: List of abbreviations used in this review for water masses in the world's Ocean. In cases when multiple names represent the same or closely related water masses found in the literature, the names have been grouped together. Atl.=Atlantic, Pac.=Pacific, Ind.=Indian, Int.=Intermediate, Wat.=Water, Sh.=Shelf.

Acronym(s)	Water Mass Name(s)	Acronym(s)	Water Mass Name(s)
AABW	Antarctic Bottom Wat.	MCDW, WCSW, WC, MWDW	Modified Circumpolar Deep Wat., Warm Core Sh. Wat., Warm Core, Modified Warm Deep Wat., Modified Weddell Deep Wat.
(M)AAIW	(Modified) Antarctic Int. Wat.	M(S)(O)W	Mediterranean (Sea) (Overflow) Wat.
AASW	Antarctic Surface Wat.	MTW	Mesothermal Wat.
ACCBW	Antarctic Circumpolar Current Bottom Wat.	NACW	North Atl. Central Wat.
ALBW	Adelie Land Bottom Wat.	NADW	North Atl. Deep Wat.
ArSSW	Arabian Sea Surface Wat.	NEADW	North East Atl. Deep Wat.
ASW, HSASW	Arctic Sh. Wat., High Salinity ASW	NPDW	North Pac. Deep Wat.
AW, ALW, AAW, MAW, RAW, AIW, LAIW	Atl. Wat., Atl. Layer Wat., Arctic Atl. Wat., Modified Atl. Wat., Recirculating Atl. Wat., Arctic Int. Wat., Lower Arctic Int. Wat.	NPESSMW	North Pac. Eastern Shallow Salinity Minimum Wat.
BBSW	Baffin Bay Surface Wat.	NPESTMW	North Pac. Eastern STMW
BBW	Bay of Bengal Wat.	NPIW	North Pac. Int. Wat.
CBDW	Canadian Basin Deep Wat.	NPSASW	North Pac. Subarctic Surface Wat.
CDW	Circumpolar Deep Wat.	NSDW	Norwegian Basin Deep Wat.
CMW	Central Mode Wat.	ODSW	Okhostk Dense Sh. Wat.
CLSW, LLSW	Classical/Lower Labrador Sea Wat.	OSMW	Okhostk Dense Mode Wat.
DS/ISOW	Denmark Strait/Iceland-Scotland Overflow Wat.	PBBW	Prydz Bay Bottom Wat.
DTW	Dichothermal Wat.	PDW	Pac. Deep Wat.
E/W/NEqSW	Eastern/Western/Northern Equatorial Surface Wat.	PG(O)W	Persian Gulf (Overflow) Wat.
EBDW	Eurasian Basin Deep Wat.	PIW	Polar Int. Wat.
EDW	Eighteen Degree Wat.	RS(O)W	Red Sea (Overflow) Wat.
ENAW	Eastern North Atl. Wat.	RSBW	Ross Sea Bottom Wat.
ESTMW(s)	Eastern STMW(s)	SAMW	Subantarctic Mode Wat.
GNAIW	Glacial North Atl. Int. Wat.	SPESTMW	South Pac. Eastern STMW
GSDW	Greenland Sea Deep Wat.	SPMW(s)	Subpolar Mode Wat.(s)
HDSTMW(s)	High Density STMW	SSMW	Shallow Salinity Minimum Wat.
HSSW, WSW	High Salinity Sh. Wat., Western Sh. Wat.	STMW(s)	Subtropical Mode Wat.(s)
HSSUW	High Salinity Subtropical UnderWat.	STUW	Subtropical UnderWat.
IDW	Ind. Deep Wat.	UAIW	Upper Arctic Int. Wat.
IOCW	Ind. Ocean Central Wat.	UCDW	Upper Circumpolar Deep Wat.
IrSW	Irminger Sea Wat.	UHW	Upper Halocline Wat.
ISW	Ice Sh. Wat.	ULSW	Upper Labrador Sea Wat.
IT(F)W	Indonesian Throughflow Wat.	WDW	Warm/Weddell Deep Wat.
LAIW	Lower Arctic Int. Wat.	WISW	Western Ind. Surface Wat.
LCDW	Lower Circumpolar Deep Wat.	WMDW	Western Mediterranean Deep Wat.
LHW	Lower Halocline Wat.	WSBW	Weddell Sea Bottom Wat.
LIW	Levantine Int. Wat.	WSDW	Weddell Sea Deep Wat.
LSSW, ESW	Low Salinity Sh. Wat., Eastern Sh. Wat.	WSTMW	Western STMW
LSW	Labrador Sea Wat.	WW	Winter Wat.

Table 3: Mode Water systematics, adapted and extended from Hanawa & Talley (2001).

Type	*Class*	*Characteristics*
I	**WSTMW** (Western Subtropical Mode Water)	Found in all basins, they are the archetypical mode waters. Their formation is associated with the Western boundary currents extensions of the subtropical gyres (Kuroshio, Gulf Stream, East Australian Current, Brazil Current, Agulhas Current).
II	**ESTMW** (Eastern Subtropical Mode Water)	Found on the Eastern side of the subtropical gyres, formation region bounded to the East by the Western edge of Eastern Boundary Currents (Canary, California, Peru Currents), and poleward by the equatorward edge of zonal fronts (Azores Front, subtropical fronts).
III	**HDSTMW** (High density Subtropical Mode Water)	Originate poleward of subtropical gyres, but equatorward of the North Pacific subarctic front, North Atlantic Current and subantarctic front. The typical example is SAMW.
IV	**SPMW** (Subpolar Mode Water)	Deep mixed layers reported around the outside of subpolar gyres in the North Pacific and North Atlantic/Nordic Seas. In the North Atlantic subpolar gyre, culmination of the densification process results in the formation of LSW.
V	**HSSUW** (High Salinity Subtropical Underwater)	Shallow high-salinity subsurface layer found in every subtropical basin. Their formation is mostly driven by Ekman pumping and subduction from the high-evaporation regions found within subtropical gyre.

References

Aagaard, K., & Carmack, E. (1989). The role of sea ice and other fresh water in the arctic circulation. *Journal Of Geophysical Research*, *94*, 14485–14498.

Aagaard, K., & Carmack, E. (1994). The polar oceans and their role in shaping the global environment. chapter The Arctic ocean and climate: a perspective (pp. 33–46). American Geophysical Union volume Geophysical Monograph 85.

Aagaard, K., Swift, J., & Carmack, E. (1985). Thermohaline circulation in the arctic mediterranean seas. *Journal of Geophysical Research*, *90*, 4833–4846.

Adkins, J. F., McIntyre, K., & Schrag, D. P. (2002). The salinity, temperature, and delta o-18 of the glacial deep ocean. *Science*, *298*, 1769–1773.

Ahmad, E., & Sultan, S. (1991). Annual mean surface heat fluxes in the arabian gulf and the net heat trasnport through the strait of hormuz. *Atmos. Ocean*, *29*, 54–61.

Ambar, I., & Howe, M. R. (1979). Observations of the mediterranean outflow.1. mixing in the mediterranean outflow. *Deep-Sea Research Part A, Oceanographic Research Papers*, *26*, 535–554.

Ambar, I., Serra, N., Brogueira, M. J., Cabecadas, G., Abrantes, F., Freitas, P., Goncalves, C., & Gonzalez, N. (2002). Physical, chemical and sedimentological aspects of the mediterranean outflow off iberia. *Deep-Sea Research Part II-Topical Studies In Oceanography*, *49*, 4163–4177.

Anderson, L., & Jones, P. (1991). The transport of co2 into arctic and antarctic seas: Similarities and differences in the driving processes. *Journal of Marine Systems*, *2*, 81–95.

Arhan, M. (1987). On the large-scale dynamics of the mediterranean outflow. *Deep-Sea Research Part A-Oceanographic Research Papers*, *34*, 1187–1208. 0198-0149.

Assmann, K., & Timmermann, R. (2005). Variability of dense water formation in the ross sea. *Ocean Dynamics*, *55*, 68–87.

Auad, G., Kennett, J., & Miller, A. (2003). North pacific intermediate water response to a modern climate warming shift. *Journal of Geophysical Research*, *108*, 3349.

Bacon, S. (1998). Decadal variability in the outflow from the nordic seas to the deep atlantic ocean. *Nature*, *394*, 871–874.

Bagriantsev, N., Gordon, A., & Huber, B. (1989). Weddell gyre: Temperature maximum stratum. *Journal of Geophysical Research*, *94*, 8331–8334.

Baines, P. (2009). A model for the structure of the antarctic slope front. *Deep Sea Research II*, *56*, 859–873.

Baringer, M. O., & Price, J. F. (1997). Mixing and spreading of the mediterranean outflow. *Journal Of Physical Oceanography*, *27*, 1654–1677.

Baringer, M. O., & Price, J. F. (1999). A review of the physical oceanography of the mediterranean outflow. *Marine Geology*, *155*, 63–82.

Bates, N., & Mathis, J. (2009). The arctic ocean marine carbon cycle: evaluation of air-sea co2 exchanges, ocean acidification impacts and potential feedbacks. *Biogeosciences*, *6*, 2433–2459.

Bates, N. R., Pequignet, A. C., Johnson, R. J., & Gruber, N. (2002). A short-term sink for atmospheric co2 in subtropical mode water of the north atlantic ocean. *Nature*, *420*, 489–493.

Beal, L., Wilhelmus, P., de Ruijter, W. P. M., Biastoch, A., & Zahn, R. (2011). On the role of the agulhas system in ocean circulation and climate. *Nature*, *472*, 429–436.

Beal, L. M., Ffield, A., & Gordon, A. L. (2000). Spreading of red sea overflow waters in the indian ocean. *Journal Of Geophysical Research-Oceans*, *105*, 8549–8564.

Belchansky, G., Douglas, D., & Platonov, N. (2008). Fluctuating arctic sea ice thickness changes estimated by an in situ learned and empirically forced neural network model. *Journal of Climate*, *21*, 716–729.

Belkin, I., Levitus, S., Antonov, J., & Malmberg, S.-A. (1998). "grean salinity anomalies" in the north atlantic. *Progress in Oceanography*, *41*, 1–68.

Bersch, M. (2002). North atlantic oscillation-induced changes of upper layer circulation in the northern north atlantic ocean. *Journal of Geophysical Research*, *107*.

Bezbodorov, A., & Ovsyany, E. (1991). Influence of the mediterranean intermediate waters on oxygen distribution in the atlantic ocean. *Sov. J. Phys Oceanogr.*, *2*, 321–328.

Blanke, B., Arhan, M., Lazar, A., & Prevost, G. (2002). A lagrangian numerical investigation of the origins and fates of the salinity maximum water in the atlantic. *Journal of Geophysical Research*, *107*, 3163.

Blanke, B., Arhan, M., & Speich, S. (2006). Salinity changes along the upper limb of the atlantic thermohaline circulation. *Geophysical Research Letters*, *33*.

Boé, J., Hall, A., & Qu, X. (2009a). Current gcms' unrealistic negative feedback in the arctic. *Journal of Climate*, *22*, 4682–4695.

Boé, J., Hall, A., & Qu, X. (2009b). Deep ocean heat uptake as a major source of spread in transient climate change simulations. *Geophysical Research Letters*, *36*.

Boening, C., Bryan, F., Holland, W., & Doscher, R. (1996). Deep-water formation and meridional overturning in a high-resolution model of the north atlantic. *Journal of Physical Oceanography*, *26*, 1142–1164.

Boenisch, G., Blindheim, J., Bullister, J., Schlosser, P., & Wallace, D. (1997). Long-term trends of temperature, salinity, density and transient tracers in the central greenland sea. *Journal of Geophysical Research*, *102*, 18553–18571.

Bonisch, G., & Schlosser, P. (1995). Deep-water formation and exchange-rates in the greenland norwegian seas and the eurasian basin of the arctic-ocean derived from tracer balances. *Progress In Oceanography*, *35*, 29–52.

Born, A., Levermann, A., & Mignot, J. (2009). Sensitivity of the atlantic ocean circulation to a hydraulic overflow parameterisation ina coarse resolution model: response of the subpolar gyre. *Ocean Modelling*, *27*, 130–142.

Bower, A., Armi, L., & Ambar, I. (1995). Direct evidence of meddy formation off the southwestern coast of portugal. *Deep-Sea Research I*, *42*, 1621–1630.

Bower, A., Fratantoni, D., Johns, W., & Peters, H. (2002a). Gulf of aden eddies and their impact on red sea water. *Geophysical Research Letters*, *29*, 2025.

Bower, A., Johns, W., Fratantoni, D., & Peters, H. (2005). Equilibration and circulation of red sea overflow water in the western gulf of aden. *Journal of Physical Oceanography*, *35*, 1963–1985.

Bower, A., Lozier, M., & Gary, S. (2011). Export of labrador sea water from the subpolar north atlantic: A lagrangian perspective. *Deep-Sea Research II*, *58*, 1798–1818.

Bower, A., Rossby, H., & Lillibridge, J. (1985). The gulf-stream barrier or blender? *Journal of Physical Oceanography*, *15*, 24–32.

Bower, A., Serra, N., & Ambar, I. (2002b). Structure of the mediterranean undercurrent and mediterranean water spreading around the southwestern iberian penninsula. *Journal of Geophysical Research*, *107*, 3161.

Bower, A. S., Hunt, H. D., & Price, J. F. (2000). Character and dynamics of the red sea and persian gulf outflows. *Journal Of Geophysical Research-Oceans*, *105*, 6387–6414. 0148-0227.

Bower, A. S., Lozier, M. S., Gary, S., & Boning, C. (2009). Interior pathways of the north atlantic meridional overturning circulation. *Nature*, *459*, 243–247.

de Boyer Montegut, C. D., Madec, G., Fischer, A. S., Lazar, A., & Iudicone, D. (2004). Mixed layer depth over the global ocean: An examination of profile data and a profile-based climatology. *Journal Of Geophysical Research-Oceans*, *109*.

Boyle, E., & Keigwin, L. (1987). North atlantic thermohaline circulation during the past 20000 yearsa linked to high-latitude surface temperature. *Nature*, *330*, 35–40.

Bozec, A., Lozier, M., Chassignet, E., & Halliwell, G. (2011). On the variability of the mediterranean outflow water in the north atlantic from 1948 to 2006. *Journal of Geophysical Research*, *116*.

Brambilla, E., & Talley, L. (2008). Subpolar Mode Water in the northern Atlantic: 1. averaged properties and mean circulation. *Journal of Geophysical Research*, *113*.

Brambilla, E., Talley, L., & Robbins, P. E. (2008). Subpolar Mode Water in the northern Atlantic: 2. origin and transformation. *Journal of Geophysical Research*, *113*.

Broecker, W., Peng, T., Jouzel, J., & Russell, G. (1990). The magnitude of global fresh-water transports of importance to ocean circulation. *Climate Dynamics*, *4*, 73–79.

Broecker, W. S. (1974). "no", a conservative water-mass tracer. *Earth And Planetary Science Letters*, *23*, 100–107.

Broecker, W. S. (1997). Thermohaline circulation, the achilles heel of our climate system: Will man-made co2 upset the current balance? *Science*, *278*, 1582–1588.

Broecker, W. S., Peacock, S. L., Walker, S., Weiss, R., Fahrbach, E., Schroeder, M., Mikolajewicz, U., Heinze, C., Key, R., Peng, T. H., & Rubin, S. (1998). How much deep water is formed in the southern ocean? *Journal Of Geophysical Research-Oceans*, *103*, 15833–15843.

Broecker, W. S., Peng, T. H., Ostlund, G., & Stuiver, M. (1985a). The distribution of bomb radiocarbon in the ocean. *Journal Of Geophysical Research-Oceans*, *90*, 6953–6970.

Broecker, W. S., Takahashi, T., & Takahashi, T. (1985b). Sources and flow patterns of deep-ocean waters as deduced from potential temperature, salinity, and initial phosphate concentration. *Journal Of Geophysical Research-*

Oceans, *90*, 6925–6939.

Bruhwiler, L., Michalak, A., & Tans, P. (2011). Spatial and temporal resolution of carbon flux estimates for 1983-2002. *Biogeosciences*, *8*, 1309–1331.

Bryan, F. (1986). High-latitude salinity effects and interhemispheric thermohaline circulations. *Nature*, *323*, 301–304.

Bryzgalo, V., & Ivanov, V. (2000). The inflow of dissolved matter through river runoff into the russia arctic seas. annual and seasonal variability. *Ecological Chemistry*, *9*, 76–89.

Cabecadas, G., Brogueira, M. J., & Goncalves, C. (2002). The chemistry of mediterranean outflow and its interactions with surrounding waters. *Deep-Sea Research Part Ii-Topical Studies In Oceanography*, *49*, 4263–4270 0967-0645.

Candela, J. (2001). Ocean circulation and climate. chapter 5.7. Mediterranean Water and global climate. (pp. 419–430). Academic Press volume 77 of *International Geophysics Series*.

Carmack, E. (1977). Water characteristics of the southern ocean south of the polar front. In M. Angel (Ed.), *A voyage of Discovery* Suppl. to vol. 24 (pp. 15–41). Deep Sea Research.

Carmack, E. (1990). Polar oceanography, part a: physical science. chapter 4. Large-scale physical oceanography of polar oceans.. (pp. 171–222). Academic Press.

Carmack, E. (2007). The alpha/beta ocean distinction: a perspective on freshwater fluxes, convection, nutrients and productivity in high-latitude seas. *Deep-Sea Research II*, *54*, 2578–2598.

Carmack, E., & Foster, T. (1975). On the flow of water out of the weddell sea. *Deep-Sea Research*, *22*, 711–724.

Carmack, E., & Killworth, P. D. (1978). Formation and interleaving of abyssal water masses off wilkes land, antarctica. *Deep-Sea Research*, *25*, 357–369.

Carmack, E., McLaughlin, F., Yamamoto-Kawai, M., Itoh, M., Shimada, K., Krishfield, R., & Proshutinsky, A. (2008). Arctic-subarctic ocean fluxes defining the role of the northern seas in climate. chapter 7. Freshwater storage in the Northern Ocean and the special role of the Beaufort gyre. (pp. 145–169). Springer-Verlag.

Carman, J., & McClean, J. (2011). Investigation of IPCC AR4 coupled climate model North Atlantic mode water formation. *Ocean Modelling*, *40*, 14–34.

Carsey, F., & Roach, D. (1994). The polar oceans and their rol in shaping the global environment. chapter Oceanic convection in the Greenland Sea Odden region as interpreted in satellite data. (pp. 159–176). American Geophysical Union volume Geophysical monograph.

Centurioni, L., & Gould, W. (2004). Winter conditions in the irminger sea observed with profiling floats. *Journal of Marine Research*, *62*, 313–336.

Chapman, W., & Walsh, J. (2007). Simulations of arctic temperature and pressure by global coupled models. *Journal of climate*, *20*, 609–632.

Chavanne, C., Heywood, K., Nicholls, K., & Fer, I. (2010). Observations of the antarctic slope undercurrent in the southeastern weddell sea. *Geophysical Research Letters*, *37*.

Chen, C. T. A., Jones, E. P., & Lin, K. (1990). Wintertime total carbon-dioxide measurements in the norwegian and greenland seas. *Deep-Sea Research Part A-Oceanographic Research Papers*, *37*, 1455–1473.

Clarke, R. A., & Coote, A. R. (1988). The formation of labrador sea-water.3. the evolution of oxygen and nutrient concentration. *Journal Of Physical Oceanography*, *18*, 469–480.

Clarke, R. A., & Gascard, J. C. (1983). The formation of labrador sea-water.1. large-scale processes. *Journal Of Physical Oceanography*, *13*, 1764–1778.

Comiso, J. (2010). Polar oceans from space. 41 chapter 8: Polynyas and other polar phenomena. (pp. 365–402). Atmospheric and Oceanographic Sciences Library.

Comiso, J., & Gordon, A. (1996). Cosmonaut polynya in the Southern Ocean: Structure and variability. *Journal Of Geophysical Research-Oceans*, *101*, 18297–18313.

Condie, S. (1995). Descent of dense water masses along continental slopes. *Journal of Marine Research*, *53*, 897–928.

Cunningham, S. A., Kanzow, T., Rayner, D., Baringer, M. O., Johns, W. E., Marotzke, J., Longworth, H. R., Grant, E. M., Hirschi, J. J. M., Beal, L. M., Meinen, C. S., & Bryden, H. L. (2007). Temporal variability of the Atlantic Meridional Overturning Circulation at 26.5 ^{o}N. *Science*, *317*, 935–938.

Cuny, J., Rhines, P., & Kwok, R. (2005a). Davis strait volume, frshwater and heat fluxes. *Deep-Sea Research I*, *52*, 519–542.

Cuny, J., Rhines, P. B., Schott, F., & Lazier, J. (2005b). Convection above the labrador continental slope. *Journal Of Physical Oceanography*, *35*, 489–511.

Curry, R., McCartney, M. S., & Joyce, T. M. (1998). Oceanic transport of subpolar climate signals to mid-depth subtropical waters. *Nature*, *391*, 575–577.

Dai, A., Qian, T., Trenberth, K. E., & Milliman, J. (2009). Changes in continental freshwater discharge from 1948 to 2004. *Journal of Climate*, *22*, 2773–2792.

Dai, A., & Trenberth, K. E. (2002). Estimates of freshwater dischargeorm continents: latitudinal and seasonal variations. *Journal Of Hydrometeorology*, *3*, 660–687.

Daniault, N., Maze, J., & Arhan, M. (1994). Circulation and mixing of mediterranean water west of the iberian peninsula. *Deep-Sea Research I*, *41*, 1685–1714.

Davis, X., Rothstein, L., Dewar, W., & Menemenlis, D. (2011). Numerical investigations of seasonal and interannual variability of north pacific subtropical mode water and its implication for pacific climate variability. *Journal of Climate*, *24*, 2648–2665.

Deacon, G. (1933). A general account of the hydrology of the south atlantic ocean. *Discovery Reports*, *7*, 171–238.

Deacon, G. (1937). The hydrology of the southern ocean. *Discovery Reports*, *15*, 1–124.

Dickson, R., Gmitrowicz, E., & Watson, A. (1990). Deep-water renewal in the northern north-atlantic. *Nature*, *344*, 848–850.

Dickson, R., Lazier, J., Meincke, J., Rhines, P., & Swift, J. (1996). Long-term coordinated changes in the convective activity of the north atlantic. *Progress In Oceanography*, *38*, 241.

Dickson, R., Meincke, J., Malmberg, S.-A., & A.J., L. (1988). The "great salinity anomaly" in the northern north atlantic 1968-1982. *Progress In Oceanography*, *20*, 103–151.

Döös, K. (1995). Interocean exchange of water masses. *Journal of Geophysical Research*, *100*, 13499–13514.

Doyle, J., & Shapiro, M. (1999). Flow response to large-scale topography: the greenland tip jet. *Tellus*, *51*, 728–748.

Emery, W. J., & Meincke, J. (1986). Global water masses - summary and review. *Oceanologica Acta*, *9*, 383–391.

Endoh, T., Mitsudera, H., Xie, S.-P., & Qiu, B. (2004). Thermohaline structure in the subarctic north pacific simulated in a general circulation model. *Journal of Physical Oceanography*, *34*, 360–371.

England, M. H. (1992). On The Formation Of Antarctic Intermediate And Bottom Water In Ocean General-Circulation Models. *Journal of Physical Oceanography*, *22*, 918–926.

Fahrbach, E., Hoppema, M., Rohardt, G., Schroder, M., & Wisotzki, A. (2004). Decadal-scale variations of water mass properties in the deep weddell sea. *Ocean Dynamics*, *54*, 77–91.

Fahrbach, E., Peterson, R., Rohdardt, G., Schlosser, P., & Bayer, R. (1994). Suppression of bottom water foramtion in the southeastern weddell sea. *Deep-Sea Research II*, *41*, 389–411.

Faure, V., & Speer, K. (2005). Labrador sea water circulation in the northern atlantic ocean. *Deep-Sea Research II*, *52*, 565–581.

Favorite, F., Dodimead, A., & Nasu, K. (1976). *Oceanography of the subarctic Pacific region, 1960-1971* volume 33 of *Bulletin*. International North Pacific Fisheries Commission.

Fine, R. A. (1993). Circulation of antarctic intermediate water in the south indian-ocean. *Deep-Sea Research Part I-Oceanographic Research Papers*, *40*, 2021–2042.

van de Flierdt, T., Frank, M., Halliday, A., Hein, J., Hattendorf, B., Guenther, D., & Kubik, P. (2004). Deep and bottom water export from the southern ocean to the pacific over the past 38 million years. *Paleoceanography*, *19*.

van de Flierdt, T., Hemming, S. R., Goldstein, S., & Abouchami, W. (2006). Radiogenic isotope fingerprint of wilkes land-adelie coast bottom water in teh circum-antarctic ocean. *Geophysical Research Letters*, *33*.

Fogelqvist, E., Blindheim, J., Tanhua, T., Osterhus, S., Buch, E., & Rey, F. (2003). Greenland-scotland overflow studied by hydro-chemical multivariate analysis. *Deep-Sea Research Part I-Oceanographic Research Papers*, *50*, 73–102.

Foldvik, A., & Gammelsrod, T. (1988). Notes on southern ocean hydrography, sea-ice and bottom water formation. *Palaeogeography, Palaeoclimatology, Palaeoecology*, *67*, 3–17.

Foldvik, A., Gammelsrod, T., Osterhus, S., Fahrbach, E., Rohardt, G., Schroder, M., Nicholls, K. W., Padman, L., & Woodgate, R. A. (2004). Ice shelf water overflow and bottom water formation in the southern weddell sea. *Journal Of Geophysical Research-Oceans*, *109*.

Foldvik, A., Gammelsrod, T., & Torresen, T. (1985). Hydrographic observations from the weddell sea during the norwegian antarctic research expedition 1976/77. *Polar Research*, *3 n.s.*, 177–193.

Forget, G., Maze, G., Buckley, M., & Marshall, J. (2011). Estimated seasonal cycle of north atlantic eighteen degree water volume. *Journal of Physical Oceanography*, *41*, 269–286.

Foster, T., & Carmack, E. (1976). Frontal zone mixing and Antarctic Bottom Water formation in the southern Weddell Sea. *Deep-Sea Research*, *23*, 301–317.

Foster, T., Foldvik, A., & Middleton, J. (1987). Mixing and bottom water formation in the shelf break region of the southern Weddell Sea. *Deep-Sea Research*, *34*, 1771–1794.

Frankcombe, L., & Dijkstra, H. (2011). The role of Atlantic-Arctic exchange in North Atlantic multidecadal climate variability. *Geophysical Research Letters*, *38*.

Fukamachi, Y., Rintoul, S., Church, J., Aoki, S., Sokolov, S., & Rosenberg, M. M.A.and Wakatsuchi (2010). Strong export of antarctic bottom water east of the kerguelen plateau. *Nature Geosciences*, *3*, 327–331.

Gascard, J. C., & Clarke, R. A. (1983). The formation of labrador sea-water.2. mesoscale and smaller-scale processes. *Journal Of Physical Oceanography*, *13*, 1779–1797.

Gebbie, G., & Huybers, P. (2011). How is the ocean filled? *Geophysical Research Letters*, *38*.

Gent, P. R., & McWilliams, J. C. (1990). Isopycnal Mixing In Ocean Circulation Models. *Journal of Physical Oceanography*, *20*, 150–155.

Gent, P. R., Willibrand, J., McDougall, T. J., & McWilliams, J. C. (1995). Parameterizing Eddy-Induced Tracer Transports In Ocean Circulation Models. *Journal of Physical Oceanography*, *25*, 463–474.

Georgi, D. T. (1979). Modal properties of antarctic intermediate water in the southeast pacific and the south-atlantic. *Journal Of Physical Oceanography*, *9*, 456–468.

Gibson, J., & Trull, T. (1999). Annual cycle of co2 under sea-ice and in open water in prydz bay, east antarctica. *Marine Chemistry*, *66*, 187–200.

Gill, A. (1973). Circulation and bottom water production in the Weddell Sea. *Deep-Sea Research*, *20*, 111–140.

Gladyshev, S., Talley, L., Kantakov, G., Khen, G., & Wakatsuchi, M. (2003). Distribution, formation, and seasonal variability of okhotsk sea mode water. *Journal Of Geophysical Research-Oceans*, *108*, 3186.

Gordon, A. (1974). Varieties and variability of antarctic bottom water. In C. I. du CNRS (Ed.), *Processus de formation des eaux oceaniques profondes* (pp. 33–47).

Gordon, A. (1978). Deep antarctic convection west of maud rise. *Journal of Physical Oceanography*, *8*, 600–612.

Gordon, A. (1981). Seasonality of southern ocean sea ice. *Journal of Geophysical Research*, *86*, 4193–4197.

Gordon, A., Chen, C., & Metcalf, W. (1984). Winter mixed layer entrainment of weddell deep water. *Journal of Geophysical Research*, *89*, 637–640.

Gordon, A., & Comiso, J. C. (1988). Polynyas in the southern ocean. *Scientific American*, *258*, 90–97.

Gordon, A., Georgi, D., & Taylor, H. (1977). Antarctic polar front zone in the western scotial sea - summer 1975. *Journal of Physical Oceanography*, *7*, 309–328.

Gordon, A., & Huber, B. (1984). Thermohaline stratification below the southern ocean sea ice. *Journal of Geophysical Research*, *89*, 641–648.

Gordon, A., & Huber, B. (1995). Warm weddell deep water west of maud rise. *Journal of Geophysical Research*, *100*, 13747–13753.

Gordon, A., Huber, B., Hellmer, H., & Ffield, A. (19934). Deep and bottom water of the weddell sea's western rim. *Science*, *262*, 95–97.

Gordon, A., Huber, B., McKee, D., & Visbeck, M. (2010). A seasonal cycle in teh export of bottom water from the weddell sea. *Nature Geosciences*, *3*, 551–556.

Gordon, A., Orsi, A., Muench, R., Huber, B., Zambianchi, E., & Visbeck, M. (2009). Western ross sea continental slope gravity currents. *Deep-Sea Research II*, *56*, 796–817.

Gordon, A., & Tchernia, P. (1972). Waters of the continental margin off adelie coast, antarctica. In D. Hayes (Ed.), *Antarctic Oceanology II: The Australian - New Zealand sector* number 19 in Antarctic Res. Ser. (pp. 59–69).

Gordon, A. L., & Fine, R. A. (1996). Pathways of water between the pacific and indian oceans in the indonesian seas. *Nature*, *379*, 146–149. 0028-0836.

Gordon, A. L., Visbeck, M., & Comiso, J. C. (2007). A possible link between the Weddell Polynya and the Southern Annular Mode. *Journal of Climate*, *20*, 2558–2571.

Gordon, A. L., Weiss, R. F., Smethie, W. M., & Warner, M. J. (1992). Thermocline and intermediate water communication between the south-atlantic and indian oceans. *Journal Of Geophysical Research-Oceans*, *97*, 7223–7240.

Gordon, A. L., Zambianchi, E., Orsi, A., Visbeck, M., Giulivi, C. F., Whitworth, T., & Spezie, G. (2004). Energetic plumes over the western ross sea continental slope. *Geophysical Research Letters*, *31*.

Gow, A. J., & Tucker, W. (1990). Polar oceanography, part a: physical science. chapter 2. Sea Ice in the Polar Regions. (pp. 171–222). Academic Press.

Graham, J., Stevens, D., Heywood, K., & Wang, Z. (2011). North atlantic climate responses to perturbations in antarctic intermediate water. *Climate Dynamics*, *37*, 297–311.

Griesel, A., Gille, S., Sprintall, J., J.H., M., & Maltrud, M. (2010). Isopycnal diffusivities in the antarctic circumpolar current inferred from lagrangian floats in an eddying model. *Journal of Geophysical Research*, *115*.

Grosfeld, K., Gerdes, R., & Determann, J. (1997). Thermohaline circulation and interaction between ice shelf cavities and the adjacent open ocean. *Journal of Geophysical Research*, *102*, 15595–15610.

Gruber, N., & Sarmiento, J. (2002). The sea: biological-physical interactions in the oceans. chapter Biogeochemical/physical interactions in elemental cycles. (pp. 337–399). Hoboken, N.J.: John Wiley volume 12.

Gruber, N., & Sarmiento, J. L. (1997). Global patterns of marine nitrogen fixation and denitrification. *Global Biogeochemical Cycles*, *11*, 235–266.

Grundlingh, M. L. (1985). Occurence of red sea water in the southwestern indian ocean. *Journal of Physical Oceanography*, *15*, 207–212.

Gu, D., & Philander, S. (1997). Interdecadal climate fluctuations that depend on exchanges between the tropics and extratropics. *Science*, *275*, 805–807.

Haine, T., Boening, C., Brandt, P., Fischer, J., Funk, A., Kieke, D., Kvaleberg, E., Rhein, M., & Visbeck, M. (2008). Arctic-subarctic ocean fluxes: defining the role of the northern seas in climate. chapter 27. North Atlantic Deep Water formation in the Labrador Sea, recirculation through the subpolar gyre, and discharge to the subtropics.. (pp. 653–702). Springer-Verlag.

Hakkinen, S. (1993). An arctic source for the great salinity anomaly: a simulation of the arctic ice-ocean system for 1955-1975. *Journal Of Geophysical Research*, *98*, 16397–16410.

Hakkinen, S., & Rhines, P. (2009). Shifting surface currents in the northern north atlantic ocean. *Journal of Geophysical Research*, *114*.

Hakkinen, S., & Rhines, P. B. (2004). Decline of subpolar North Atlantic circulation during the 1990s. *Science*, *304*, 555–559.

Haley, B., Frank, M., Spielhagen, R., & Eisenhauer, A. (2008). Influence of brine formation on arctic ocean circulation over the past 15 million years. *Nature Geosciences*, *1*, 68–72.

Hall, M., & Bryden, H. (1982). Direct estimates and mechanisms of ocean heat transport. *Deep Sea Research*, *29*, 339–359.

Hallberg, R. (2000). Time integration of diapycnal diffusion richardson number dependent mixing in isopycnal coordinate ocean models. *Mon. Weath. Rev.*, *128*, 1402–1419.

Hamilton, L. (1990). Temperature inversions at intermediate depths in the antarctic intermediate waters of the southwestern pacific. *Aust. J. Freshwater Res.*, *41*, 325–351.

Hanawa, K., & Kamada, J. (2001). Variability of core layer temperature (clt) of the north pacific subtropical mode water. *Geophysical Research Letters*, *28*, 2229–2232.

Hanawa, K., & Talley, L. D. (2001). Ocean circulation and climate. chapter Mode Waters. (pp. 373–386). San Diego, CA: Academic Press.

Hansen, B., Osterhus, S., Quadfasel, D., & Turrell, W. (2004). Already the day after tomorrow? *Science*, *305*, 953–954.

Hansen, B., Osterhus, S., Turrell, W., Jonsson, S., Valdimarsson, H., Hatun, H., & Malskaer Olsen, S. (2008). Arctic-subarctic ocean fluxes: defining the role of the northern seas in climate. chapter Ch1. The inflow of Atlantic water, heat and salt to the Nordic Seas across the Greenland-Scotland Ridge. Springer.

Hartin, C., A., F. R., Sloyan, B., Talley, L., & Chereskin, T. (2011). Formation rates of subantarctic mode water and antarctic intermediate water within the south pacific. *Deep-Sea Research I*, *58*, 524–534.

Harvey, J. (1982). θ-s relationships and water masses in the eastern north-atlantic. *Deep-Sea Research Part A-Oceanographic Research Papers*, *29*, 1021–1033.

Harvey, J., & Arhan, M. (1988). The water masses of the central north-atlantic in 1983-84. *Journal Of Physical Oceanography*, *18*, 1855–1875.

Hatun, H., Sando, A. B., Drange, H., Hansen, B., & Valdimarsson, H. (2005).

Influence of the atlantic subpolar gyre on the thermohaline circulation. *Science*, *309*, 1841–1844.

Hautala, S., & Roemmich, D. H. (1998). Subtropical mode water in the northeast pacific basin. *Journal of Geophysical Research*, *103*, 13055–13066.

Hawkins, E., Smith, R., Allison, L., Gregory, J., Woolings, T., Pohlmann, H., & de Cuevas, B. (2011). Bistability of the Atlantic overturning circulation in a global climate model and links to ocean freshwater transport. *Geophysical Research Letters*, *38*.

Hay, W. (1993). The role of polar deep water formation in global climate change. *Annual Reviews of Earth and Planetary Sciences*, *21*, 227–254.

Hazeleger, W., & Drijfhout, S. (2006). Subtropical cells and meridional overturning circulation pathways in the tropical atlantic. *Journal Of Geophysical Research-Oceans*, *111*.

Hellmer, H. H., & Bersch, M. (1985). *The Southern Ocean: A survey of oceanographic and marine meteorological research work*. Technical Report 26 Reports on Polar Research.

Helm, K., Bindoff, N., & Church, J. (2010). Changes in the global hydrological cycle inferred from ocean salinity. *Geophysical Research Letters*, *37*.

Hendy, I., & Kennett, J. (2003). Tropical forcing of north pacific intermediate water distribution during late quaternary rapid climate change? *Quaternary Science Reviews*, *22*, 673–689.

Herraiz-Borreguero, L., & Rintoul, S. R. (2011). Subantarctic mode water: distribution and circulation. *Ocean Dynamics*, *61*, 103–126.

Heywood, K. J., Garabato, A. C. N., Stevens, D. P., & Muench, R. D. (2004). On the fate of the antarctic slope front and the origin of the weddell front. *Journal Of Geophysical Research-Oceans*, *109*.

Hickey, H., & Weaver, A. . (2004). The southern ocean as a source region for tropical atantic variability. *Journal of Climate*, *17*, 3960–3972.

Hillaire-Marcel, C., de Vernal, A., Bilodeau, G., & Weaver, A. (2001). Absence of deep-water formation in the Labrador Sea during the last interglacial period. *Nature*, *410*, 1073–1077.

Hofmann, E., Busalacchi, A. J., & O'Brien, J. (1981). Wind generation of the costa rica dome. *Science*, *214*, 552–554.

Holbrook, N., & Maharaj, A. (2008). Southwest pacific subtropical mode water: a climatology. *Progress in Oceanography*, *77*, 298–315.

Holland, D. (2001). Explaining the weddell polynya - a large ocean eddy shed at maud rise. *Science*, *292*, 1697–1700.

Holland, M., Finnis, J., Barrett, A., & Serreze, M. (2007). Projected changes in arctic ocean freshwater budgets. *Journal of Geophysical Research*, *112*.

Holland, M., Serreze, M., & Stroeve, J. (2010). The sea ice mass budget of the arctic and its future change as simulated by coupled climate models. *Climate Dynamics*, *34*, 185–200.

Hoppema, M., Fahrbach, E., Schroder, M., Wisotzki, A., & deBaar, H. J. W. (1995). Winter-summer differences of carbon dioxide and oxygen in the weddell sea surface layer. *Marine Chemistry*, *51*, 177–192.

Hosoda, S., Xie, S. P., Takeuchi, K., & Nonaka, M. (2001). Eastern north pacific subtropical mode water in a general circulation model: Formation mechanism and salinity effects. *Journal Of Geophysical Research-Oceans*, *106*, 19671–19681.

Huang, R. X., & Qiu, B. (1998). The structure of the wind-driven circulation in the subtropical south pacific ocean. *Journal Of Physical Oceanography*, *28*, 1173–1186.

Huang, R. X., & Russell, S. (1994). Ventilation of the subtropical north pacific. *Journal Of Physical Oceanography*, *24*, 2589–2605.

Hurrell, J. W. (1995). Decadal trends in the north atlantic oscillation regional temperatures and precipiations. *Science*, *269*, 676–679.

Hurrell, J. W., Visbeck, M., Busalacchi, A., Clarke, R. A., Delworth, T. L., Dickson, R. R., Johns, W. E., Koltermann, K. P., Kushnir, Y., Marshall, D., Mauritzen, C., McCartney, M. S., Piola, A., Reason, C., Reverdin, G., Schott, F., Sutton, R., Wainer, I., & Wright, D. (2006). Atlantic climate variability and predictability: A clivar perspective. *Journal Of Climate*, *19*, 5100–5121.

Iorga, M. C., & Lozier, M. (1999a). Signatures of the mediterranean outflow from a north atlantic climatology. 1. salnity and density fields. *Journal of Geophysical Research*, *104*, 25985–26009.

Iorga, M. C., & Lozier, M. (1999b). Signatures of the mediterranean outflow from a north atlantic climatology. 2. diagnostic velocity fields. *Journal of Geophysical Research*, *104*, 26011–26029.

Iudicone, D., Rodgers, K. B., Schopp, R., & Madec, G. (2007). An exchange window for the injection of Antarctic Intermediate Water into the South Pacific. *Journal of Physical Oceanography*, *37*, 31–49.

Ivanov, V. V., Shapiro, G. I., Huthnance, J. M., Aleynik, D. L., & Golovin, P. N. (2004). Cascades of dense water around the world ocean. *Progress In Oceanography*, *60*, 47–98.

Jacobs, S. (1991). On the nature and significance of the antarctic slope front. *Marine Chemistry*, *35*, 9–24.

Jacobs, S., Fairbanks, R., & Horibe, Y. (1985). Oceanology of the antarctic continental shelf. chapter Origin and evolution of water masses near the Antarctic continental margin: Evidence from H218O/H216O ratios in seawater. (pp. 59–85). AGU volume 43 of *Antarctic Res. Ser.*.

Jacobs, S., & Georgi, D. (1977). Observations in the southwest indian/antarctic ocean. In M. Angel (Ed.), *A voyage of Discovery* Suppl. to vol. 24 (pp. 43–89). Deep Sea Research.

Jacobs, S., Gordon, A., & Amos, A. (1979a). Effect of glacial ice melting on the antarctic surface water. *Nature*, *277*, 469–471.

Jacobs, S., Gordon, A., & Ardai, J. (1979b). Circulation and melting beneath the ross ice shelf. *Sciences*, *203*, 439–443.

Jacobs, S. S. (2004). Bottom water production and its links with the thermohaline circulation. *Antarctic Science*, *16*, 427–437.

Jennings, J. J., Gordon, L., & Nelson, D. (1984). Nutrient depletion indicates high primary productivity in the weddell sea. *Nature*, *309*, 51–54.

Joyce, T., & Robbins, P. (1996). The long-term hydrographic record at bermuda. *Journal of Climate*, *9*, 3121–3131.

Joyce, T. M. (2011). New perspectives on eighteen-degree water formation in the north atlantic. *J. Oceanogr.*, *67*.

Joyce, T. M., & Dunworth-Baker, J. (2003). Long-term hydrographic variability in the northwest pacific ocean. *Geophysical Research Letters*, *30*, 1043.

Juliano, M., & Alves, M. (2007). The atlantic subtropical front/current systesms of the azores and st. helena. *Journal of Physical Oceanography*, *37*, 2573–2598.

Jung, S., Kroon, D., Ganssen, G., Peeters, F., & Ganeshram, R. (2010). Southern hemisphere intermediate water formation and the bi-polar seesaw. *PAGES news*, *18*, 36–38.

Kang, I., Jin, K., Wang, B., Lau, K., Shukla, J., Krishnamurthy, V., Schubert, S., Wailser, D., Stern, W., Kitoh, A., Meehl, G., Kanamitsu, M., Galin, V., Satyan, V., Park, C., & Liu, Y. (2002). Intercomparison of the climatologial variations of asian summer monsoon precipiatation simulated by 10 gcms. *Climate Dynamics*, *19*, 383–395.

Karcher, M., Gerdes, R., & Kauker, F. (2008). Arctic-subarctic ocean fluxes: defining the role of the northern seas in climate. chapter Ch 5. Long-term variability of Atlantic Water inflow to the Northern Seas: insight from model experiments. Springer.

Karl, D., Michaels, A., Bergman, B., Capone, D., Carpenter, E., Letelier, R., Lipschultz, F., Paerl, H., Sigman, D., & Stal, L. (2002). Dinitrogen fixation in the world's oceans. *Biogeochemistry*, *57/58*, 47–98.

Karstensen, J., & Quadfasel, D. (2002a). Formation of southern hemisphere thermocline waters: Water mass conversion and subduction. *Journal Of Physical Oceanography*, *32*, 3020–3038.

Karstensen, J., & Quadfasel, D. (2002b). Water subducted into the indian ocean subtropical gyre. *Deep-Sea Research Part Ii-Topical Studies In Oceanography*, *49*, 1441–1457.

Karstensen, J., Schlosser, P., Wallace, D. W. R., Bullister, J. L., & Blindheim, J. (2005). Water mass transformation in the greenland sea during the 1990s. *Journal Of Geophysical Research-Oceans*, *110*.

Kasajima, Y., & Johannessen, T. (2009). Role of cabbeling in water densification in the greenland basin. *Ocean Science*, *5*, 247–257.

Kase, R., Zenk, W., Sanford, T., & Hiller, W. (1985). Currents, fronts and eddy fluxes in the canary basin. *Prog. Oceanog.*, *14*, 231–257.

Katsumata, K., Ohshima, K. I., Kono, T., Itoh, M., Yasuda, I., Volkov, Y., & Wakatsuchi, M. (2004). Water exchange and tidal currents through the bussol' strait revealed by direct current measurements. *Journal of Geophysical Research*, *109*.

Kawase, M., & Sarmiento, J. L. (1985). Nutrients in the atlantic thermocline. *Journal of Geophysical Research*, *90*, 8961–8979.

Kawase, M., & Sarmiento, J. L. (1986). Circulation and nutrients in middepth atlantic waters. *Journal Of Geophysical Research-Oceans*, *91*, 9749–9770.

Keeling, R., & Stephens, B. (2001). Antarctic sea ice and the control of pleistocene climate instability. *Paleoceanography*, *16*, 112–131.

Kelley, D. E. (1994). Temperature-salinity criterion for inhibition of deep convection. *Journal Of Physical Oceanography*, *24*, 2424–2433.

Kelly, K., Small, R., Samelson, R., Qiu, B., Joyce, T., Kwon, Y., & Cronin, M. (2010). Western boundary currents and frontal air-sea interaction: Gulf

stream and kuroshio extension. *Journal of Climate*, *23*, 5644–5667.
Kerr, R., Wainer, I., & Mata, M. (2009). Representation of the weddell sea deep water masses in the ocean component of the ncar-ccsm model. *Antarctic Science*, *21*, 301–312.
Key, R. M., Kozyr, A., Sabine, C. L., Lee, K., Wanninkhof, R., Bullister, J. L., Feely, R. A., Millero, F. J., Mordy, C., & Peng, T. H. (2004). A global ocean carbon climatology: Results from global data analysis project (glodap). *Global Biogeochemical Cycles*, *18*, GB4031.
Khatiwala, S., Fairbanks, R., & Houghton, R. A. (1999). Freshwater sources to the coastal ocean off northeastern north america: Evidence from h218o/h216o. *Journal of Geophysical Research*, *104*, 18241–18255.
Khatiwala, S., Schlosser, P., & Visbeck, M. (2002). Rates and mechanisms of water mass transformation in the labrador sea as inferred from tracer observations. *Journal Of Physical Oceanography*, *32*, 666–686.
Khatiwala, S., & Visbeck, M. (2000). An estimate of the eddy-induced circulation in the labrador sea. *Geophysical Research Letters*, *27*, 2277–2280.
Kieke, D., Klein, B., Stramma, L., Rhein, M., & Koltermann, K. P. (2009). Variability and propagation of labrador sea water in the southern subpolar north atlantic. *Deep-Sea Research I*, *56*, 1656–1674.
Kieke, D., Rhein, M., Stramma, L., Smethie, W., LeBel, D., & Zenk, W. (2006). Changes in the cfc inventories and formation rates of upper labrador sea water, 1997-2001. *Journal of Physical Oceanography*, *36*, 64–86.
Killworth, P. D. (1977). Mixing of the weddell sea continental slope. *Deep Sea Research*, *24*.
Killworth, P. D. (1983). Deep convection in the world ocean. *Reviews Of Geophysics*, *21*, 1–26.
Knox, F., & McElroy, M. (1984). Changes in atmospheric co2: influence of the marine biota a high latitude. *Journal of Geophysical Research*, *89*, 4629–4637.
Kosters, F. (2004). Denmark strait overflow: comparing model results and hydraulic transport estimates. *Journal of Geophysical Research*, *109*.
Kouketsu, S., Tomita, H., Oka, E., Hosoda, S., Kobayashi, T., & Sato, K. (2011). The role of mesoscale eddies in mixed layer deepening and mode water formation in the western north pacific. *J. Oceanogr.*, *67*.
Krémeur, A., Lévy, M., Aumont, O., & Reverdin, G. (2009). Impact of the subtropical mode water biogeochemical properties on primary production in the north atlantic: new insights from an idealized model study. *Journal of Geophysical Research*, *114*.
Kuhlbrodt, T., Griesel, A., Montoya, M., Levermann, A., Hofmann, M., & Rahmstorf, S. (2007). On the driving processes of the Atlantic meridional overturning circulation. *Reviews Of Geophysics*, *45*, 1–32.
Lachkar, Z., Orr, J., ¡.C., D., & Delecluse, P. (2009). On the role of mesoscale eddies in the ventilation of antarctic intermediate water. *Deep-Sea Research I*, *56*, 909–925.
Ladd, C., & Thompson, L. (2000). Formation mechanisms for north pacific central and eastern subtropical mode waters. *Journal Of Physical Oceanography*, *30*, 868–887.
Larque, L., Maamaatuaiahutapu, K., & Garcon, V. (1997). On the intermediate and deep water flows in the south atlantic ocean. *Journal Of Geophysical Research-Oceans*, *102*, 12425–12440.
Latif, E., M.and Roeckner, Mikolajewicz, U., & Voss, R. (2000). Tropical stabilization of the thermohaline circulation in a greenhouse warming simulation. *Journal of Climate*, *13*, 1809–1813.
Lavender, K., Davis, R., & Owens, B. (2000). Mid-depth recirculation observed in the interior labrador and irminger seas by direct velocity measurements. *Nature*, *407*, 66–69.
Lazier, J., Hendry, R., Clarke, A., Yashayaev, I., & Rhines, P. (2002). Convection and restratification in the labrador sea, 1990-2000. *Deep-Sea Research Part I-Oceanographic Research Papers*, *49*, 1819–1835.
Lazier, J. R. N. (1973). The renewal of labrador sea water. *Deep Sea Research*, *20*, 341–353.
Lazier, J. R. N. (1980). Oceanographic conditions at ocean weather ship bravo, 1964-1974. *Atmos.-Ocean*, *18*, 227–238.
Legg, S., Briedleb, B., Chang, Y., & et al. (2009). Improving oceanic overflow representation in climate models. *BAMS*, *May*, 657–670.
Legg, S., Hallberg, R. W., & Girton, J. (2006). Comparison of entrainment in overflows simulated by a z-coordinate, isopycnal and non-hydrostatic models. *Ocean Modelling*, *11*, 69–97.
Lewis, E., & Perkin, R. (1986). Ice pumps and their rates. *Journal of Geophysical Research*, *91*, 11756–11762.
Lherminier, P., Mercier, H., Gourcuff, C., Alvarez, M., Bacon, S., & Kermabon, C. (2007). Transports across the 2002 greenland-portugal ovide section and comparison with 1997. *Journal of Geophysical Research*, *112*, C07003.
Li, C., & Battisti, D. S. (2008). Reduced atlantic storminess during last glacial maximum: evidence from a coupled climate model. *Journal of Climate*, *21*, 3561–3579.
Lilly, J., & Rhines, P. (2002). Coherent eddies in the labrador sea observed from a morring. *Journal of Physial Oceanography*, *32*, 585–598.
Lilly, J., Rhines, P., Schott, F., Lavender, K., Lazier, J., Send, U., & D'Asaro, E. A. (2003). Observations of the labrador sea eddy field. *Progress in Oceanography*, *59*, 75–176.
Locarini, R., Mishonov, A., Antonov, J., Boyer, T., & Garcia, H. (2006). *World Ocean Atlas 2005, vol. 1, Temperature NOAA Atlas NESDIS*. edited by S. Levitus et al. vol. 61 NOAA Silver Spring, Md.
Losch, M. (2008). Modeling ice shelf cavities in a z coordinate ocean general circulation model. *Journal of Geophysical Research*, *113*.
Lovenduski, N. S., & Gruber, N. (2005). Impact of the southern annular mode on southern ocean circulation and biology. *Geophysical Research Letters*, *32*.
Lovenduski, N. S., Gruber, N., Doney, S., & Lima, I. (2007). Enhanced co2 outgassing in the southern ocean from a positive phase of the southen annular mode. *Global Biogeochemical Cycles*, *21*.
Lozier, M. (2010). Deconstructing the conveyor belt. *Science*, *328*, 1507–1511.
Lozier, M., Owens, W., & Curry, R. (1995). The climatology of the north atlantic. *Prog. Oceanog.*, *36*, 1–44.
Lozier, M., & Sindlinger, L. (2009). On the source of mediterranean overflow water property changes. *Journal of Physical Oceanography*, *39*, 1800–1817.
Lozier, M., & Stewart, N. (2008). On the temporally varying northward penetration of mediterranean overflow water and eastward penetration of labrador sea water. *Journal of Physical Oceanography*, *38*, 2097–2103.
Lozier, M. S. (1999). The impact of mid-depth recirculations on the distribution of tracers in the north atlantic. *Geophysical Research Letters*, *26*, 219–222.
Lumpkin, R., & Speer, K. (2007). Global ocean meridional overturning. *Journal Of Physical Oceanography*, *37*, 2550–2562.
Luyten, J. R., Pedlosky, J., & Stommel, H. (1983). The ventilated thermocline. *Journal of Physical Oceanography*, (pp. 292–309).
Maamaatuaiahutapu, K., Garcon, V. C., Provost, C., Boulahdid, M., & Osiroff, A. P. (1992). Brazil-malvinas confluence - water mass composition. *Journal Of Geophysical Research-Oceans*, *97*, 9493–9505.
MacAyeal, D. (1984). Thermohaline circulation below the ross ice shelf: a consequence of tidally induced vertical mixing and basal melting. *Journal of Geophysical Research*, *89*, 597–606.
Macdonald, A. M., Mecking, S., Robbins, P., Toole, J., Johnson, G., Talley, L., Cook, M., & Wijffels, S. (2009). The woce-era 3-d pacific ocean circulation and heat budget. *Progress in Oceanography*, *82*, 281–325.
MacDonald, R., & Carmack, E. (1993). Tritium and radiocarbon dating of canada basin deep waters. *Science*, *259*, 103–104.
Mackintosh, A., & et al. (2011). Retreat of the east antarctic ice sheet during the last glacial termination. *Nature Geosciences*, *4*, 195–202.
Madelain, F. (1970). nfluence de la topogrpahie du fond sur l'ecoulement medterraneen entre le detroit de gibraltar et le cap saint-vincent. *Cah. Oceanogr.*, *22*, 43–61.
Mahlstein, I., & Knutti, R. (2011). Ocean heat transport as a cause for model uncertainty in projected Arctic warming. *Journal of Climate*, *24*, 1451–1460.
Mamayev, O. (1975). Temperature-salinity analysis of world ocean waters. translation from russian by robert j. burton. Elsevier Scientific Publishing.
Manabe, S., & Stouffer, R. J. (1995). Simulation of abrupt climate-change induced by fresh-water input to the north-atlantic ocean. *Nature*, *378*, 165–167.
Marinov, I., Gnanadesikan, A., Toggweiler, J. R., & Sarmiento, J. L. (2006). The southern ocean biogeochemical divide. *Nature*, *441*, 964–967.
Marotzke, J., & Scott, J. R. (1999). Convective mixing and the thermohaline circulation. *Journal Of Physical Oceanography*, *29*, 2962–2970.
Marshall, D. (1997). Subduction of water masses in an eddying ocean. *Journal of Marine Research*, *55*, 201–222.
Marshall, J., & Schott, F. (1999). Open-ocean convection: observations, theory, and models. *Reviews Of Geophysics*, *37*, 1–64.
Martinson, D. (1990). Evolution of the southern ocean winter mixed layer and sea ice: Open ocean deepwater formation and ventilation. *Journal of Geophysical Research*, *95*, 11641–11654.
Martinson, D., Killworth, P., & Gordon, A. (1981). A convective model for the

weddell polynya. *Journal of Physical Oceanography*, *11*, 466–488.
Masuda, S., Awaji, T., Sugiura, N., Toyoda, T., Ishikawa, Y., & Horiuchi, K. (2006). Interannual variability of temperature inversions in the subarctic north pacific. *Geophysical Research Letters*, *33*.
Masujima, M., & Yasuda, I. (2009). Distribution and modification of north pacific intermediate water around the subarctic frontal zone east of 150e. *Journal of Physical Oceanography*, *39*, 1462–1474.
Masuzawa, J. (1969). Subtropical mode water. *Deep-Sea Research*, *16*, 463–472.
Matsumoto, K., Sarmiento, J. L., Key, R. M., Aumont, O., Bullister, J. L., Caldeira, K., Campin, J. M., Doney, S. C., Drange, H., Dutay, J. C., Follows, M., Gao, Y., Gnanadesikan, A., Gruber, N., Ishida, A., Joos, F., Lindsay, K., Maier-Reimer, E., Marshall, J. C., Matear, R. J., Monfray, P., Mouchet, A., Najjar, R., Plattner, G. K., Schlitzer, R., Slater, R., Swathi, P. S., Totterdell, I. J., Weirig, M. F., Yamanaka, Y., Yool, A., & Orr, J. C. (2004). Evaluation of ocean carbon cycle models with data-based metrics. *Geophysical Research Letters*, *31*.
Matt, S., & Johns, W. (2007). Transport and entrainment in the red sea outflow plume. *Journal of Physical Oceanography*, *37*, 819–836.
Mauritzen, C. (1996). Production of dense overflow waters feeding the north atlantic across the greenland-scotland ridge. part 1: Evidence for a revised circulation scheme. *Deep-Sea Research I*, *43*, 769–806.
Mauritzen, C., & et al. (2011). Closing the loop - approaches to monitoring the state of the arctic mediterranean during the international polar year 2007-2008. *Progress In Oceanography*, *in press*.
Maze, G., Forget, G., Buckely, M., & Marshall, J. (2009). Using transformation and formation maps to study the role of air-sea heat fluxes in north atlantic eighteen degree water formation. *Journal of Physical Oceanography*, *39*, 1818–1835.
Maze, J. P., Arhan, M., & Mercier, H. (1997). Volume budget of the eastern boundary layer off the iberian peninsula. *Deep-Sea Research Part I-Oceanographic Research Papers*, *44*, 1543–1574.
McCarthy, M. C., & Talley, L. D. (1999). Three-dimensional isoneutral potential vorticity structure in the indian ocean. *Journal Of Geophysical Research-Oceans*, *104*, 13251–13267.
McCartney, M. (1977). A voyage of discovery: George deacon 70th anniversary. chapter Subantarctic Mode Water. (pp. 103–119). Deep Sea Research (Suppl.).
McCartney, M. S. (1992). Recirculating components to the deep boundary current of the northern north-atlantic. *Progress In Oceanography*, *29*, 283–383.
McCartney, M. S., & Mauritzen, C. (2001). On the origin of the warm inflow to the nordic seas. *Progress In Oceanography*, *51*, 125–214.
McCartney, M. S., & Talley, L. D. (1982). The subpolar mode water of the north-atlantic ocean. *Journal Of Physical Oceanography*, *12*, 1169–1188.
McKee, D., Yuan, X., Gordon, A., Huber, B., & Dong, Z. (2011). Climate impact on interannual variability of weddell sea bottom water. *Journal of Geophysical Research*, *116*.
McManus, J., Francois, R., Gherardhi, J.-M., Keigwin, L., & Brown-Leger, S. (2004). Collapse and rapid resumption of atlantic meridional circulation linked to deglacial climate changes. *Nature*, *428*, 834–837.
McPhee, M., Proshutinsky, A., Morison, J., Steele, M., & Alkire, M. (2009). Rapid change in freshwater content of the arctic ocean. *Geophysical Research Letters*, *36*.
Mecking, S., & Warner, M. J. (2001). On the subsurface cfc maxima in the subtropical north pacific thermocline and their relation to mode waters and oxygen maxima. *Journal Of Geophysical Research-Oceans*, *106*, 22179–22198.
Meincke, J., Rudels, B., & Friedrich, H. (1997). The arctic ocean-nordic seas thermohaline system. *Ices Journal Of Marine Science*, *54*, 283–299.
Melling, H., Agnew, T., Falkner, K., Greenberg, D., Lee, C., Muenchow, A., Petrie, B., Prinsenberg, S., Samelson, R., & Woodgate, R. (2008). Arctic subarctic ocean fluxes: defining the role of the northern seas in climate. chapter 9. Fresh-water fluxes via Pacific and Arctic outflows across the Canadian polar shelf. (pp. 193–247). Springer-Verlag.
Menemenlis, D., Fukumori, I., & Lee, T. (2007). Atlantic to mediterranean sea level difference driven by winds near gibraltar strait. *Journal of Physical Oceanography*, *37*, 359–376.
Meredith, M., Gordon, A., Naveira Garabato, A., Abrahamsen, E., Huber, B., Jullion, L., & Venables, H. (2011). Synchonous intensification and warming of antarctic bottom water outflow from the weddell gyre. *Geophysical Research Letters*, *38*.
Meredith, M. P., Garabato, A. C. N., Gordon, A. L., & Johnson, G. C. (2008). Evolution of the deep and bottom waters of the Scotia Sea, Southern Ocean, during 1995-2005. *Journal of Climate*, *21*, 3327–3343.
Meschanov, S. L., & Shapiro, G. I. (1998). A young lens of red sea water in the arabian sea. *Deep Sea Research I*, *45*, 1–13.
Messias, M. J., Watson, A., Johannessen, T., & et al. (2008). The greenland sea tracer experiment 1996-2002: horizontal mixing and transport of greenland sea intermediate water. *Progress In Oceanography*, *78*, 85–105.
Mikaloff-Fletcher, S. E., Gruber, N., Jacobson, A., & et al. (2007). Inverse estiamtes of the oceanic sources and sinks of natural co2 and the implied oceanic carbon transport. *Global Biogeochemical Cycles*, *21*.
Millot, C., Candela, J., Fuda, J., & Tber, Y. (2006). Large warming and salinification of the mediterranean outflow due to changes in its composition. *Deep-Sea Research I*, *53*, 656–666.
Miura, T., Suga, T., & Hanawa, K. (2002). Winter mixed layer and formation of dichothermal water in the bering sea. *Journal Of Oceanography*, *58*, 815–823.
Miura, T., Suga, T., & Hanawa, K. (2003). Numerical study of formation of dichothermal water in the bering sea. *Journal of Oceanography*, *59*, 369–376.
Molinari, R., Fine, R., & Johns, E. (1992). The deep western boundary current in the tropical north atlantic ocean. *Deep-Sea Research*, *39*, 1967–1984.
Molinari, R., Fine, R., Wilson, W., Curry, R., Abell, J., & McCartney, M. (1998). The arrival of recently formed labrador sea water in the deep western boundary current at 26.5n. *Geophysical Research Letters*, *25*, 2249–2252.
Molinelli, E. (1978). Isohaline thermoclines in southeast pacific ocean. *Journal Of Physical Oceanography*, *8*, 1139–1145.
Molinelli, E. J. (1981). The antarctic influence on antarctic intermediate water. *Journal Of Marine Research*, *39*, 267–293.
Moore, G., & Renfrew, I. (2005). Tip jets and barrier winds: a quikscat climatology of high wind speed events around greenland. *Journal of Climate*, *18*, 3713–3725.
Mosby, H. (1934). The waters of the atlantic antarctic ocean. *Scientific Results of the Norwegian Antarctic Expeditions 1927-1928*, *1*, 131 p.
Murray, S., & Johns, W. (1997). Direct observations of seasonal exchange through the bab el mandab strait. *Geophysical Research Letters*, *24*, 2557–2560.
Myers, P. (2005). Impact of freshwater from the canadian arctic archipelago on labrador sea water formation. *Geophysical Research Letters*, *32*.
Myers, P., & Donnelly, C. (2008). Water mass transformation and formation in the labrador sea. *Journal of Climate*, *21*, 1622–1638.
Mysak, L., Manak, D., & Marsden, R. (1990). Sea-ice anomalies observed in the greenland and labrador seas during 1901-1984 and their relation to an interdecadal arctic climate cycle. *Climate Dynamics*, *5*, 111–133.
Nakamura, H. (1996). A pycnostad on the bottom of the ventilated portion in the central subtropical north pacific: its distribution and formation. *Journal of Oceanography*, *52*, 171–188.
Naveira Garabato, A., Jullion, L., Stevens, D., Heywood, K., & King, B. (2009). Variability of subantarctic mode water and antarctic intermediate water in the drake passage during the late-twenty-first centuries. *Journal of Climate*, *22*, 3661–3688.
Naveira-Garabato, A. C., McDonagh, E. L., Stevens, D. P., Heywood, K. J., & Sanders, R. J. (2002). On the export of antarctic bottom water from the weddell sea. *Deep-Sea Research Part II-Topical Studies In Oceanography*, *49*, 4715–4742.
Nilsen, J., & Falck, E. (2006). Variations of mixed layer properties in the norwegian sea for the period 1948-1999. *Progress in Oceanography*, *70*, 58–90.
Ninnemann, U. S., & Charles, C. (1997). Regional differences in quaternary subantarctic nutrient cycling: link to intermediate and deep water ventilation. *Paleoceanography*, *12*, 560–567.
Nishikawa, S., Tsujino, H., Sakamoto, K., & Nakano, H. (2010). Effects of mesoscale eddies on subduction and distribution of subtropical mode water in an eddy resolving ogcm of the western north pacific. *Journal of Physical Oceanography*, *40*, 1748–1765.
Nitishinsky, M., Anderson, L., & Hoelmann, J. (2007). Inorganic carbon and nutrient fluxes on the arctic shelf. *Continental Shelf Research*, *27*, 1584–1599.
Nunez Vaz, R., & Lennon, G. (1996). Physical oceanography of the prydz bay region of antarctic waters. *Deep-Sea Research I*, *43*, 603–641.
O'Connor, B., Fine, R., & Olson, D. (2005). A global comparison of subtropical underwater formation rates. *Deep-Sea Research I*, *52*, 1569–1590.

O'Connor, B., Fine, R. A., Maillet, K., & Olson, D. (2002). Formation rates of subtropical underwater in the pacific ocean. *Deep-Sea Research I*, *49*, 1571–1590.

Ohshima, K. I., Nakanowatari, T., Riser, S., & Wakatsuchi, M. (2010). Seasonal variation in the in- and outflow of the okhotsk sea with the north pacific. *Deep-Sea Research II*, *57*, 1247–1256.

Oka, E., & Qiu, B. (2011). Progress of north pacific mode water research in the past decade. *J. Oceanogr.*, *67*.

Oka, E., & Suga, T. (2003). Formation region of north pacific subtropical mode water in the late winter of 2003. *Geophysical Research Letters*, *30*. 2205.

Oka, E., & Suga, T. (2005). Differential formation and circulation of north pacific central mode water. *Journal Of Physical Oceanography*, *35*, 1997–2011.

Olsson, K., Jeansson, E., Anderson, L., Hansen, B., Eldevik, T., Kristiansen, R., Messias, M., Johannessen, T., & Watson, A. (2005). Intermediate water from the greenland sea in the faroe bank channgel: spreading of released sulphur hexafluoride. *Deep-Sea Research I*, *52*, 279–294.

Ono, K., Ohshima, K., Kono, T., Itoh, M., Katsumata, K., Volkov, Y., & Wakatsuchi, M. (2007). Water mass exchange and diapycnal mixing at bussol' strait revealed by water mass properties. *Journal of Oceanography*, *63*, 281–291.

Ono, T., Sasaki, K., & Yasuda, I. (2003). Re-estimation of annual anthropogenic carbon input from oyashio into north pacific intermediate water. *Journal Of Oceanography*, *59*, 883–891.

Orsi, A. (2010). Recycling bottom waters. *Nature Geosciences*, *3*, 307–309.

Orsi, A. H., Jacobs, S. S., Gordon, A. L., & Visbeck, M. (2001). Cooling and ventilating the abyssal ocean. *Geophysical Research Letters*, *28*, 2923–2926.

Orsi, A. H., Johnson, G. C., & Bullister, J. L. (1999). Circulation, mixing, and production of Antarctic Bottom Water. *Progress in Oceanography*, *43*, 55–109.

Orsi, A. H., Nowlin, W. D., & Whitworth, T. (1993). On the circulation and stratification of the weddell gyre. *Deep-Sea Research Part I-Oceanographic Research Papers*, *40*, 169–203.

Orsi, A. H., Smethie, W. M., & Bullister, J. L. (2002). On the total input of Antarctic waters to the deep ocean: A preliminary estimate from chlorofluorocarbon measurements. *Journal Of Geophysical Research-Oceans*, *107*. doi:10.1029/2001JC000976.

Orsi, A. H., Whitworth, T., & Nowlin, W. D. (1995). On the meridional extent and fronts of the antarctic circumpolar current. *Deep-Sea Research Part I-Oceanographic Research Papers*, *42*, 641–673.

Orsi, A. H., & Wiederwohl, C. (2009). A recount of ross sea waters. *Deep-Sea Research II*, *56*, 778–795.

Orvik, K., & Niiler, P. (2002). Major pathways of atlantic water in teh northern north atlantic and nordic seas toward arctic. *Geophysical Research Letters*, *29*, 1896.

Ou, H. W. (2007). Watermass properties of the antarctic slope front: A simple model. *Journal Of Physical Oceanography*, *37*, 50–59.

Pahnke, K., & Zahn, R. (2005). Southern hemispere water mass conversion linked with north atlantic climate variability. *Science*, *307*, 1741–1746.

Paillet, J., & Arhan, M. (1996). Shallow pycnoclines and mode water subduction in the eastern north atlantic. *Journal Of Physical Oceanography*, *26*, 96–114.

Paillet, J., Arhan, M., & McCartney, M. (1998). Spreading of labrador sea water in the eastern north atlantic. *Journal of Geophysical Research*, *103*, 10223–10239.

Palter, J. B., Lozier, M. S., & Barber, R. T. (2005). The effect of advection on the nutrient reservoir in the north atlantic subtropical gyre. *Nature*, *437*, 687–692.

Papadakis, M., Chassignet, E., & Hallberg, R. W. (2003). Numerical simulations of the mediterranean sea outflow: impact of the entrainment parameterization in an isopycnic coordinate ocean model. *Ocean Modelling*, *5*, 325–356.

Park, Y. H., & Gamberoni, L. (1997). Cross-frontal exchange of antarctic intermediate water and antarctic bottom water in the crozet basin. *Deep-Sea Research Part Ii-Topical Studies In Oceanography*, *44*, 963–986.

Peters, H., & Johns, W. (2005). Mixing and entrainment in the red sea outflow plume. part ii: turbulence characteristics. *Journal of Oceanography*, *35*, 584–600.

Peters, H., Johns, W., Bower, A., & Fratantoni, D. (2005). Mixing and entrainment in the red sea outflow plume. part i: Plume structure. *Journal of Physical Oceanography*, *35*, 569–583.

Peterson, B., McClelland, J., Curry, R., Holmes, R., Walsh, J., & Aagaard, K. (2006). Trajectory shifts in the arctic and subarctic freshwater cycle. *Science*, *313*, 1061–1066.

Pickart, R. (1992). Water mass component of the north atlantic deep western boundary current. *Deep-Sea Research*, *39*, 1553–1572.

Pickart, R., & Spall, M. (2007). Impact of labrador sea convection on the north atlantic meridional overturning circulation. *Journal of Physical Oceanography*, *37*, 2207–2227.

Pickart, R. S., & Smethie, W. (1993). How does the deep western boundary current cross the gulf stream? *Journal of Physical Oceanography*, *23*, 2602–2616.

Pickart, R. S., Smethie, W. M., Lazier, J. R. N., Jones, E. P., & Jenkins, W. J. (1996). Eddies of newly formed upper labrador sea water. *Journal Of Geophysical Research-Oceans*, *101*, 20711–20726.

Pickart, R. S., Spall, M., Ribergaard, M., Moore, G., & Milliff, R. (2003a). Deep convection in teh irminger sea forced by the greenland tip jet. *Nature*, *424*, 152–156.

Pickart, R. S., Straneo, F., & Moore, G. W. K. (2003b). Is labrador sea water formed in the irminger basin? *Deep-Sea Research Part I-Oceanographic Research Papers*, *50*, 23–52.

Pickart, R. S., Torres, D. J., & Clarke, R. A. (2002). Hydrography of the labrador sea during active convection. *Journal Of Physical Oceanography*, *32*, 428–457.

Piola, A. R., & Georgi, D. T. (1981). Sea-air heat and fresh-water fluxes in the drake passage and western scotia sea. *Journal Of Physical Oceanography*, *11*, 121–126.

Piola, A. R., & Georgi, D. T. (1982). Circumpolar properties of antarctic intermediate water and sub-antarctic mode water. *Deep-Sea Research Part A-Oceanographic Research Papers*, *29*, 687–711.

Piola, A. R., & Gordon, A. L. (1989). Intermediate waters in the southwest south-atlantic. *Deep-Sea Research Part A-Oceanographic Research Papers*, *36*, 1–16.

Pollard, R., Griffith, M., Cunningham, S., Read, J., Perez, F. F., & Rios, A. F. (1996). Vivaldi 1991 - a study of the formation, circulation and ventilation of easter north atlantic central water. *Progress In Oceanography*, *37*, 167–192.

Pollard, R. T., & Pu, S. (1985). Structure and circulation of the upper atlantic ocean northeast of the azores. *Progress In Oceanography*, *14*, 443–462. 0079-6611.

Price, J., & Baringer, M. (1994). Outflows and deep water production by marginal seas. *Prog. Oceanog.*, *33*, 161–200.

Price, M., Heywood, K. J., & Nicholls, K. W. (2008). Ice-shelf - ocean interactions at fimbul ice shefl, antarctica, from oxygen isotope ratio measurements. *Ocean Science*, *4*, 89–98.

Proshutinsky, A., Bourke, R., & McLaughlin, F. (2002). The role of the beaufort gyre in arctic climate variability: Seasonal to decadal climate scales. *Geophysical Research Letters*, *29*, 2100.

Provost, C., Escoffier, C., Maamaatuaiahutapu, K., Kartavtseff, A., & Garcon, V. (1999). Subtropical mode waters in the south atlantic ocean. *Journal Of Geophysical Research-Oceans*, *104*, 21033–21049.

Qiu, B. (1995). Why is the spreading of the north pacific intermediate water confined on density surfaces around σ_θ=26.8? *Journal of Physical Oceanography*, *25*, 168–180.

Qiu, B., & Huang, R. X. (1995). Ventilation of the north-atlantic and north-pacific - subduction versus obduction. *Journal Of Physical Oceanography*, *25*, 2374–2390.

Qu, T., & Chen, J. (2009). A north pacific decadal variability in subduction rate. *Geophysical Research Letters*, *36*.

Qu, T., Gao, S., & Fukumori, I. (2011). What governs the north atlantic salinity maximum in a global gcm? *Geophysical Research Letters*, *38*.

Qu, T., Gao, S., Fukumori, I., Fine, R. A., & Lindstrom, E. J. (2008). Subduction of south pacific waters. *Geophysical Research Letters*, *35*.

Qu, T. D., & Lindstrom, E. J. (2004). Northward intrusion of antarctic intermediate water in the western pacific. *Journal Of Physical Oceanography*, *34*, 2104–2118.

Rahmstorf, S. (1996). On the freshwater forcing and transport of the Atlantic thermohaline circulation. *Climate Dynamics*, *12*, 799–811.

Reid, J. (1965). *Intermediate waters of the Pacific Ocean*. Johns Hopkins Press.

Reid, J. L. (1969). Sea-surface temperature, salinity, and density of pacific ocean in summer and in winter. *Deep-Sea Research*, *S*, 215. Suppl. S.

Reynolds, R., Rayner, N., Smith, T., Stokes, D., & Wang, W. (2002). An im-

proved in situ and satellite sst analysis for climate. *Journal of Climate*, *15*, 1609–1625.

Rhein, M., Fischer, J., Smethie, W., Smythe-Wright, D., Weiss, R., Mertens, C., Min, D.-H., Fleischmann, U., & Putzka, A. (2002). Labrabor sea water: Pathways, cfc inventory, and formation rates. *Journal of Physical Oceanography*, *32*, 648–665.

Rhein, M., Kieke, D., Huttl-Kabus, S., Roessler, A., Mertens, C., Meissner, R., Klein, B., Boening, C., & Yashayaev, I. (2011). Deep water formation, the subpolar gyre, and the meridional overturning circulation int eh subpolar north atlantic. *Deep-Sea Research II*, *in press*.

Rhein, M., Stramma, L., & Send, U. (1995). The atlantic deep western boundary current - water masses and transports near the equator. *Journal Of Geophysical Research-Oceans*, *100*, 2441–2457.

Richardson, P., Bower, A., & Zenk, W. (2000). A census of meddies tracked by floats. *Progress in Oceangraphy*, *45*, 209–250.

Rickaby, R. E. M., & Elderfield, H. (2005). Evidence from the high-latitude north atlantic for variations in antarctic intermediate water flow during the last deglaciation. *Geochemistry Geophysics Geosystems*, *6*.

Ridgway, K., & Dunn, J. (2003). Mesoscale structure of the mean East Australian Current System and its relationship with topography. *Progress in Oceanography*, *56*, 189–222.

Riemenschneider, U., & Legg, S. (2007). Regional simulations of the faroe bank channel overflow in a level model. *Ocean Modelling*, *17*, 93–122.

Rintoul, S. (1998). Ocean, ice, and atmosphere: interactions at the antarctic continental margin. chapter On the origin and influence of Adelie Land Bottom Water. (pp. 151–171). AGU volume 75 of *Antarctic Res. Ser.*.

Rintoul, S. R., & England, M. H. (2002). Ekman transport dominates local air-sea fluxes in driving variability of subantarctic mode water. *Journal Of Physical Oceanography*, *32*, 1308–1321.

Rio, M.-H., Schaeffer, P., Moreaux, G., Lemoine, J.-M., & Bronner, E. (2009). A new mean dynamic topography computed over the global ocean from GRACE data, altimetry and in-situ measurments. Poster communication at OceanObs09 symposium, Venice.

Robertson, R., Visbeck, M., Gordon, A. L., & Fahrbach, E. (2002). Long-term temperature trends in the deep waters of the weddell sea. *Deep-Sea Research Part Ii-Topical Studies In Oceanography*, *49*, 4791–4806.

Rodehacke, C., Hellmer, H., Beckmann, A., & Roether, W. (2007a). Formation and spreading of antarctic deep and bottom waters inferred from a chloroflu oroacrbon (cfc) simulation. *Journal of Geophysical Research*, *112*.

Rodehacke, C., Hellmer, H., Huhn, O., & Beckmann, A. (2007b). Ocean/ice shelf interaction in the southern weddell sea: results of a regional numerical helium/neon simulation. *Ocean Dynamics*, *57*, 1–11.

Roemmich, D., & Cornuelle, B. (1992). The subtropical mode waters of the south-pacific ocean. *Journal Of Physical Oceanography*, *22*, 1178–1187.

Rogerson, M., Rohling, E., & Weaver, P. (2006). Promotion of meridional overturning by mediterranean-derived salt during the last deglaciation. *Paleoceanography*, *21*.

Rudels, B., Jones, E., Anderson, L., & Kattner, G. (1994). The polar oceans and their role in shaping the global environment. chapter On the intermediate depth waters of the Arctic Ocean. (pp. 33–46). American Geophysical Union volume Geophysical Monograph 85.

Rudels, B., Larsson, A.-M., & Sehlstedt, P.-I. (1991). Stratification and water mass foramtion in the arctic ocean: some implications for the nutrient distribution. In E. Sakshaug, C. Hopkins, & N. Oristland (Eds.), *Proceedings ofthe Pro Mare Symposium on Polar Marine Ecology* (pp. 19–31). volume Polar Research 10.

Rudels, B., & Quadfasel, D. (1991). Convection and deep water formation in the arctic ocean - greenland sea system. *Journal of Marine Systems*, *2*, 435–450.

Rudnick, D. L., & Luyten, J. (1996). Intensive surveys of the azores front. 1. tracers and dynamics. *Journal of Geophysical Research*, *101*, 923–939.

Russell, J. L., & Dickson, A. G. (2003). Variability in oxygen and nutrients in south pacific antarctic intermediate water. *Global Biogeochemical Cycles*, *17*. 1033.

Rutgers Van Der Loeff, M. M., Key, R., Scholten, J., Bauch, D., & Michel, A. (1995). 228ra as a tracer for shelf water in the arctic ocean. *Deep-Sea Research II*, *42*, 1533–1553.

Saafani, M. A., & Shenoi, S. S. C. (2007). Water masses in the gulf of aden. *Journal Of Oceanography*, *63*, 1–14.

Sabine, C. L., Feely, R. A., Gruber, N., Key, R. M., Lee, K., Bullister, J. L., Wanninkhof, R., Wong, C. S., Wallace, D. W. R., Tilbrook, B., Millero, F. J., Peng, T. H., Kozyr, A., Ono, T., & Rios, A. F. (2004). The oceanic sink for anthropogenic co2. *Science*, *305*, 367–371.

Saenko, O. A., Schmittner, A., & Weaver, A. J. (2004). The Atlantic-Pacific seesaw. *Journal of Climate*, *17*, 2033–2038.

Saenko, O. A., Weaver, A. J., & England, M. H. (2003a). A region of enhanced northward Antarctic Intermediate Water transport in a coupled climate model. *Journal of Physical Oceanography*, *33*, 1528–1535.

Saenko, O. A., Weaver, A. J., & Gregory, J. M. (2003b). On the link between the two modes of the ocean thermohaline circulation and the formation of global-scale water masses. *Journal of Climate*, *16*, 2797–2801.

Sallée, J. B., Morrow, R., & Speer, K. (2008). Eddy heat diffusion and subantarctic mode water formation. *Geophysical Research Letters*, *35*.

Sallée, J. B., Speer, K., & Rintoul, S. (2010a). Zonally asymmetric response of the southern ocean mixed-layer depth to the southern annular mode. *Nature Geosciences*, *3*.

Sallée, J. B., Speer, K. G., Rintoul, S., & Wijffels, S. (2010b). Southern ocean thermocline ventilation. *Journal of Physical Oceanography*, *40*, 509–529.

Sallée, J.-B., Wienders, N., Speer, K., & Morrow, R. (2006). Formation of subantarctic mode water in the southeastern Indian Ocean. *Ocean Dynamics*, *56*, 525–542.

Santoso, A., & England, M. (2008). Antarctic Bottom Water variability in a coupled climate model. *Journal of Physical Oceanography*, *38*, 1870–1893.

Santoso, A., & England, M. H. (2004). Antarctic intermediate water circulation and variability in a coupled climate model. *Journal of Physical Oceanography*, *34*, 2160–2179.

Sarafanov, A. (2009). On the effect of the north atlantic oscillation on temperature and salinity of the subpolar north atlantic intermediate and deep waters. *Ices Journal Of Marine Science*, *66*, 1448–1454.

Sarmiento, J. L., Gruber, N., Brzezinski, M. A., & Dunne, J. P. (2004a). High-latitude controls of thermocline nutrients and low latitude biological productivity. *Nature*, *427*, 56–60.

Sarmiento, J. L., Slater, R., Barber, R., Bopp, L., Doney, S. C., Hirst, A. C., Kleypas, J., Matear, R., Mikolajewicz, U., Monfray, P., Soldatov, V., Spall, S. A., & Stouffer, R. (2004b). Response of ocean ecosystems to climate warming. *Global Biogeochemical Cycles*, *18*.

Sarmiento, J. L., & Toggweiler, J. R. (1984). A new model for the role of the oceans in determining atmospheric pco2. *Nature*, *308*, 621–624.

Sathiyamoorthy, S., & Moore, G. (2002). Buoyancy flux at ocean weather station bravo. *Journal of Physical Oceanography*, *32*, 458–474.

Saunders, P. (1990). Cold outflow from the faroe bank channel. *Journal of Physical Oceanography*, *20*, 29–43.

Saunders, P. (1994). The flux of overflow water through the charlie-gibbs fracture zone. *Journal of Geophysical Research*, *99*, 12343–12355.

Saunders, P. (2001). Ocean circulation and climate. chapter 5.6. The dense Northern overflows. (pp. 401–417). Academic Press volume 77 of *International Geophysics Series*.

Schlosser, P., Bullister, J., & Bayer, R. (1991). Studies of deep water formation and circulation in the weddell sea using natural and anthropogenic tracers. *Marine Chemistry*, *35*, 97–122.

Schmid, C., Siedler, G., & Zenk, W. (2000). Dynamics of intermediate water circulation in the subtropical south atlantic. *Journal Of Physical Oceanography*, *30*, 3191–3211.

Schmidt, S., & Send, U. (2007). Origin and composition of seasonal labrador sea freshwater. *Journal of Physical Oceanography*, *37*, 1445–1454.

Schmitt, R. (1994). Double diffusion in oceanography. *Annu. Rev. Fluid Mech.*, *26*, 255–285.

Schmitz, W. J., & McCartney, M. (1993). On the north atlantic circulation. *Reviews of Geophysics*, *31*, 29–49.

Schouten, M. W., & Matano, R. P. (2006). Formation and pathways of intermediate water in the parallel ocean circulation model's southern ocean. *Journal Of Geophysical Research-Oceans*, *111*.

Screen, J., Gillett, N., Karpechko, A., & Stevens, D. (2010). Mixed layer temperature response to the southern annular mode: Mechanisms and model representation. *Journal of Climate*, *23*, 664–678.

Seager, R., Battisti, D. S., Yin, J., Gordon, N., Naik, N., Clement, A. C., & Cane, M. A. (2002). Is the gulf stream responsible for europe's mild winters? *Quarterly Journal Of The Royal Meteorological Society*, *128*, 2563–2586. Part B.

Seidov, D., & Haupt, B. (2002). On the role of inter-basin surface salinity contrasts in global ocean circulation. *Geophysical Research Letters*, *29*, 1800.

Sen Gupta, A., & England, M. H. (2007). Evaluation of interior circulation in a high-resolution global ocean model. part ii: Southern hemisphere intermediate, mode, and thermocline waters. *Journal Of Physical Oceanography*, *37*, 2612–2636.

Sen Gupta, A., Santoso, A., Taschetto, A., Ummenhoffer, C., Trevena, J., & England, M. (2009). Projected changes to the Southern Hemisphere Ocean and sea ice in the IPCC AR4 models. *Journal of Climate*, *22*, 3047–3078.

Serreze, M., Barrett, A., Slater, A., Woodgate, R., Aagaard, K., Lammers, R., Steele, M., Moritz, R., Meredith, M., & Lee, C. (2006). The large-scale freshwater cycle of the arctic. *Journal of Geophysical Research*, *111*.

Serreze, M., & Francis, J. (2006). The arctic amplification debate. *Climatic Change*, *76*, 241–264.

Shapiro, G. I., & Meschanov, S. L. (1991). Distribution and spreading of red sea water and salt lens formation in the northwest indian ocean. *Deep Sea Research Part A. Oceanographic Research Papers*, *38*, 21.

Shcherbina, A. Y., Talley, L. D., & Rudnick, D. L. (2003). Direct observations of north pacific ventilation: Brine rejection in the okhotsk sea. *Science*, *302*, 1952–1955.

Shcherbina, A. Y., Talley, L. D., & Rudnick, D. L. (2004a). Dense water formation on the northwestern shelf of the okhotsk sea: 1. direct observations of brine rejection. *Journal Of Geophysical Research-Oceans*, *109*.

Shcherbina, A. Y., Talley, L. D., & Rudnick, D. L. (2004b). Dense water formation on the northwestern shelf of the okhotsk sea: 2. quantifying the transports. *Journal Of Geophysical Research-Oceans*, *109*.

Shodlock, M., Rodehacke, C., Hellmer, H., & Beckmann, A. (2001). On the origin of the deep cfc maximum in the eastern weddell sea - numerical model results. *Geophysical Research Letters*, *28*, 2859–2862.

Siedler, G., Kuhl, A., & Zenk, W. (1987). The madeira mode water. *Journal of Physical Oceanography*, *17*, 1561–1570.

Siegenthaler, U., & Wenk, T. (1984). Rapid atmospheric co2 variations and ocean circulation. *Nature*, *308*, 624–626.

Sloyan, B., Talley, L., Chereskin, T., Fine, R., & Holte, J. (2010). Antarctic intermediate water and subantarctic mode water foramtion in the southeast pacific: the role of turbulent mixing. *Journal of Physical Oceanography*, *40*, 1558–1574.

Sloyan, B. M., & Kamenkovich, I. V. (2007). Simulation of subantarctic mode and antarctic intermediate waters in climate models. *Journal Of Climate*, *20*, 5061–5080.

Sloyan, B. M., & Rintoul, S. R. (2001). The southern ocean limb of the global deep overturning circulation. *Journal Of Physical Oceanography*, *31*, 143–173.

Smethie, W. M. (1993). Tracing the thermohaline circulation in the western north-atlantic using chlorofluorocarbons. *Progress In Oceanography*, *31*, 51–99. 0079-6611.

Smethie, W. M., & Fine, R. A. (2001). Rates of north atlantic deep water formation calculated from chlorofluorocarbon inventories. *Deep-Sea Research Part I-Oceanographic Research Papers*, *48*, 189–215.

Smethie, W. M., Fine, R. A., Putzka, A., & Jones, E. P. (2000). Tracing the flow of north atlantic deep water using chlorofluorocarbons. *Journal Of Geophysical Research-Oceans*, *105*, 14297–14323. 0148-0227.

Smith, J., Hillenbrand, C.-D., Pudsey, C., Allen, C., & Graham, A. (2010). The presence of polynyas in the weddell sea during the last glacial period with implications for the reconstruction of sea-ice limits and ice-sheet history. *Earth And Planetary Science Letters*, *296*, 287–298.

Sorensen, J. V. T., Ribbe, J., & Shaffer, G. (2001). Antarctic intermediate water mass formation in ocean general circulation models. *Journal Of Physical Oceanography*, *31*, 3295–3311.

Spall, M. A., & Pickart, R. S. (2001). Where does dense water sink? a subpolar gyre example. *Journal Of Physical Oceanography*, *31*, 810–826.

Spall, M. A., & Pickart, R. S. (2003). Wind-driven recirculations and exchange in the labrador and irminger seas. *Journal Of Physical Oceanography*, *33*, 1829–1845.

Sprintall, J. (2008). Long-term trends and interannual variability of temperature in drake passage. *Progress in Oceanography*, *77*, 316–330.

Stammerjohn, S., Martinson, D., Smith, R., Yuan, X., & Rind, D. (2008). Trends in antarctic annual sea ice retreat and advance and their relation to el nino-southern oscillation and southern annular mode variability. *Journal of Geophysical Research*, *113*.

Steinfeldt, R., Rhein, M., Bullister, J., & Tanhua, T. (2009). Inventory changes in anthropogenic carbon from 1997-2003 in the atlantic ocean between 20s and 65n. *Global Biogeochemical Cycles*, *23*, GB3010.

Stephens, B., & Keeling, R. (2000). The influence of antarctic sea ice on glacial-interglacial co2 variations. *Nature*, *404*, 171–174.

de Steur, L., Holland, D., Muench, R., & M.G., M. (2007). The warm-water "halo" around maud rise: properties, dynamics and impact. *Deep-Sea Research I*, *54*, 871–896.

Stommel, H. (1961). Thermohaline convection with two stable regimes of flow. *Tellus*, *13*, 224–230.

Stommel, H. (1979). Determination of water mass properties of water pumped down from the ekman layer to the geostrophic flow below. *Proceedings Of The National Academy Of Sciences Of The United States Of America*, *76*, 3051–3055.

Stommel, H., & Arons, A. B. (1960a). On the abyssal circulation of the world ocean.1. stationary planetary flow patterns on a sphere. *Deep-Sea Research*, *6*, 140–154.

Stommel, H., & Arons, A. B. (1960b). On the abyssal circulation of the world ocean.2. an idealized model of the circulation pattern and amplitude in oceanic basins. *Deep-Sea Research*, *6*, 217–233.

Stott, F., Xie, S.-P., & McCreary, J. (2009). Indian ocean circulation and climate variability. *Reviews of Geophysics*, *47*, 1–46.

Stouffer, R., & et al. (2006). GFDL's CM2 global coupled climate models. Part IV: Idealized climate response. *Journal of Climate*, *19*, 723–740.

Stouffer, R., Yin, J., Gregory, J., & et al. (2006a). Investigating the causes of the response of the thermohaline circulation to past and fugure climate changes. *Journal of Climate*, *19*, 1365–1387.

Stouffer, R. J., Russell, J., & Spelman, M. J. (2006b). Importance of oceanic heat uptake in transient climate change. *Geophysical Research Letters*, *33*.

Stramma, L., Kieke, D., Rhein, M., Schott, F., Yashayaev, I., & Koltermann, K. P. (2004). Deep water changes at the western boundary of the subpolar north atlantic during 1996 to 2001. *Deep-Sea Research I*, *51*, 1033–1056.

Straneo, F. (2006). Heat and freshwater transport through the central labrador sea. *Journal of Physical Oceanography*, *36*, 606–628.

Straneo, F., & Kawase, M. (1999). Comparisons of localized convection due to localized forcing and to preconditioning. *Journal of Physical Oceanography*, *29*, 55–68.

Straneo, F., & Saucier, F. (2008). The outflow from hudson strait and its contribution to the labrador current. *Deep-Sea Research I*, *55*, 926–946.

Strass, V., Fahrbach, E., Schauer, U., & Sellmann, L. (1993). Formation of denmark strait overflow water by mixing in the east greenland current. *Journal of Geophysical Research*, *98*, 6907.

Suga, T., Aoki, Y., Saito, H., & Hanawa, K. (2008). Ventilation of the north pacific subtropical pycnocline and mode water formation. *Progress in Oceangraphy*, *77*, 285–297.

Suga, T., & Hanawa, K. (1995). The subtropical mode water circulation in the north pacific. *Journal Of Physical Oceanography*, *25*, 958–970.

Suga, T., Motoki, K., Aoki, Y., & MacDonald, A. (2004). The north pacific climatology of winter mixed layer and mode waters. *Journal of Physical Oceanography*, *34*, 3–22.

Suga, T., Motoki, K., & Hanawa, K. (2003). Subsurface water masses in the central north pacific transition region: The repeat section along the 180 degrees meridian. *Journal Of Oceanography*, *59*, 435–444.

Suga, T., Takei, Y., & Hanawa, K. (1997). Thermostad distribution in the north pacific subtropical gyre: The general mode water and the subtropical mode water. *Journal Of Physical Oceanography*, *27*, 140–152.

Suga, T., & Talley, L. D. (1995). Antarctic intermediate water circulation in the tropical and subtropical south-atlantic. *Journal Of Geophysical Research-Oceans*, *100*, 13441–13453.

Sutton, P., & Roemmich, D. (2011). Decadal steric and sea surface height changes in the Southern Hemisphere. *Geophysical Research Letters*, *38*.

Sverdrup, H., Johnson, M., & Fleming, R. (1942). The oceans: Their physics, chemistry and general biology. chapter Chapter XV: The Water Masses and Currents of the Oceans. (pp. 605–761). Englewood Cliff, NJ: Prentice-Hall.

Swift, J., Aagaard, K., Timokhov, L., & Nikiforov, E. (2005). Long-term variability of arctic ocean waters: Evidience from a reanalysis of the ewg data set. *Journal of Geophysical Research*, *110*.

Swift, J., & Aagaard, S., K.a nd Malmberg (1980). The contribution of the denmark strait overflow to the deep north atlantic. *Deep Sea Research Part A*, *27*, 29–42.

Swift, J. H. (1984). The circulation of the denmark strait and iceland scotland overflow waters in the north-atlantic. *Deep-Sea Research Part A-Oceanographic Research Papers*, *31*, 1339–1355.

Swift, J. H., & Aagaard, K. (1981). Seasonal transitions and water mass forma-

tion in the iceland and greenland seas. *Deep-Sea Research*, *28*, 1107–1129.
Swift, S., & Bower, A. (2003). Formation and circulation of dense water in the persian/arabian gulf. *Journal of Geophysical Research*, *108*, 3004.
Sy, A., Rhein, M., Lazier, J. R. N., Koltermann, K. P., Meincke, J., Putzka, A., & Bersch, M. (1997). Surprisingly rapid spreading of newly formed intermediate waters across the north atlantic ocean. *Nature*, *386*, 675–679.
Tagliabue, A., & Arrigo, K. R. (2006). Processes governing the supply of iron to phytoplankton in stratified seas. *Journal Of Geophysical Research-Oceans*, *111*.
Tagliabue, A., Bopp, L., Dutay, J. C., & et al. (2010). Hydrothermal contribution to the oceanic dissolved iron inventory. *Nature Geosciences*, *3*, 252–256.
Talley, L. (1996). The south atlantic: Present and past circulation. chapter Antarctic Intermediate Water in the South Atlantic. (pp. 219–238). Berlin: Springer-Verlag.
Talley, L. (2008). Freshwater transport estimates and the global overturning circulation: Shallow, deep and throughflow components. *Progress In Oceanography*, *78*, 257–303.
Talley, L., Pickard, G., Emery, W., & Swift, J. (2011). *Descriptive physical oceanography: an introduction*. (Sixth edition ed.). Amsterdam, The Netherlands: Elsevier.
Talley, L. D. (1991). An okhotsk sea-water anomaly - implications for ventilation in the north pacific. *Deep-Sea Research Part A-Oceanographic Research Papers*, *38*, S171–S190.
Talley, L. D. (1993). Distribution and formation of north pacific intermediate water. *Journal Of Physical Oceanography*, *23*, 517–537.
Talley, L. D. (1997). North pacific intermediate water transports in the mixed water region. *Journal Of Physical Oceanography*, *27*, 1795–1803.
Talley, L. D. (2003). Shallow, intermediate, and deep overturning components of the global heat budget. *Journal of Physical Oceanography*, *33*, 530–560.
Talley, L. D., & McCartney, M. S. (1982). Distribution and circulation of labrador sea-water. *Journal Of Physical Oceanography*, *12*, 1189–1205.
Talley, L. D., Nagata, Y., Fujimura, M., Iwao, T., Kono, T., Inagake, D., Hirai, M., & Okuda, K. (1995). North pacific intermediate water in the kuroshio-oyashio mixed water region. *Journal Of Physical Oceanography*, *25*, 475–501.
Talley, L. D., Reid, J. L., & Robbins, P. E. (2003). Data-based meridional overturning streamfunctions for the global ocean. *Journal of Climate*, *16*, 3213–3226.
Talley, L. D., & Sprintall, J. (2005). Deep expression of the indonesian throughflow: Indonesian intermediate water in the south equatorial current. *Journal Of Geophysical Research-Oceans*, *110*.
Talley, L. D., & Yun, J. Y. (2001). The role of cabbeling and double diffusion in setting the density of the north pacific intermediate water salinity minimum. *Journal Of Physical Oceanography*, *31*, 1538–1549.
Tamura, T., Ohshima, K., & Nihashi, S. (2008). Mapping of sea ice production for antarctic coastal polynyas. *Geophysical Research Letters*, *35*.
Taneda, T., Suga, T., & Hanawa, K. (2000). Subtropical mode water variation in the northwestern part of the north pacific subtropical gyre. *Journal of Geophysical Research*, *105*, 19591–19598.
Tanhua, T., Jones, P., Jeansson, E., Jutterstrom, S., Smethie, W., Wallace, D. W. R., & Anderson, L. (2009). Ventilation of the Arctic Ocean: mean ages and inventories of anthropogenic CO2 and CFC-11. *Journal of Geophysical Research*, *114*.
Tanhua, T., Waugh, D. W., & Wallace, D. W. R. (2008). Use of sf6 to estimate anthropogenic co2 in the upper ocean. *Journal of Geophysical Research*, *113*.
Thierry, V., de Boisséson, E., & Mercier, H. (2008). Interannual variability of the subpolar mode water properties over teh reykjanes ridge during 1990-2006. *Journal of Geophysical Research*, *113*.
Thompson, B. (1800). *Essays, Political, Economical, and Philosophical*. London.
Thompson, R., & Edwards, R. J. (1981). Mixing and water-mass formation in the australian sub-antarctic. *Journal Of Physical Oceanography*, *11*, 1399–1406.
Thornalley, D.J.R. and Barker, S. and Broecker W.S. and Elderfield H. and McCave I.N. (2011). The deglacial evolution of north atlantic deep convection. *Science*, *331*, 202–205.
Toggweiler, J. R., Gnanadesikan, A., Carson, S., Murnane, R., & Sarmiento, J. L. (2003a). Representation of the carbon cycle in box models and GCMs 1. Solubility pump. *Global Biogeochemical Cycles*, *17*, 1026.
Toggweiler, J. R., Murnane, R., Carson, S., Gnanadesikan, A., & Sarmiento, J. L. (2003b). Representation of the carbon cycle in box models and GCMs - 2. Organic pump. *Global Biogeochemical Cycles*, *17*, 1027.
Toggweiler, J. R., & Samuels, B. (1995). Effect Of Sea-Ice On The Salinity Of Antarctic Bottom Waters. *Journal of Physical Oceanography*, *25*, 1980–1997.
Toggweiler, J. R., & Samuels, B. (1998). On the ocean's large-scale circulation near the limit of no vertical mixing. *Journal of Physical Oceanography*, *28*, 1832–1852.
Tomczak, M., & Godfrey, J. S. (1994). *Regional Oceanography: an Introduction*. (First edition ed.). Pergamon.
Toyama, K., & Suga, T. (2011). Roles of mode waters in the formation and maintenance of central water in the north pacific. *J. Oceanogr.*, *67*.
Toyoda, T., Awaji, T., Ishikawa, Y., & Nakamura, T. (2004). Preconditioning of winter mixed layer in the formation of north pacific eastern subtropical mode water. *Geophysical Research Letters*, *31*.
Trumbore, S. E., Jacobs, S. S., & Smethie, W. M. (1991). Chlorofluorocarbon evidence for rapid ventilation of the ross sea. *Deep-Sea Research Part A-Oceanographic Research Papers*, *38*, 845–870.
Tsubouchi, T., Suga, T., & Hanawa, K. (2007). Three types of south pacific subtropical mode waters: their relation to the large-scale circulation of the south pacific subtropical gyre and their temporal variability. *Journal of Physical Oceanography*, *37*, 2478–2490.
Tsuchiya, M. (1989). Circulation of the antarctic intermediate water in the north-atlantic ocean. *Journal Of Marine Research*, *47*, 747–755.
Tsuchiya, M., Talley, L. D., & McCartney, M. S. (1992). An eastern atlantic section from iceland southward across the equator. *Deep-Sea Research Part A-Oceanographic Research Papers*, *39*, 1885–1917.
Turner, J. (1986). Turbulent entrainment: the development of the entrainment assumption, and its application to geophysical flows. *J. Fluid Mech.*, *173*, 431–471.
Uda, M. (1963). Oceanography of the subarctic pacific ocean. *J. Fish. Res. Board Can.*, *20*, 119–179.
Uehara, H., Suga, T., Hanawa, K., & Shikama, N. (2003). A role of eddies in formation and transport of north pacific subtropical mode water. *Geophysical Research Letters*, *30*. 1705.
Ueno, H., Oka, E., Suga, T., Onishi, H., & Roemmich, D. (2007). Formation and variation of temperature inversions in the eastern subarctic north pacific. *Geophysical Research Letters*, *34*.
Ueno, H., & Yasuda, I. (2000). Distribution and formation of the mesothermal structure (temperature inversions) in the north pacific subarctic region. *Journal of Geophysical Research*, *105*, 16885–16897.
Ueno, H., & Yasuda, I. (2003). Intermediate water circulation in the north pacific subarctic and northern subtropical regions. *Journal of Geophysical Research*, *108*, 3348.
Ueno, H., & Yasuda, I. (2005). Temperature inversions in the subarctic north pacific. *Journal of Physical Oceanography*, *35*, 2444–2456.
Vage, K., Pickart, R., Moore, G., & Ribergaard, M. (2008a). Winter mixed layer development in the central irminger sea: the effect of strong, intermittent wind events. *Journal of Physical Oceanography*, *38*, 541–565.
Vage, K., Pickart, R., Sarafanov, A., Knutsen, O., Mercier, H., Lherminier, P., van Aken H.M., Meincke, J., Quadfasel, D., & Bacon, S. (2011). The Irminger gyre: circulation, convection, and interannual variability. *Deep-Sea Research I*, *58*, 590–614.
Vage, K., Pickart, R., Thierry, V., Reverdin, G., Lee, C., Petrie, B., Agnew, T., Wong, A., & Ribergaard, M. (2008b). Surprising return of deep convection to the subpolar north atlantic ocean in winter 2007-2008. *Nature Geosciences*, *2*, 67–72.
Van Scoy, K., Olson, D., & Fine, R. (1991). Ventilation of north pacific intermediate waters: the role of the alaskan gyre. *Journal of Geophysical Research*, *96*, 16801–16810.
Volkov, D., & Fu, L.-L. (2010). On the reasons for the formation and variability of the azores current. *Journal of Physical Oceanography*, *40*, 2197–2220.
Vranes, K., Gordon, A. L., & Ffield, A. (2002). The heat transport of the indonesian throughflow and implications for the indian ocean heat budget. *Deep-Sea Research Part Ii-Topical Studies In Oceanography*, *49*, 1391–1410.
de Vries, P., & Weber, S. (2005). The Atlantic freshwater budget as a diagnostic for the existence of a stable shut down of the meridional overturning circulation. *Geophysical Research Letters*, *32*.
Waelbroeck, C., Skinner, L., Labeyrie, L., Duplessy, J. C., Michel, E.,

Vazquez Riveiros, N., Gherardhi, J.-M., & Devilde, F. (2011). The timing of deglacial circulation changes in the atlantic. *Paleoceanography*, *26*.

Walin, G. (1982). On the relation between sea-surface heat-flow and thermal circulation in the ocean. *Tellus*, *34*, 187–195. 0040-2826.

Wang, Q., Danilov, S., Hellmer, H., & Schroeter, J. (2010). Overflow dynamics and bottom water formation in the western Ross Sea: influence of tides. *Journal of Geophysical Research*, *115*.

Warner, M., M. J., & Weiss, R., R. F. (1992). Chlorofluoromethanes in South Atlantic Antarctic Intermediate Water. *Deep Sea Research Part A. Oceanographic Research Papers*, *39*, 2053–2075.

Weepernig, R., Schlosser, P., Khatiwala, S., & Fairbanks, R. (1996). Isotope data from ice station weddell: implications for deep water formation in the weddell sea. *Journal of Geophysical Research*, *101*, 25723–25739.

Weiss, R., Bullister, J., Gammon, R., & Waner, M. (1985). Atmospheric chlorofluoromethanes in the deep equatorial atlantic. *Nature*, *314*, 608–610.

Weiss, R. F., Ostlund, H. G., & Craig, H. (1979). Geochemical studies of the weddell sea. *Deep-Sea Research Part A-Oceanographic Research Papers*, *26*, 1093–1120.

Whitehead, J. (1998). Topographic control of oceanic flows in deep passages and straits. *Reviews of Geophysics*, *36*, 423–440.

Whitworth, I., T (2002). Two modes of bottom water in the australian-antarctic basin. *Geophysical Research Letters*, *29*, 1073.

Whitworth, T., Nowlin, W., Pillsbury, D., Moore, M., & Weiss, R. (1991). Observations of the antarctic circumpolar current and deep boundary current in the southwest atlantic. *Journal of Geophysical Research*, *96*, 15105–15118.

Whitworth, T., & Orsi, A. H. (2006). Antarctic bottom water production and export by tides in the ross sea. *Geophysical Research Letters*, *33*. L12609.

Williams, G., Aoki, S., Jacobs, S., Rintoul, S., Tamura, T., & Bindoff, N. (2010). Antarctic bottom water from the adelie and george v land coast, east antarctica (140-149e). *Journal of Geophysical Research*, *115*.

Williams, R. (1991). The role of the mixed layer in setting the potential vorticity of the main thermocline. *Journal of Physical Oceanography*, *21*, 1803–1814.

Winton, M., Hallberg, R., & Gnanadesikan, A. (1998). Simulation of density-driven frictional downslope flow in z-coordinate ocean models. *Journal Of Physical Oceanography*, *28*, 2163–2174.

Wong, A. P. S. (2005). Subantarctic mode water and antarctic intermediate water in the south indian ocean based on profiling float data 2000-2004. *Journal Of Marine Research*, *63*, 789–812.

Wong, A. P. S., Bindoff, N., & Forbes, A. (1998a). Ocean, ice, and atmosphere: interactions at the antarctic continental margin. chapter Ocean-ice interaction and possible bottm water formation in Prydz Bay, Antarctica (pp. 173–187). AGU volume 75 of *Antarctic Res. Ser.*.

Wong, A. P. S., & Johnson, G. C. (2003). South pacific eastern subtropical mode water. *Journal Of Physical Oceanography*, *33*, 1493–1509.

Wong, C., Matear, R., Freeland, H., Whitney, F., & Bychkov, A. (1998b). Woce line p1w in the sea of okhotsk. 2. cfcs and the formation rate of intermediate water. *Journal of Geophysical Research*, *103*, 15625–15642.

Worthington, L. V. (1959). The 18-degree water in the sargasso sea. *Deep-Sea Research*, *5*, 297–305.

Wüst, G. (1935). *The stratosphere of the Atlantic Ocean* volume VI of *Scientific results of the German Atlantic expedition of the research vessel "Meteor" 1925-27*. American Publishing Co. Pvt. Ltd.

Xie, S.-P., Xu, L., Liu, Q., & Kobashi, F. (2011). Dynamical role of mode water ventilation in decadal variability in the central subtropical gyre of the north pacific. *Journal of Climate*, *24*, 1212–1225.

Yabuki, T., Suga, T., Hanawa, K., Matsuoka, K., Kiwada, H., & Watanabe, T. (2006). Possible source of the antarctic bottom water in the prydz bay region. *Journal Of Oceanography*, *62*, 649–655.

Yamamoto-Kawai, M., McLaughlin, F., Carmack, E., Nishino, S., Shimada, K., & Kurita, N. (2009). Surface freshening of the canada basin, 2003-2007: river runoff versus sea ice meltwater. *Journal Of Geophysical Research*, *114*.

Yashayaev, I. (2007). Hydrographic changes in the labrador sea, 1960-2005. *Progress In Oceanography*, *73*, 242–276.

Yashayaev, I., Bersch, M., & van Aken, H. M. (2007). Spreading of the labrador sea water to the irminger and iceland basins. *Geophysical Research Letters*, *34*.

Yashayaev, I., & Clarke, A. (2008). Evolution of north atlantic water masses inferred from labrador sea salinity series. *Oceanography*, *21*, 30–45.

Yashayaev, I., Holliday, N. P., Bersch, M., & van Aken H.M. (2008). Arctic-subarctic ocean fluxes: defining the role of the northern seas in climate. chapter Ch 24. The history of the Labrador Sea Water: Production, Spreading, Transformation and Loss. (pp. 569–612). Springer.

Yashayaev, I., & Loder, J. (2009). Enhanced production of labrador sea water in 2008. *Geophysical Research Letters*, *36*.

Yasuda, I. (1997). The origin of the north pacific intermediate water. *Journal Of Geophysical Research-Oceans*, *102*, 893–909.

Yasuda, I., Kouketsu, S., Katsumata, K., Ohiwa, M., Kawasaki, Y., & Kusaka, A. (2002). Influence of okhotsk sea intermediate water on the oyashio and north pacific intermediate water. *Journal Of Geophysical Research-Oceans*, *107*.

Yeager, S. G., & Jochum, M. (2009). The connection between labrador sea buoyancy loss, deep western boundary current strength, and gulf stream path in an ocean circulation model. *Ocean Modelling*, *30*, 207–224.

Yoshikawa, C., Nakatsuka, T., & Wakatsuchi, M. (2006). Distribution of n* in the sea of okhostk and its use as a biogeochemical tracer of the okhostk sea intermediate water formation process. *Journal of Marine Systems*, *63*, 49–62.

You, Y. (2002a). A global ocean climatological atlas of the turner angle: implications for double-diffusion and water-mass structure. *Deep-Sea Research Part I-Oceanographic Research Papers*, *49*, 2075–2093.

You, Y. Z. (1996). Dianeutral mixing in the thermocline of the indian ocean. *Deep-Sea Research Part I-Oceanographic Research Papers*, *43*, 291–320.

You, Y. Z. (2000). Contribution of salt-fingering to the conveyor belt circulation in the abyssal northern indian ocean. *Geophysical Research Letters*, *27*, 3913–3916.

You, Y. Z. (2002b). Quantitative estimate of antarctic intermediate water contributions from the drake passage and the southwest indian ocean to the south atlantic. *Journal Of Geophysical Research-Oceans*, *107*. 3031.

You, Y. Z., Chern, C. S., Yang, Y., Liu, C. T., Liu, K. K., & Pai, S. C. (2005). The south china sea, a cul-de-sac of north pacific intermediate water. *Journal Of Oceanography*, *61*, 509–527.

You, Y. Z., Suginohara, N., Fukasawa, M., Yasuda, I., Kaneko, I., Yoritaka, H., & Kawamiya, M. (2000). Roles of the Okhotsk Sea and Gulf of Alaska in forming the North Pacific Intermediate Water. *Journal Of Geophysical Research-Oceans*, *105*, 3253–3280.

You, Y. Z., Suginohara, N., Fukasawa, M., Yoritaka, H., Mizuno, K., Kashino, Y., & Hartoyo, D. (2003). Transport of north pacific intermediate water across japanese woce sections. *Journal Of Geophysical Research-Oceans*, *108*. 3196.

Yuan, X., & Martinson, D. (2000). Antarctic sea ice extent variability and its global connectivity. *Journal of Climate*, *13*, 1697–1717.

Yuan, X., & Martinson, D. (2001). The antarctic dipole and its predictability. *Geophysical Research Letters*, *28*, 3609–3612.

Yun, J., & Talley, L. (2003). Cabbeling and the density of the North Pacific Intermediate Water quantified by an inverse method. *Journal Of Geophysical Research-Oceans*, *108*, 3118.

Zenk, W., & Armi, L. (1990). The complex spreading pattern of mediterranean water off the portuguese continental slope. *Deep-Sea Research*, *37*, 1805–1823.

Zhang, D., McPhaden, M., & Johns, W. (2003). Observational evidence for flow between the subtropical and tropical atlantic: the atlantic tropical cells. *Journal of Physical Oceanography*, *33*, 1783–1797.

Zhang, R. (2010). Latitudinal dependence of Atlantic meridional overturning circulation (AMOC) variabions. *Geophysical Research Letters*, *37*.

Zhang, R., & Vallis, G. (2007). The role of bottom vortex stretching on the path of the North Atlantic Western Boundary current and on the Northern recirculation gyre. *Journal of Physical Oceanography*, *37*, 2053–2080.